2008

Combustion dynamics of swirl-stabilized lean premixed flames in an acoustically-driven environment

Yun Huang
University of Iowa

COMBUSTION DYNAMICS OF SWIRL-STABILIZED LEAN PREMIXED FLAMES IN AN ACOUSTICALLY-DRIVEN ENVIRONMENT

by

Yun Huang

An Abstract

Of a thesis submitted in partial fulfillment
of the requirements for the Doctor of
Philosophy degree in Mechanical Engineering
in the Graduate College of
The University of Iowa

December 2008

Thesis Supervisor: Assistant Professor Albert Ratner

ABSTRACT

Combustion instability is a process which involves unsteady chemical kinetic, fluid mechanic, and acoustic processes. It can lead to unstable behavior and be detrimental in ways ranging from faster part fatigue to catastrophic system failure. In terms of combustion methodology, combustion instability has been a key issue for lean premixed combustion. The primary objective of this work is to improve understanding of combustion dynamics through an experimental study of lean premixed combustion using a low swirl combustor. This special burner was developed at the Lawrence Berkeley National Laboratory and has recently received significant interest from the gas turbine industry.

In these experiments, acoustic perturbations (chamber modes) are imposed on a low swirl stabilized methane-air flame using loudspeakers. The flame response is examined and quantified with OH planar laser induced fluorescence. Rayleigh index maps of the flame are computed for each frequency and operating condition. Examining the structures in the Rayleigh maps, it is evident that, while the flame shows no significant response in some cases, acoustic forcing in the 70-150 Hz frequency range induces vortex shedding in the flame shear layer. These vortices distort the flame front and generate locally compact and sparse flame areas. This information about the flow field shows that, besides illuminating the combustion dynamics, the Rayleigh index is a useful way to reveal interesting aspects of the underlying flow.

The experiments also revealed other interesting aspects of this flame system. It was found that the flame becomes unstable when the perturbation amplitude reaches 0.7% of the mean pressure. Decreasing the swirl number makes the flame shape more jet-like, but does little to alter the shear-layer coupling. In a similar fashion, increasing the pressure was found to alter the flame shape and flame extent, but the thermo-acoustic

coupling and induced large scale structure persisted to 0.34MPa, the highest pressure tested.

Abstract Approved: _____
Thesis Supervisor

_____
Title and Department

_____
Date

COMBUSTION DYNAMICS OF SWIRL-STABILIZED LEAN PREMIXED FLAMES IN AN ACOUSTICALLY-DRIVEN ENVIRONMENT

by

Yun Huang

A thesis submitted in partial fulfillment
of the requirements for the Doctor of
Philosophy degree in Mechanical Engineering
in the Graduate College of
The University of Iowa

December 2008

Thesis Supervisor: Assistant Professor Albert Ratner

Graduate College
The University of Iowa
Iowa City, Iowa

CERTIFICATE OF APPROVAL

_____

PH.D. THESIS

_____

This is to certify that the Ph.D. thesis of

Yun Huang

has been approved by the Examining Committee
for the thesis requirement for the Doctor of Philosophy
degree in Mechanical Engineering at the December 2008 graduation.

Thesis Committee: _____
Albert Ratner, Thesis Supervisor

_____
James Buchholz

_____
P. Barry Butler

_____
Lea-Der Chen

_____
Ching-Long Lin

_____
Charles Stanier

To Shuiqing and Jonathan

ACKNOWLEDGEMENTS

First, I would like to express my sincere gratitude to my advisor, Professor Albert Ratner, for all of his help and support throughout my PhD study in Iowa. His guidance, understanding and encouragement have provided a foundation for the present thesis.

I would like to express my sincere thanks to my thesis committee members, Prof. James Buchholz, Prof. P. Barry Butler, Prof. Lea-Der Chen, Prof. Ching-Long Lin and Prof. Charles Stanier. I learned much about being a good professor by learning in your classes, working as teaching assistant, and getting advices on my research and career development.

I thank all the members in our lab; in particular, Dr. Dal Mo Kang, who taught me the experimental techniques needed to carry out combustion instability research during his visit; former graduate students Brett Bathel and Hui Gao for their support and their help with the first portion of the experiments; Ilker Yilmaz and Majid Emadi for helping me with elevated pressure experiments; and Anthony Dix, Bihua Wei, Yongli Zhao, Xinghui Zhang, Yan Zhang, Neeraj Kumar Mishra, Eric DeCristofaro, for making my time here so enjoyable.

I am deeply grateful to Professor C.K. Law at Princeton University for providing me the opportunity to study and learn in his laboratory during my summer visit. The members of Prof. Law's group also have my gratitude for their help and kindness during my stay.

I would like to thank the University of Iowa, the Richard B. Stewart Thermal-Fluids Graduate Scholarship foundation, the Lawrence Berkeley National Laboratory (R.K. Cheng as the project monitor), and Siemens (Scott Martin as the project monitor), for financial support.

Finally I want to thank my dearest family for their love and encouragement.

ABSTRACT

Combustion instability is a process which involves unsteady chemical kinetic, fluid mechanic, and acoustic processes. It can lead to unstable behavior and be detrimental in ways ranging from faster part fatigue to catastrophic system failure. In terms of combustion methodology, combustion instability has been a key issue for lean premixed combustion. The primary objective of this work is to improve understanding of combustion dynamics through an experimental study of lean premixed combustion using a low swirl combustor. This special burner was developed at the Lawrence Berkeley National Laboratory and has recently received significant interest from the gas turbine industry.

In these experiments, acoustic perturbations (chamber modes) are imposed on a low swirl stabilized methane-air flame using loudspeakers. The flame response is examined and quantified with OH planar laser induced fluorescence. Rayleigh index maps of the flame are computed for each frequency and operating condition. Examining the structures in the Rayleigh maps, it is evident that, while the flame shows no significant response in some cases, acoustic forcing in the 70-150 Hz frequency range induces vortex shedding in the flame shear layer. These vortices distort the flame front and generate locally compact and sparse flame areas. This information about the flow field shows that, besides illuminating the combustion dynamics, the Rayleigh index is a useful way to reveal interesting aspects of the underlying flow.

The experiments also revealed other interesting aspects of this flame system. It was found that the flame becomes unstable when the perturbation amplitude reaches 0.7% of the mean pressure. Decreasing the swirl number makes the flame shape more jet-like, but does little to alter the shear-layer coupling. In a similar fashion, increasing the pressure was found to alter the flame shape and flame extent, but the thermo-acoustic coupling and induced large scale structure persisted to 0.34MPa, the highest pressure tested.

TABLE OF CONTENTS

LIST OF TABLES

LIST OF FIGURES

LIST OF NOMENCLATURE

c	Speed of sound
D	Diameter
E	Energy
f	Frequency
g	Gravity
k	Wave number
K	Stretch rate
l	Markstein length
$\dot{m}_a$	Mass flow rate of air
$\dot{m}_f$	Mass flow rate of fuel
Le	Lewis number
P	Mean pressure
p'	Pressure oscillation
Pr	Prandtl number
p_{rms}	Root mean square of p'
q	Heat release fluctuation
Re	Reynolds number
Rf	Rayleigh Index
Ru	universal gas constant
s	Area
S	Swirl number
Sf	Flame speed
S_L	Laminar flame speed
St	Strouhal number
T	Time

T	Temperature
u	Velocity fluctuation
U	Velocity
V	Volume
β	Zeldovich number
γ	Ratio of specific heats
λ	Wavelength
Φ	Equivalence ratio
ε	Energy of the oscillation cycle
σ	Growth rate
σ	Unburned to burned density ratio

CHAPTER 1

INTRODUCTION

1.1 Background

Gas turbines have a multitude of applications and are available in a wide range of sizes, are used in applications from power generation to mechanical drive, for the exploration, production and transmission of oil and gas, as well as marine propulsion systems including transport, ferryboat and cruise ship installations. Gas turbines have become a dominant technology for new power generating capacity in the United States and worldwide. A gas turbine is a heat engine that uses high temperature, high-pressure gas as a working fluid to spin a turbine and generate power. Combustion of fuel with air is usually used to produce the needed temperatures and pressures to efficiently drive the turbine. Gas turbines are both more efficient and typically burn lower carbon fuels compared to other types of combustion-based power generation and mechanical drive systems.

Gas turbine manufacturers are currently facing two broad challenges- to reduce pollutant emission and improve efficiency. The Clean Air Act of 1990 imposes strict emission and control regulations on the production of NOx, which is emitted by combustion of fossil fuels. On the other hand, prices of natural gas have risen due to steady growth in demand and insufficient supply. High prices and strong price volatility, due to the inability to find natural gas at secure locations, are two additional challenges that the gas turbine industry now faces. After energy conservation and the use of renewable resources, the construction and use of clean, efficient gas turbine power plants will be the most effective way to reduce greenhouse gases and regional air pollution.

Lean premixed combustion has become an important technology option for reducing emissions for both gas-based heating and gas turbine power systems. With lean premixed combustion, the flame temperature is reduced by use of excess air. In turn, the

low temperature reduces the NOx formation rate (Turns, 2001). Lean premixed combustion has already been adopted by industry. For example, in 2005 General Electric reported that they were using a Dry Low NOx combustion system for the company's 12 MW class 10-2 gas turbine, to reduce NOx emissions from 25 to 15 ppm. These emission levels are guaranteed over any operating condition for 50-100% of load and ambient temperatures of -29°C to 38°C. The combustion chamber for this system incorporates four GE5 premixed pilot burners and includes flame detection, flashback thermocouples, and a humming detection system for full flame control. Research has shown that lean premixed combustion is the most promising technique for achieving the current reliability, efficiency, pollution, and economic utility goals.

There are several other techniques which could reduce NOx emissions, including exhaust stream clean-up using ammonia, direct water injection into the combustion liner to reduce the exhaust temperature, catalytic combustion (which allows for combustion below the flammability limit), and Rich-burn/Quick-quench/Lean-burn (RQL) combustion. Among these, the RQL system is usually hampered by soot formation and incomplete mixing while catalytic combustion tends to be too expensive, but research on these technologies is still ongoing (McKinney et al., 2007).

The greatest drawback of lean premixed combustion is that it can generate instabilities. Combustion instabilities are characterized by large-amplitude oscillations of one or more natural acoustic modes of the combustor. The instabilities generally occur when the unsteady heat release from combustion couples with the natural acoustic modes of the combustor, resulting in self-excited oscillations. Combustion driven pressure oscillations can make the flame unstable, reduce part life, and lead to structural damage and failure. This aspect of lean premixed systems has been hindering its development and use in gas turbines (Dowling, 2005).

Even with current high swirl burner combustion systems, combustion instability has been a serious problem when operating conditions have been adjusted in attempts to

reduce emissions (Lieuwen, 2003). It was reported that the cost for the repair and replacement of hot section components, where much of the damage was directly attributable to combustion instability, now exceeds $1 billion annually and constitutes up to 70% of the nonfuel costs for F-class gas turbines. Combustion instability is also not unique to gas turbines. It has been encountered in a variety of combustors, for example, propulsion systems (rockets, ramjets, and afterburners), power generation (land-based gas turbines), boiler and heating systems, and industrial furnaces (Lieuwen and Yang, 2006).

1.2 Combustion Instability

Historically, the first observation of combustion oscillation was the 'singing flame' which was discovered by Higgins in 1777. This phenomenon caught the interest of researchers and prompted broader, more systematic study. Rijke showed that sound can be generated in a vertical tube open at both ends by placing a heated metal gauze inside the tube. The sound was generated only when the heating element was placed in certain positions inside the tube. Rayleigh was the first to hypothesize the onset of the instability, and defined a criterion for the positive coupling which is now well known as the Rayleigh Criterion (Swift, 1999). The criterion states that a periodic heat transfer process adds energy to the acoustic field if the heat is added to or removed from the gas when the local pressure is above or below its mean value, respectively. This statement was later developed into a mathematical formulation by various researchers, including Putnam (1964), Chu (1956), Zinn (1987), and Culick (1987).

Combustion instabilities observed in different combustion systems display different properties depending on the geometry of the combustion chamber, fuel injector, burner, and so on. Some general classifications have been established to help understand the mechanisms behind the phenomena. Williams (1985) classified combustion instabilities into three categories- intrinsic instabilities, chamber instabilities, and system instabilities. Intrinsic instabilities are inherent to the combustion and fluid physics. There

are several types of instabilities which can be categorized as intrinsic instability, including but not limited to Darrieus-Landau instability (hydrodynamic instability) and diffusive-thermal instability. Chamber instabilities result from the interaction between the combustion process and chamber acoustics. System instabilities are consequence of the interactions of combustion process, chamber property, upstream supply, and/or downstream exhaust systems.

The term thermoacoustic instability generally refers to combustion instabilities which are caused by the interaction of acoustics and combustion. It can be an intrinsic instability, chamber instability, or system instability. Various areas of engineering research have examined thermoacoustic instabilities. The 1950s saw a surge in research related to combustion instability experienced in liquid propellant rocket engines (Culick, 1989; Culick, 1995). In the 1970s, the furnace industry also found thermoacoustic instability to be a problem and some focused research was initiated (Rodriguez-Martinez et al., 2006). During the 1980s, the emphasis on Ramjets and pulse combustors focused research on attempts to understand combustion instability so as to harness this effect to enhance propulsion system performance (Zinn, 1987). Starting in the 1990s, attention switched to gas turbines as the industry modified their designs to reduce NOx pollution (Keller, 1995). Currently, there continues to be a variety of research on many aspects and implications of combustion instability.

1.3 Objectives and Outline

Combustion instability is a complicated process that involves unsteady kinetic, fluid mechanic and acoustic processes. Even though a lot of research has been done in the area of combustion instability, the mechanisms causing combustion instabilities in gas turbines are still not fully understood. There is no clear criterion for the design of industrial combustors to avoid combustion instability. The present work aims to improve this situation through an experimental study of lean premixed combustion using a low

swirl combustor. The low swirl burner is a promising design for gas turbine systems and was developed at the Lawrence Berkeley National Laboratory (LBNL).

The objectives of this work are: to characterize the interplay of multiple, unstable physical phenomena of combustion instability so as to garner insights which can be applied during the design process; to develop tools and techniques to assess and refine new burner and combustor technology with minimal full-scale testing; to construct a database of combustor response functions as a starting point for a structured approach for modeling and active control of combustion instability.

The experimental system for the work utilizes laser diagnostics which are capable of Planar Laser Induced Fluorescence (PLIF). Compared with chemiluminescence (Venkataraman et al., 1999; Lee and Santavicca, 2003; Ghoniem et al., 2005), PLIF captures detailed information through a cross-section of the flame (Lee et al., 1995; Shepherd and Cheng, 2001). In addition, the acoustic system (installed in the chamber to create acoustic waves) enables fully-selectable direct acoustic forcing of the flame. Compared with other commonly used methods for studying combustion instability, such as installing speakers upstream of the fuel injector (Santhanam et al., 2002; Lawn et al., 2004; Li et al., 2007), this method allows study of acoustics-flame interaction while greatly reducing the impact on pre-flame mixing.

Chapter 2 presents a literature review of combustion instability mechanisms, models, and measurement techniques. Chapter 3 has a detailed description of the experimental system including the acoustic chamber, the burner, the mixer and the laser system layout; the OH-PLIF techniques including the beam spectrum scan and the beam distribution correction are then discussed. The last section lays out the experimental procedure.

Chapter 4 examines thermo-acoustic instability of the low-swirl-stabilized lean premixed methane-air flame at atmospheric conditions. Acoustic perturbations are imposed on the flame, and the flame's response is recorded. The Rayleigh index map of

the flame, including the methodology for constructing these, is computed and is used as an indicator of flame-acoustic coupling. These maps are also used to assess underlying flow field structure and to examine in detail the mechanisms behind the coupling. This work has been accepted for publication (Huang and Ratner, 2009).

Chapter 5 expands these studies to elevated chamber pressures of up to 0.34MPa. A similar methodology of calculating Rayleigh index as used in chapter 4 is employed and comparisons are drawn across the range of pressures. The goal is to characterize how the flame response evolves and how the flow structures change due to pressure increases.

Chapter 6 examines how other factors affect the measured flame behavior. The first parameter assessed is the effect of swirl on thermoacoustic coupling. This is acchomplished by comparing two swirl burners of the same type but with swirl numbers of 0.2 and 0.5. Then, the flame response to different acoustic forcing amplitudes is investigated.

Chapter 7 concludes the thesis by summarizing the achievement of the current work and laying out possible future works to advance our understanding of thermo-acoustic instability.

CHAPTER 2

LITERATURE REVIEW

There has been a significant amount of research performed and literature published on the topic of combustion instability. This chapter gives a brief review of some of these works and focuses on several particular aspects. The first part reviews work which focuses on the study of physical factors that lead to amplification of system oscillations. The second part of this chapter reviews theoretical models developed to assess and predict oscillations. The third part examines measurement techniques relevant to, and some previously employed for, the assessment of oscillatory behavior. The last portion of this chapter focuses on the history, development, and application of the low swirl burners.

2.1 Amplifications of Oscillatory Combustion Instabilities

Combustion instability is a physical process resulting from the coupling of heat release and pressure oscillation. The factors responsible for driving combustion instabilities either affect the heat release fluctuation, the pressure oscillations, or both. The physical phenomena capable of inducing pressure fluctuation include acoustic motions in the chamber (chamber acoustic property), hydrodynamic instabilities, injection system fluctuations, chamber noise, local heat release, etc. Heat release is largely controlled by the local air-to-fuel mixture ratio and mass flow rate, along with the instantaneous local pressure and temperature. Specifically, for methane-fueled premixed flames, the instability may arise from equivalence ratio fluctuations, mass flow rate oscillations, and vortex shedding processes due to hydrodynamics instabilities (Lieuwen et al., 1998; Najm and Ghoniem, 1994). For liquid-fuel-based systems, atomization and droplet vaporization are additional sources of heat-release fluctuations. Some specific

discussions on sources of pressure and heat release fluctuations for premixed gas phase combustion are presented in later sub-sections.

2.1.1 Chamber Acoustic Property

Often, the combustion oscillations observed in the laboratory or in full-scale industrial systems occur at frequencies that are close to the natural acoustic modes of the combustion chamber (Samaniego, 1993). The famous Rijke tube is a good example of a self-excited combustor. As demonstrated by many researchers, when the two ends of the tube are open and the air inside is locally heated, the sound frequency produced corresponds to the half-wave mode of the tube; it becomes a quarter-wave mode if one end is open and the other end is closed (Swift, 2002). Systems with confined combustor geometry, such as dump combustors, are, as expected, more prone to combustion oscillations in the same manner as the Rijke tube.

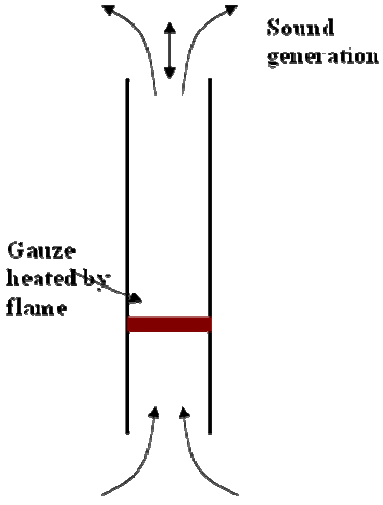

Figure2.1 Rijke tube

For these systems, simplified one dimensional modeling is typically used (and is typically sufficient) to predict the frequency of the chamber instability. For a duct with

uniform cross sectional area, a mean temperature, and a time-constant density distribution (no variations due to mean flow) can be described by functions of purely the axial coordinate x and time t. The acoustic wave takes the form of (Dowling and Stow, 2003)

$$\hat{p}(x) = \hat{f}e^{-i\omega x/\bar{c}} + \hat{g}e^{i\omega x/\bar{c}},\ \hat{u}(x) = \frac{1}{\bar{\rho}\bar{c}}\left(\hat{f}e^{-i\omega x/\bar{c}} - \hat{g}e^{i\omega x/\bar{c}}\right) \tag{2.1}$$

If the chamber has one end open (open to the atmosphere or attached to a large plenum) and one end closed, the frequency ω of the plane wave is

$$\omega_n = \frac{(2n-1)\pi\bar{c}}{2l} \tag{2.2}$$

If the duct is not uniform in diameter, it can be first divided into sections and then the previous analysis performed section by section. Poinsot et al. (1987) applied this method using a transfer matrix, where a combustor was first divided into many sections and then each section was assumed to have uniform properties. The computed frequencies found by this method matched the experimentally measured frequencies.

Other experiments have shown the validity of this technique in other combustor configurations. Samaniego (1993) examined combustion instability in a side-dump combustor. The self excited frequency (400-600Hz) measured from the experiment is reasonably close to the quarter-wave mode of the combustor (550-700 Hz). In another instance, Pun et al. (2003) observed that the frequency of the pressure oscillation of a landfill gas flare (for one of the largest flares in the country) was excited at the quarter-wave mode.

The one dimensional model is also important because it introduces key concepts, although the direct analysis is not applicable for annular combustors where the longest combustor dimension is typically the circumference. The 1-D model analysis was extended to annular and cylindrical geometries by Culick and Yang (1995) to:

$$p' = \sum_{l,m,n} A_{lmn} J_m\left(k_{rmn} r\right)\cos\left(m\theta + \gamma_{lmn}\right)\cos\left(k_{zl} z\right)e^{j\varpi_{lmn}t} \tag{2.3}$$

where l, m, and n are integers, J_m is the Bessel function of the first kind of order m, L is the chamber length, k_{rmn} is the wave number in the radial direction; γ_{lmn} is the wave number in the azimuthal direction; k_{zl} is the wave number in the longitudinal direction which satisfies $k_{zl}\ L=l\pi$. The estimated frequencies of the oscillation obtained from the above equation lie within 10-15% of the frequencies observed in the experiments (Culick, 2001). Unfortunately, this equation doesn't specify which frequency will be excited most and it doesn't predict the amplitude of the oscillation observed in the experiment. Dowling and Morgan (2005) and Bellows et al. (2006) introduced nonlinear modifications so as to predict the amplitude of the resulting cycle limit.

Chamber acoustic property analysis is an analysis technique that has been applied to reduce system oscillations. Acoustic oscillation can be eliminated if the dissipation of acoustic waves within the combustor is increased sufficiently through the introduction of acoustic absorbers, such as perforated plates and Helmholtz resonators, and this method provides direction to the type and location of needed damping.

2.1.2 Equivalence Ratio Fluctuation

Equivalence ratio fluctuation is a source factor for heat-release fluctuations. There are two possible ways that equivalence ratio fluctuation can be created. One is through incomplete mixing of the fuel and air, typically due to premixing system inefficiency. The other common cause is mass flow fluctuations in the fuel and/or air supply systems. This can be caused by acoustic waves propagating upstream and perturbing, thereby generating the equivalence ratio fluctuations.

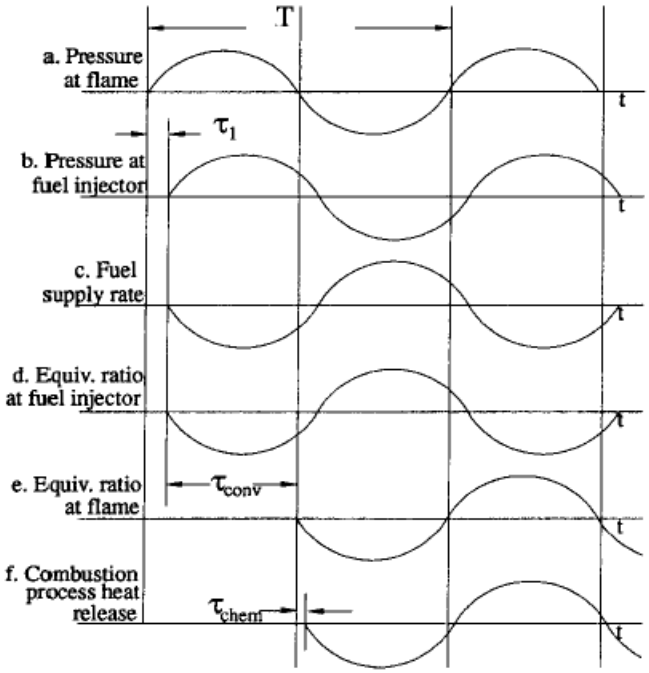

Figure2.2 An equivalence ratio perturbations driven instability

Source: Lieuwen et al., 1998; a qualitative description of the manner in which equivalence ratio perturbations drive an instability in LNGT with a non-choked fuel injector

Lieuwen et al. (1998) presented a theoretical model of combustion instabilities in low NOx gas turbines that accounted for equivalence ratio fluctuations. It showed that the instabilities may be caused by interactions of combustor pressure oscillations with the reactants' supply rates, producing equivalence ratio perturbation in the inlet duct. This heat release fluctuation and the equivalence ratio fluctuation can form a feedback loop and drive the amplitude increases seen in combustion instability. Kang (2006) measured the response behavior of a non-premixed jet flame with acoustic perturbation and showed that the degree of mixing (and hence the local equivalence ratio) is affected by excitation frequency and the response is different for each frequency. Modulating the fuel/air mixing with high speed valves based on microphone measurement of the acoustics in fuel

feed lines has been widely used as a means of feedback control to reduce combustion instability (Dowling and Morgans, 2005). Another validation of the effect of equivalence ratio fluctuations was seen in a Rolls-Royce (Scarinci et al., 2005) study that examined a variety of candidate-injector configurations. The study showed that pressure fluctuation was reduced up to 92% in the combustion chamber when the injection-combustion scheme was tuned to maximize mixing time.

2.1.3 Naturally-occurring and Forcing-induced Coherent Flow Structures

Coherent flow structures, usually vortices, have been shown to interact with combustion in different ways. The roll-up of the mixing layer between the reactants and hot products can lead to the formation of large scale vortices that have combustion layers embedded in them. The combustion may be enhanced at certain locations by increased turbulence associated with vortex development or the vortex may retard combustion by distorting the flame surface in unfavorable ways. The transient nature of combustion can generate acoustic noise which can then coalesce into an acoustic field that will in turn affect the generation and convection of the combustion layers. In general, coherent flow structures can be a major factor inducing combustion instability.

The general idea of periodic combustion associated with unstable shear layers was first independently reported by Kaskan and Noreen (1954) and Rogers and Marble (1956). In particular, the latter work, discussing premixed gaseous fuel and air flowing past a flame holder, proposed that delayed periodic combustion in shed vortices can drive an acoustic field. Poinsot et al. (1987) measured the C_2 emission of propane-air flame with Schlieren images in a dump combustor. They showed that the phase relationship between the heat release (C_2 emission) and the pressure oscillation was determined by time delays due to vortex formation, convection and combustion. Gutmark et al. (1989) measured the effects of vortex interaction and forcing frequency for a propane diffusion

flame with OH-PLIF. They observed that there was a close similarity between the nonreactive and reactive mixing layer large-scale structures.

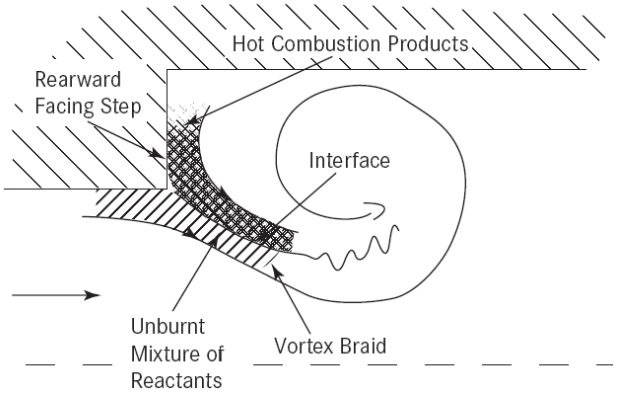

Figure2.3 Vortex roll-up in a dump combustor

Source: Schadow and Gutmark, 1992

For forced coherent flow structures, the general conclusion of those studies was that the frequency of vortex rollup can lock onto the frequency of a sound field if the amplitude of the acoustic oscillation is large enough and its frequency is sufficiently close to the natural frequency of vortex shedding (Keller, 1995). This phenomenon is often referred to as Lock-on. Gutmark et al. (1989) measured combustion dynamics of an acoustically excited flame at the preferred mode of an air jet and found that the combustion was initiated at the circumference of large scale structures. These vortices were then convected downstream as the flame burned inward towards the vortex core. Measurements with ionization probes showed that heat was released periodically due to these convecting vortices. Birbaud et.al (2006) reported such coupling on a conical laminar flame. The velocity field they measured responded differently depending on the Strouhal Number (St) of the acoustic perturbation (which came from the upstream

direction); when St <1, the response consisted of a convective wave. Detailed reviews about shear layer flow instabilities associated with jets, wakes, and mixing layers and the role of large-scale structures as the source for periodic heat release were given by Schadow and Gutmark (1992) and Coats (1996).

2.2 Models For Premixed Combustion Instability

Typical combustion instabilities are the result of one of several physical instability mechanisms, either thermo-acoustic, Darrieus-Landau, or thermal-diffusive. Models for these instabilities are developed independently, although they usually interact with each other and the type which is dominant can change across the operating range of a device. In this chapter, a general introduction of the models for these three types of instabilities is given with focus on thermo-acoustic instability.

2.2.1 Rayleigh Criterion

The condition under which the heat transfer amplifies or dumps acoustic energy was firstly stated by Lord Rayleigh (1945). The statement is:

> "If heat be communicated to, and abstracted from, a mass of air vibrating (for example) in a cylinder bounded by a piston, the effect produced will depend upon the phase of the vibration at which the transfer of heat takes place. If heat be given to the air at the moment of greatest condensation, or be taken from it at the moment of greatest rarefaction, the vibration will be encouraged. On the other hand, if heat be given at the moment of greatest rarefaction, or abstracted at the moment of greatest condensation, the vibration will be discouraged."

This criterion was reformulated by Putnam (1964), known as the Rayleigh integral, to define conditions of instability amplification:

$$\frac{1}{T}\int_0^T p'q'dt \succ 0 \qquad (2.4)$$

Where, p' and q' are pressure and heat release oscillation and T is time.

Chu (1956) incorporated the effect of boundary condition and derived the acoustic energy equation (2.5). We can see that acoustic disturbances grow in magnitude if their energy gain (the first term on the RHS) from combustion exceeds the energy losses across boundaries (the second term on the RHS). Equation 2.6 is a generalized form of Rayleigh criterion. In the equation, γ is the ratio of specific heats, c is the speed of sound, u is velocity fluctuation, s is the area, and V is the volume.

$$\frac{\partial}{\partial t}\int_V \left(\frac{1}{2}\bar{\rho}u^2 + \frac{1}{2}\frac{p'^2}{\overline{\rho c}}\right)dV = \int_V \frac{(\gamma-1)p'q}{\overline{\rho c}^2}dV - \int_S p'u.dS \tag{2.5}$$

$$\int_V \frac{(\gamma-1)p'q}{\overline{\rho c}^2}dV \succ \int_S p'u.dS \tag{2.6}$$

Culick (1976) provided an explicit formulation of the criterion so that it can be accommodated in a general analysis of the pressure oscillation in combustion chambers. The change of energy in one period was derived as follows:

$$\Delta\varepsilon_n(t) = (\gamma-1)\frac{\omega_n^2}{E_n^2}\int dV \int_t^{t+\tau_n} \frac{p_n}{\bar{p}}\frac{Q'}{\bar{p}}dt \tag{2.8}$$

Here, n denotes different modes of the acoustic oscillation, τ is a cycle of oscillation, and ε is energy. If the fluctuating heat release rate coincides with those of the fluctuating pressure or they are in phase, $\Delta\varepsilon_n(t)$ is positive, and heat addition tends to drive the nth mode.

Experimentally, Rayleigh Index can be obtained if the given pressure oscillation and heat release distribution are known. (Rayleigh index generally refers to the left hand side of eq. 2.4 and eq. 2.6.) The pressure oscillation can be monitored by a pressure transducer or microphone while the measurement of heat release is more challenging. The measurement techniques for assessing heat release, namely, chemiluminescence and fluorescence, will be addressed later.

Poinsot et al. (1987) performed experiments on a multiple-flame-holder dump combustor. The heat release was assumed to correspond to the level C_2 light emission. The authors showed that global Rayleigh index for the cavity was satisfied and that simple C_2 chemiluminescence was sufficient for this geometry. Pun (2001) compared the Rayleigh index distribution of two kinds of flames, an aerodynamically stabilized flame and a bluff-body stabilized flame. It was shown that the bluff-body stabilized flame is less sensitive to chamber acoustic excitation due to the flames ability to anchor a surface. This conclusion is consistent with that obtained from flame response function analysis. Venkataraman et al. (1999) and Lee and Santavicca (2003) measured CH chemiluminescence and computed the spatial Rayleigh index using an Abel transformation. Their results showed one positive region and one negative region in the Rayleigh Index map. The damping and gain regions in Rayleigh index were compared to the recirculation zones in the dump. Kang et al. (2007) measured the Rayleigh Index distribution of the swirl burner and observed toroidal structures in the Rayleigh Index. Kang's work provides the effective diagnostic method. However, the mechanism inside the phenomena was not investigated in detail. The current thesis continues that work to examine the toroidal structure and the combustion dynamics of the low swirl-stabilized flame.

2.2.2 The Darrieus-Landau Instability

The Darrieus-Landau instability is often called hydrodynamic instability. In purely theoretical analysis, Darrieus (1938) and Landau (1944) predicted independently that planar deflagrations are unconditionally unstable (Matalon, 2007). The Darrieus-Landau theory assumes that the flame is infinitesimally thin and propagates normal to itself at a constant speed S_L relative to the cold unburned gas. Within this framework, the linear stability of a planar flame yields

$$\omega = S_L k \omega_{DL}\,,\ \omega_{DL} \equiv \frac{-\sigma + \sqrt{\sigma^3 + \sigma^2 - \sigma}}{\sigma + 1} \tag{2.9}$$

where ω is the growth rate, S_L is the laminar flame speed, k is the transverse wave number, and $\sigma \equiv \rho_u/\rho_b$ is the unburned-to-burned density ratio. From this equation, the growth rate $\omega > 0$ for all wave numbers k as, for most combustion, $\sigma > 1$ (exothermic chemical reaction). Also, ω increases with increasing σ and vanishes as $\sigma \rightarrow 1$. Figure2.4 is an illustration of Darrieus-Landau instability by Clanet and Searby (1998).

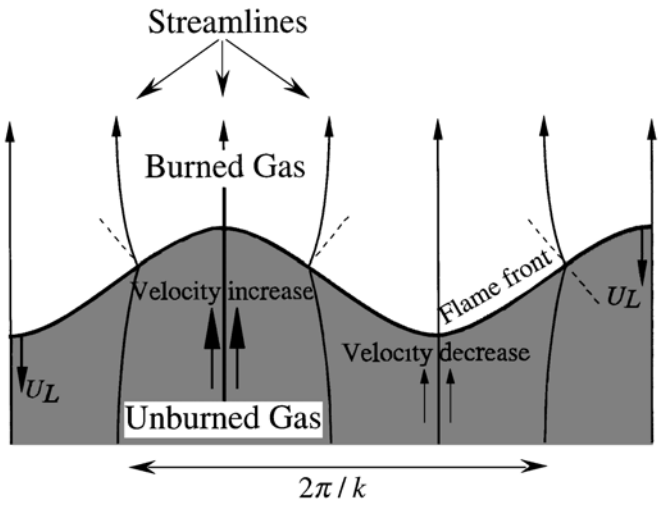

Figure 2.4 Deviation of flow lines leading to the DL instabiltiy

Source: Clanet and Searby, 1998

The extended form of Eq. 2.9 accounting for gravitational forces by Landau is

$$\omega = \frac{-\sigma + \sqrt{\left(\sigma^3 + \sigma^2 - \sigma\right) - \left(\sigma^2 - 1\right)\left(g/S_L^2 k\right)}}{\sigma + 1} S_L k \tag{2.10}$$

where g is the gravitational acceleration. For a planar flame in an upward uniform flow, corresponding to downward propagation ($g>0$), disturbances with wavelength $\lambda \succ 2\pi\sigma S_L^2/g$ are damped out by gravitational forces. Gravity, therefore, acts to stabilize

the long wavelength disturbances, and its influence is over a wider range of wavelengths for slow flames. For upward propagation, gravity acts to further destabilize the flame.

Subsequent work on hydrodynamic instability was aimed at correcting the DL theory for short-wave perturbations by taking the flame structure into consideration. Specifically, Markstein (1964) incorporated the effects of finite flame thickness by relating the flame speed to the local curvature of the flame front as in Eq. 2.11. Here the constant ℓ, which is of the order of flame thickness, is called the Markstein length. K is the flame stretch. Linear stability analysis shows that the Markstein theory yields stabilization of short-wave perturbations, which explains the existence of small scale planar flame fronts.

$$S_f = S_L - \ell K \tag{2.11}$$

Matalon and Matkowsky (1984) derived a correction to the DL equation and clarified the role of diffusion on flame stability. Thermal diffusion, which tends to smooth out temperature difference, always has a stabilizing influence.

2.2.3 Thermal Diffusive Instability

Another common instability for premixed flame is thermal–diffusive instability. Thermal-diffusive instability arises in flames as a result of the imbalance between the thermal and mass diffusion, i.e. for Lewis number differing from unity, $Le \neq 1$. There are two modes of thermal-diffusive instability, cellular and pulsating, which respectively occur for $Le < 1$ and $Le > 1$(Williams, 1985; Wang, 2007).

For Le<1, the effect of mass diffusion is stronger than that of heat conduction such that the convex section of the flame front becomes stronger and propagates faster, while the concave section weakens and propagates slower, leading to a cellular flame front. For Le>1, the effect is opposite and cellularly stable as in Figure 2.5 (Law, 2006). But when Le>1, the pulsating instability may occur.

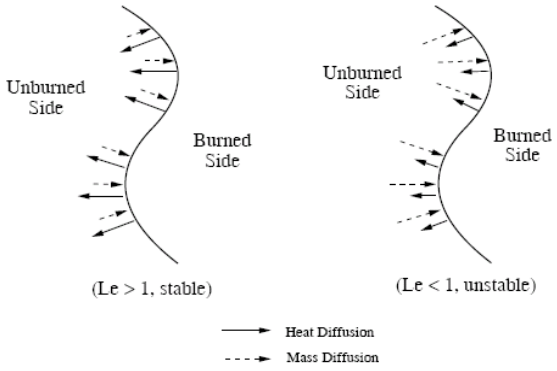

Figure2.5 Schematic of cellular instability

Source: Law, 2006

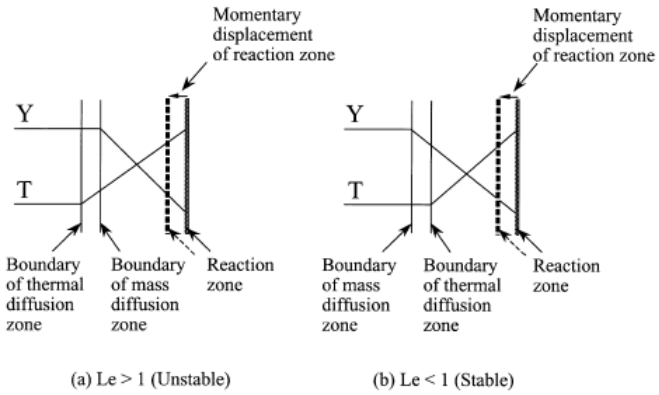

Figure2.6 Illustration of pulsating instability

Source: Wang, 2007

Figure 2.6 is the pulsating instability (Wang, 2007). For Le<1, if the reaction zone is positively perturbed with respect to the flame front, upstream heat conduction is increased by a larger extent than mass diffusion into the reaction zone. Consequently, the flame is weakened and the reaction zone relaxes back to its original position. A negative perturbation strengthens the flame and leads it back to the original position. However, for

Le>1, a positive perturbation will strengthen the flame and the reaction zone tends to outrun the flame front. At the same time, the flame is also bounded by the finite thickness of the preheat zone. As a consequence, the behavior of pulsating starts.

Barenblatt *et al.* (1962) (Wang, 2007) performed a linear analysis for the cellular mode of the thermal-diffusive instability in a planar flame subject to long-wave perturbations, and derived the dispersion relation:

$$\sigma = D_{\text{th}}\left[\tfrac{1}{2}\beta(1-Le)-1\right]k^2 \qquad (2.13)$$

It is seen that for $Le < Le_c$ (critical Lewis Number) = $1 - 2/\beta$, σ is positive and the flame is unstable to any perturbation. The stability boundary Le_c is slightly less than unity. This shifts the stability boundary for Le from unity to a slightly smaller value. Subsequently, Sivashinsky (1977) incorporated the relaxation effects of short-wave perturbations as

$$\sigma = D_{\text{th}}\left[\tfrac{1}{2}\beta(1-Le)-1\right]k^2 - 4D_{\text{th}}\ell_D^2 k^4 \qquad (2.14)$$

Where D_{th} is the thermal diffusivity of the mixture, l_D is the diffusive length. Thus, when the flame is unstable, i.e. $Le < Le_c$, there exists a critical wave number k_c that corresponds to the fastest growing mode of the perturbation. Joulin and Clavin (1979) extended Sivashinsky's theory by considering the effect of heat loss. They found that at the cellular flame boundary Le_c increases with increasing heat loss and approaches unity at the flame extinction limit.

Current work focuses on the combustion of methane and air. The Lewis number of the mixture of methane and air is approximately unity. Therefore, thermal-diffusive instability has not been examined in the current work. However, these instabilities must be considered while studying thermoacoustic instability with different fuels and while studying the effect of thermoacoustic instability on fine flame structure (Lee et al., 1995; Law and Sung, 2000).

2.3 Measurement Techniques

Combustion instability is a process where combustion (heat release fluctuation), pressure oscillation and velocity oscillation are all coupled. Of particular importance are the measurements of the fluctuations in pressure, heat release and flame structure. Spatially resolved temperature, velocity, and combustion species are needed. In this part the current state of the measurement techniques used in the field of combustion instability research will be reviewed.

2.3.1 Visualization of Combustion

Before the application of laser diagnostics in combustion, shadowgraph, schlieren and smoke were probably the three dominant methods. Shadowgraph and schlieren are quite similar and reveal non-uniformities in transparent media. Since the combustion field is not uniform in density, the flame shape can be recorded. Poinsot et al. (1987) reported the interaction of combustion and vortex convection with spark schlieren. The spark is given off by a laser source. Shadowgraph and schlieren are currently widely used in supersonic combustion where the density gradient is very sharp. Smoke is another old technique for flow field visualization and still used. Kornilov et al. (2007) compared cold flow and reacting flow field with TiO_2 smoke. The vortex structures in cold flow disappeared when combustion occurred.

For combustion instability study, instantaneous combustion (phase resolved) and heat release fluctuation are wanted as instability tends to occur when combustion and the pressure oscillation are in phase. Instead of the overall luminescence of the combustion field, that of one particular species is now widely used. For example, OH, CH, and HCO are often employed for hydrocarbon combustion (Wolfrum, 1998; Hassel and Linow, 2000; Hardalupaset al, 2004; Kohse-Hoimghaus et al., 2005).

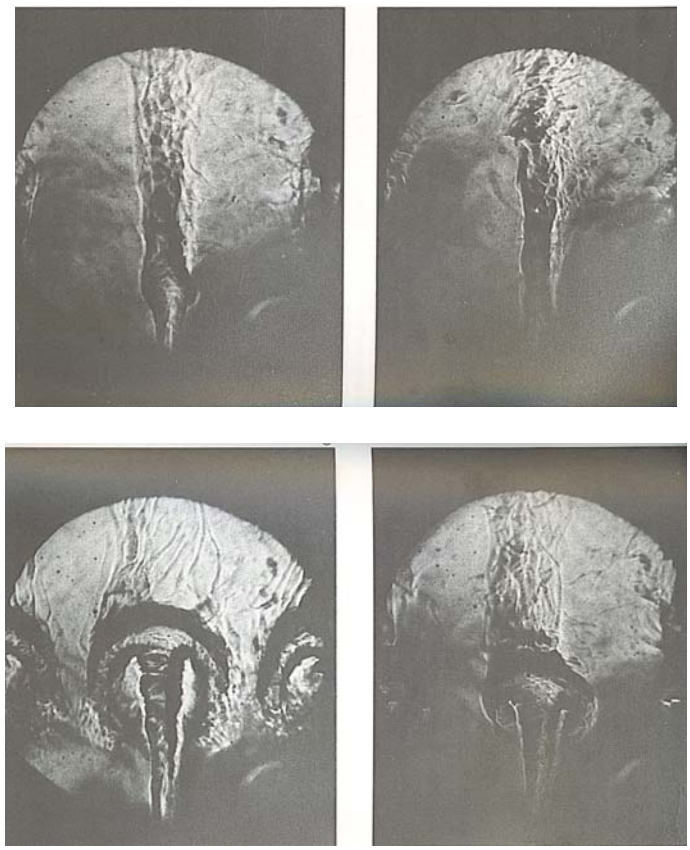

Figure 2.7 Spark-schlieren photographs of vortex-combustion interaction

Source: Poinsot et al., 1987

To capture the species concentration, there are two widely used techniques: chemiluminescence and laser induced fluorescence (LIF). Chemiluminescence is the radiative emission given off by chemically excited reactive species and serves as a good indicator of global heat release rate in premixed hydrocarbon flames. It doesn't need excitation from laser source, so the experimental implementation is simple. However, it is a line-of-sight technique with limited capability for resolving small-scale structures. Abel transformation, also called 'onion peeling' can be applied to get the two dimensional image by assuming symmetry. Due to its convenience, chemiluminescence has been widely used in combustion (Samaniego et al., 1993; Venkataraman et al., 1999; Lee and

Santavicca 2003; Hardalupas and Orain, 2004; Taupin et al., 2007). Kojima et al. (2005) measured OH, CH and C_2 chemiluminescence of a premixed laminar methane-air flame. The images of OH and CH show almost identical distribution in terms of shapes, locations and intensities while C_2 shows apparent differences from the others.

Planar laser induced fluorescence (PLIF) was introduced into combustion in the 1970's. It has been used for combustion diagnostics and to characterize gas and liquid phase fluid flow situations. PLIF measurement involves imaging the fluorescence signal from a thin sheet of flame, excited by a laser beam, and hence is able to achieve a high degree of spatial resolution (Battles and Hanson, 1995, Locke et al. 1995). Giezendanner et al. (2003) measured planar laser-induced fluorescence spectroscopy of OH, CH, and H_2CO for a turbulent diffusion flame. Qualitative correlations among the distributions of the species were found. The primary drawback of PLIF is that it requires a laser source, making the technique more expensive and harder to implement than chemiluminescence.

To get an image of the combustion, it requires optical access, therefore most experiments are limited to use in the laboratory. One of the motivations of the current work is to test the low swirl burner for its application in industry.

2.3.2 Measurement of Velocity

There are several ways to measure the velocity field including hot wire anemometry, laser doppler velocimetry, particle image velocimetry etc. Hot wire anemometry (HWA) is an old technique to measure instantaneous fluid velocity (Kulsheimer and Buchner, 2002). The technique depends on the convective heat loss to the surrounding fluid from an electrically heated sensing element or probe. If only the fluid velocity varies, then the heat loss can be interpreted as a measure of that variable. Hot wire anemometry can only get the velocity point by point. And it perturbs the flow field as it requires a sensing probe.

Laser Doppler Velocimetry (LDV) is a very accurate technique for measuring the direction and speed of fluids. In its simplest form, LDV crosses two beams of collimated, monochromatic, and coherent laser light in the flow of the fluid being measured, which are usually obtained by splitting a single beam. The two beams are made to intersect at their waists (the focal point of a laser beam), where they interfere and generate a set of straight fringes. The sensor is then aligned to the flow such that the fringes are perpendicular to the flow direction. As particles pass through the fringes, they reflect light and therefore, the local velocity can be calculated from the frequency and the width of the fringes. Aldredge and Killingsworth (2004) measured flow field of a Taylor-Couette burner and observed characteristic flow field of the different stages of flame propagation.

The drawback of LDV for combustion measurement is that it needs seeding of the particles which is an intruder to the velocity field. In addition, LDV cannot get accurate measurement for the products region because of insufficiently high-seeding particle volume density resulting from gas expansion across the flame (Hassel and Linow, 2000).

Particle Image Velocimetry (PIV) is a new technology for flow field visualization. Compared with LDV, which only measures the velocity of a point, PIV can give a velocity field. Particles are seeded into the fluid, and then the motion of particles is recorded in several frames. It is then possible to calculate the displacement vector for particles. This is converted to a velocity using the time between image exposures. PIV is now a very useful tool for cold flows. In terms of its application in combustion, it is still rare as it requires particle seeding. Littlejohn and Cheng (2007) used PIV for the low swirl burner. Analysis of the velocity statistics shows that the non-reacting and reacting flow fields of the burner exhibit similar features for hydrocarbon and hydrogen combustion.

2.3.3 Measurement of Temperature and Pressure

Thermal couple is a traditional way to get temperature. Often only the temperature of the reactants or the temperature at the combustor exit is measured. The inlet temperature was shown to affect the instability mode and amplitude (Huang et al., 2003).

To get the temperature in the combustion region is still a difficult task. Recently planar laser induced fluorescence has developed to do temperature measurement as well. Temperature is related to the ratio of fluorescence signals from the laser-excited level and from another higher level coupled to the laser-excited level through collision. This technique requires laser equipment and detailed knowledge of the collision knowledge (Chang et al., 1990). Seitzman et al. (1985) presented instantaneous temperature field measurements using single laser shot PLIF images of NO, while Gutmark et al. (1989) used OH-PLIF.

Pressure measurement is a basic way to characterize unstable combustion. Compared with measurement of all the above parameters, pressure measurement is quite simple. It is typically made using high frequency response piezoelectric pressure transducers. Microphones are sometimes used as well.

2.4 Swirl Combustors

The use of swirl stabilized combustion is widespread, including coal combustors, gas turbine combustors, and internal combustion engines. Swirl is adopted to stabilize the flame and reduce emission. Significantly different combustion characteristics have been observed by altering the swirl configuration and the swirl number (Durbin and Ballal, 1994; Syred and Beer, 1972; Syred, 2006). When the swirl number is high enough, it will create central toroidal recirculation zones. These recirculation zones circulate heat and active chemical species to the root of the flame and allow flame stabilization and flame

establishment to occur in regions of relative low velocity where flow and flame speed can be matched.

Typically, there are two methods to generate swirling. One way is to tangentially inject air to the combustor and is often called air-jet swirler. The air flow with tangential velocity then mixes with the fuel. This method has been commonly used in industry. The second way is to install a swirler with tangential blades (Roux et al., 2005). When air or premixed reactants pass through the blades, a swirling flow is generated.

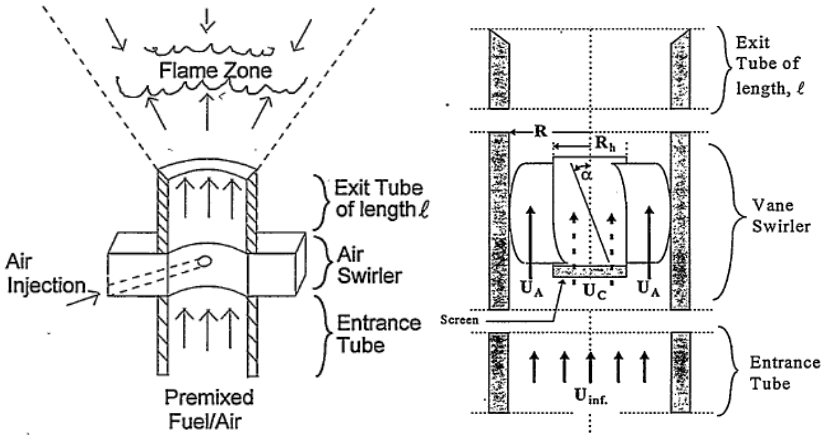

Figure 2.8 Two ways for generation of swirl

Source: Cheng et al., 2000

Normally, when swirl number exceeds 0.6-0.7, processing vortex core (PVC) and central recirculation zone (CRZ) occur (Taupin et al., 2007). Figure 2.9 shows the flow field and the location of the PVC of a swirl burner with swirl number 1.57. It is difficult to analyze the role of PVC and its influence on instability. Flows in the CRZ region are characterized by high shear stress and high turbulence intensity. These properties promote the mixing and increase the operation range. Stronger CRZs are less susceptible

to deformation by pressure oscillation, but they also make the system prone to combustion instabilities. The swirling flow also affects the flame size, flame shape, temperature distribution, and heat release distribution. The radial distribution of swirl and jet axial momentum plays very important roles on the flame thermal characteristics. Gupta et al. (2001) showed different combustion characteristics when the tangential air is injected clock wise and anti-clock wise.

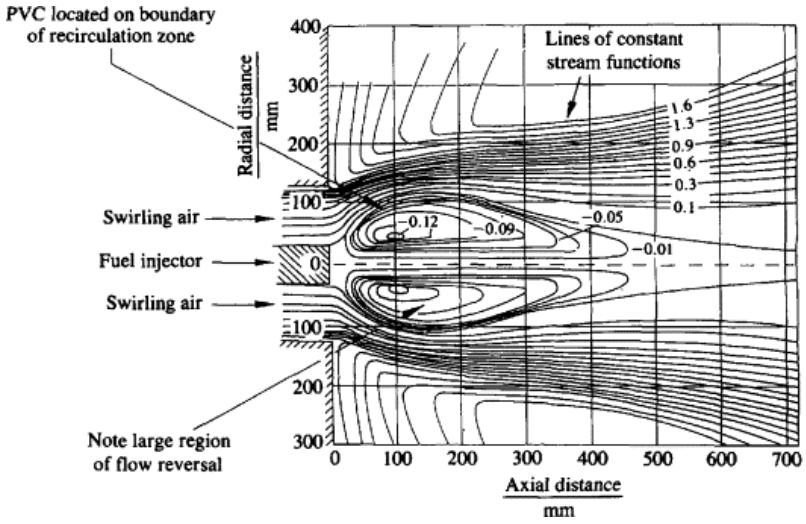

Figure 2.9 Stream line and PVC location of a swirl burner swirl number 1.57

Source: Chigier and Beer, 1964

Remedial effects have been employed to inhibit the instability from PVC and CRZs so that they cannot interact with the downstream components. As reviewed by Syred (2006), a carefully shaped exhaust section can remove the CRZ and have the flame fill the furnace; an off centered furnace exhaust may eliminate the formation of PVC and change the acoustic resonance as well (Turrell et al, 2004); some use mini vortex generators to distort the generation of PVC.

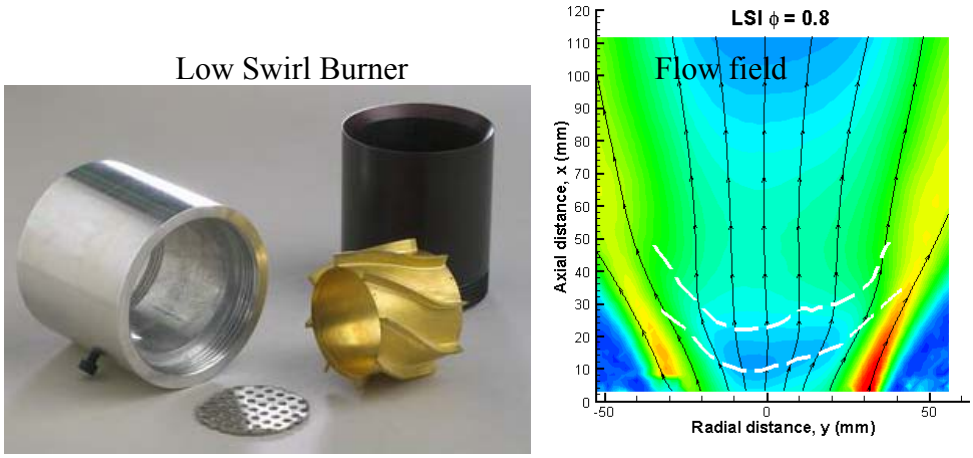

Figure 2.10 Low swirl burner by R.K.Cheng

The swirl burner for this work is a novel design by R.K. Cheng et al. (2000) and coworkers for premixed combustion (Figure 2.10). Premixed air and fuel pass through angled vanes before they get into the combustion chamber. The vanes introduce swirl which creates divergent flow field to stabilize flame. Hence, no CRZ is needed. Compared with the air-jet swirler, it is simple in geometry and less costly. The swirl number is adjustable and generally less than 0.6. Flow field measurements with Particle Image Velocimetry (PIV) showed that PVC and CRZ were not present near the burner exit (Cheng et al, 2006). The flow field also showed self-similarity as for conventional jet. The other important feature of the combustor is that it emits less than 2ppm of NOx. It is the only technology that can affordably reduce NOx emission to this near zero level. For this reason, this technology won the 2007 R&D 100 Award.

The low swirl burner has been commercialized in industry for heating and drying. Recently, it has received interest from gas turbine equipment manufacturers. This work focuses on the instability of this new generation of swirl burner. As reviewed, instability is a key problem in gas turbine industry.

CHAPTER 3

EXPERIMENTAL SYSTEM AND TECHNIQUES

The experimental system employed in this work consists of multiple components and subsystems. To systematically describe the experiment, individual subsystems are described separately in each section. The first section describes the experimental setup and unique features of the system including the acoustic chamber, swirl burner, and laser system. The second section introduces the PLIF diagnostic method and details the OH-PLIF technique, which is the major data collection tool for this work. The last section describes the experimental procedures and outlines the data analysis methodology.

3.1 Experimental System

Experimental investigation of combustion instability requires significant hardware and a complex arrangement. Figure 3.1 shows a schematic diagram of the gas flow through the system. Gas flow consists of a fuel supply, fuel/air mixer, burner, combustion-acoustics chamber, and exhaust. Flow rate of air is measured by the HASTINGS HFC-203A mass flow meter. Flow rate of fuel is measured by the LINDE 18C-202-4125 mass flow meter. The fuel and air are mixed before going to the chamber. The products are released from the adjustable exhaust valves.

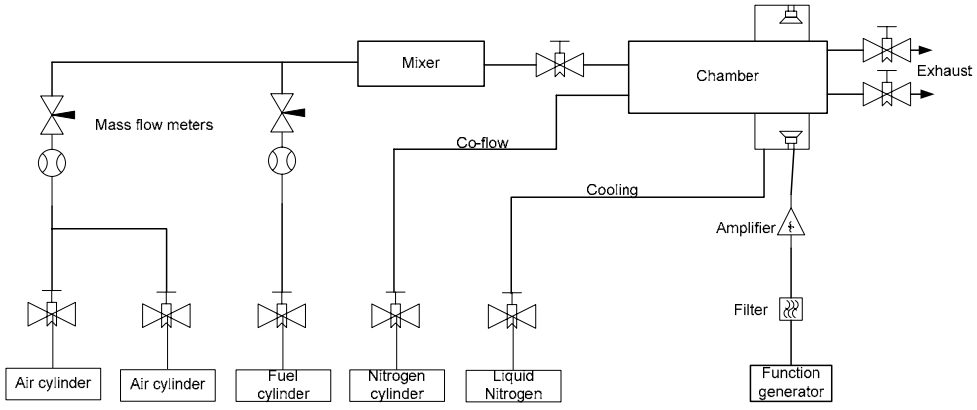

Figure 3.1 System flow schematic

3.1.1 Combustion-Acoustics Chamber

The combustion-acoustics chamber is made of several stainless steel sections that bolt together, including a vertical central section and a horizontal top that houses the loudspeakers, as shown in Figure 3.2. The inside diameter of the combustion chamber is about 30cm and the height is approximately 185cm.The bottom part of the chamber is equipped with four quartz windows to provide full optical access to the flame. The top of the chamber is acoustically closed and the exhaust has a variable restriction, enabling pressurized experiments. The chamber was tested with water up to 10 atmospheres and operation (to ensure safety) is limited to 5 atmospheres.

This chamber has several advantages for the study of combustion instability versus systems employed by most other researchers. First, it enables continuous elevated pressure operation. In many practical combustion systems, the mean pressure is much higher than one atmosphere and, therefore, it is important to study combustion instability and flame dynamics at elevated pressure conditions. Second, the chamber diameter is much bigger than that of the burner and flame. This eliminates the interaction of the flame and chamber wall as compared with smaller chamber (confined combustor) systems. In addition, the chamber geometry is quite different from that of traditional dump combustor systems. Dump combustor systems have been used in many combustion instability studies (Geoniem et al., 2002; Geoniem et al., 2005) but produce a limited range of phenomena. Third, the acoustic perturbation is driven from the downstream side of the chamber (and downstream of the burner), which distinguishes this work from many previous experiments where speakers are installed upstream of the burner and directly affect the fuel supply and mixing rather than isolating the in-chamber flow-flame-acoustics interactions as is done in the present system.

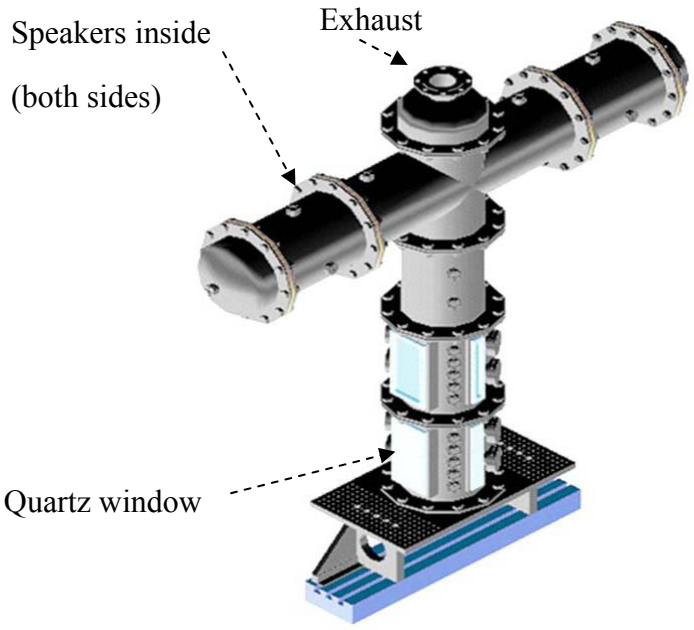

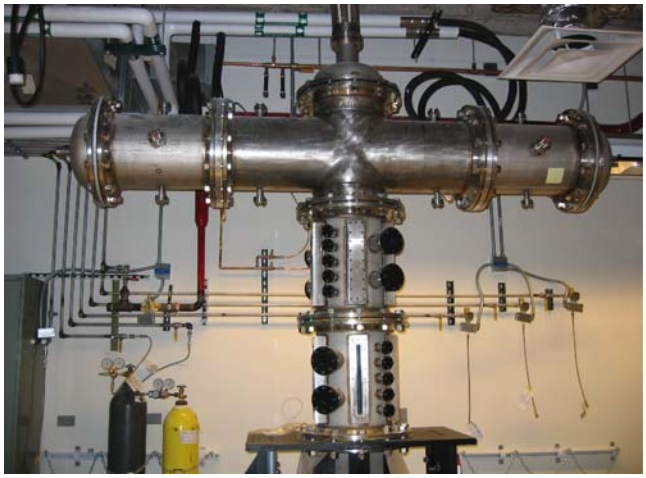

Figure 3.2 Acoustic chamber

To produce this type of driving and minimize the impact on fuel injection, the speakers are installed relatively far downstream, in the arms of the systems as viewed in Figure 3.2. Four speakers are installed and driven in-phase to generate the acoustic perturbation imposed on the flame. The symmetric design is used to balance the flow and the downstream length ensures that edge vortices generated due to the speaker motion do not interact with the flame. The speakers are powered by a 2000 W amplifier (Mackie M2600) and the signal is generated by a function generator (Wavetek 171) that provides a sine wave signal at different frequencies as the input.

During the experiment, the pressure oscillation in the chamber is monitored by a piezoelectric pressure transducer. While the pressure transducer gathers data at only a single point, the pressure wave is nearly uniform over the entire extent of the flame. This uniformity allows the single pressure reading to be applied at all flame spatial locations. To assess how much the wave varies across the flame, a transfer matrix analysis, a method commonly used in thermoacoustics (Swift, 2002), is applied. Figure 3.3 is the diagram for the transfer matrix evaluation. Eq. (3.1) shows the pressure fluctuations of the inlet and exit for a constant temperature duct.

$$\begin{bmatrix} p'_e \\ u_e \end{bmatrix} = \begin{bmatrix} \cos kx & \dfrac{-j\rho_0 c}{A}\sin kx \\ \dfrac{A}{jc}\sin kx & \cos kx \end{bmatrix} \begin{bmatrix} p'_i \\ u_i \end{bmatrix} \tag{3.1}$$

where p' is pressure fluctuation, u is the velocity fluctuation, subscript e means exit, i means inlet, k is the wave number, A is the area of the chamber cross section, and c is the sound speed.

Within the Eq. (3.1), two variables are known, p'_i from the pressure transducer and u_i at the bottom of the chamber from the nonslip boundary condition. From this, the pressure amplitude at the bottom of the chamber can be calculated. Table 3.1 lists the pressure amplitude variation between the two positions at different frequencies. At a low

frequency (37Hz), the difference is only 0.9%, while at higher frequency (110Hz), the difference is 9.1%. This qualifies the assumption of a uniform pressure field across the flame, but fundamentally, the pressure difference does increase dramatically with frequency.

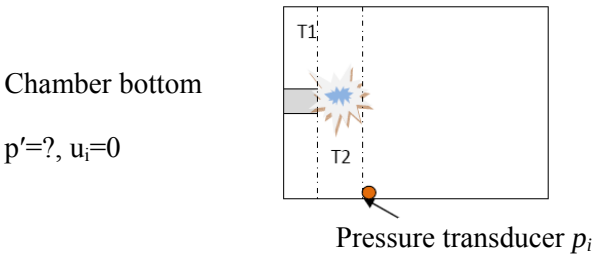

Figure 3.3 Compact chamber

Table 3.1 Pressure variation with frequency

f(Hz)	37	55	65	85	110
(Δp/p)%	0.9	2.1	2.9	5.1	9.1

3.1.2 Swirl Burner

The burner for the study of thermoacoustic coupling of the lean premixed flame is from Lawrence Berkeley National Lab as mentioned in chapter one. The burner has dimensions of 2.54cm ID and 6.5cm Height. Inside the burner a swirler is installed. Figure 3.4 is a schematic view of the burner and swirler. The swirler has a diameter of 2.54cm and the height is 1.4cm. It has 8 vanes on the outside. These vanes can be designed for different angles and numbers to adjust the intensity of the swirl. In addition, a screen, of different mesh number, can be placed in the center part to further adjust the swirl number.

As also reviewed in chapter 2, low-swirl is a unique method for stabilizing lean-burning, premixed combustion as the flame is stabilized by flow divergence, not through recirculation which is commonly seen in industrial high swirl burners. The low swirl burner produces a more stable turbulent flame (Cheng et al, 2006). The flow field also

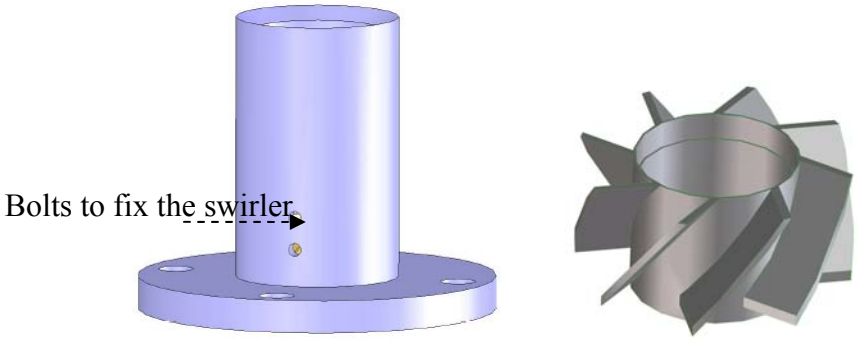

Figure 3.4 Schematic view of the burner and swirler

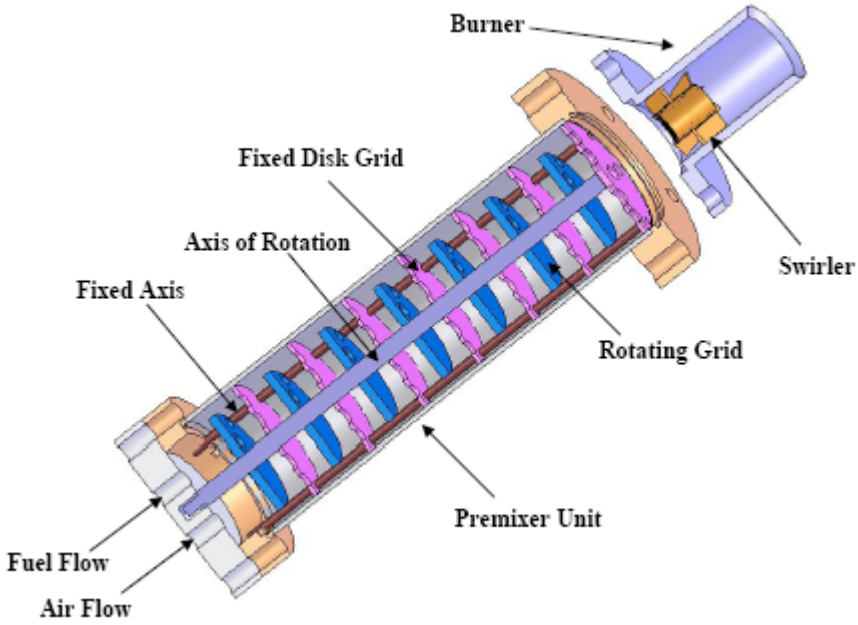

Figure 3.5 Schematic view of the mixer

showed self-similarity as for conventional jet. This type of swirler has been tested for furnaces and boilers showing reduced NOx emission, and been tested for different types of fuel including hydrogen mixtures and synthetic gases (Littlejohn and cheng, 2007).

3.1.3 Mixer

To enable both fully premixed and partially premixed experiments, a mixer was designed and fabricated as shown in figure 3.5. It is designed with a series of perforated plates where half of the plates are fixed and half can rotate. The mixer is 20cm long and the inside diameter is 4.8cm. The diameters of the disks are 4.0cm for rotating and 4.8cm for the fixed, respectively. There are four grid holes on each disk plate. The sizes of the grid holes are 0.5 and 0.6 cm. The idea is to set the alignment of the holes so as to get different degrees of mixing. When the holes in disks are in line, the least amount of mixing should be incurred. When the holes are misaligned 90 degree from each other, the greatest mixing is expected, which should be sufficient to produce fully premixed flow.

3.1.4 Laser System

The PLIF laser system consists of a pump laser, a dye laser and an optical frequency doubler. The pump laser is a high power Nd:YAG laser (Continuum Powerlite 9010). The YAG laser is capable to produce 1064 nm (infrared) or 532nm (green) beam. Thanks to its high power, Nd:YAG laser has been widely used for planar laser induced fluorescence experiments and particle image velocimetry experiments. The tunable dye laser (Continuum ND6000) uses Rodamine 590 as the dye to convert the 532nm beam to near 564nm. Rodamine 590 is mildly toxic and care must be taken when making the solution. In the final step, the beam from the dye laser is frequency doubled to a laser frequency which will excite the OH radical.

The system produces approximately 800mJ per pulse at 10Hz at 532 nm. The beam out of the dye laser, at 564 nm, drops in power to about 180mJ/pulse. The resultant doubled beam, at 282 nm, is approximately 27mJ/pulse.

The optical components employed for PLIF experiment include prisms, spherical and cylindrical lenses, and mirrors. The beam from the Doubler usually has some low frequency residuals (green and red beams). This portion is separated from the UV light by a Pellin-Broca prism. The combination of spherical and cylindrical lens is then used to produce a laser sheet having typical dimensions of 2 cm high by 200 micron thick at the image location. The direction of the beam is adjusted with mirrors.

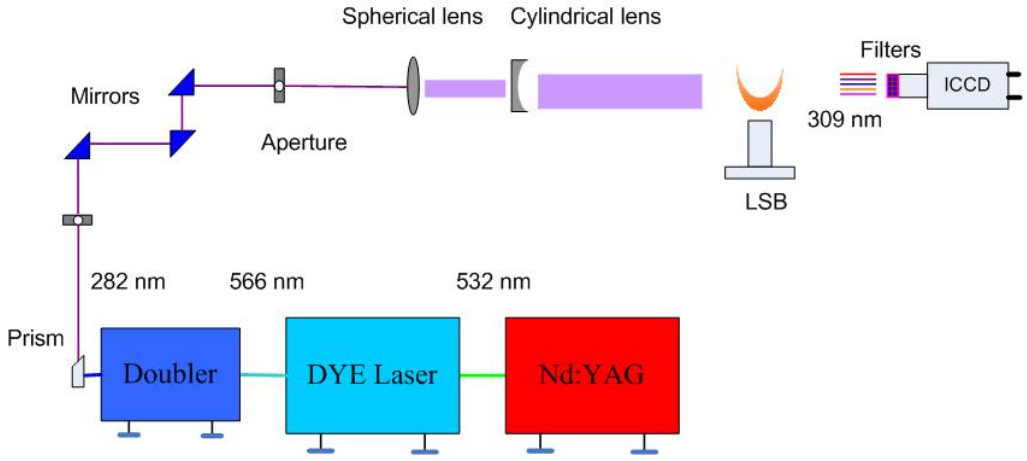

Figure 3.6 System for PLIF measurement

The laser beam passing the flame region has dimensions of 9.0 cm high by 300 to 500μm wide. The fluorescence from OH PLIF is collected at 90°from the laser sheet with a 105mm f/1.2 ultra violet (UV) lens attached to a Princeton Instruments intensified charge-coupled device (ICCD) camera. The field of view of the camera is around 10cm square and the resolution is 512×512 pixels. The electronic image intensifier for the camera is triggered synchronously with the laser pulse. A LEO (Lattice Eletro Optics) band pass filter (312.6F10-10) is attached in the ICCD camera to cut off all scattered light and to pass only the OH fluorescence in the 300-320 nm range. For PLIF measurement,

the gate time is usually 150 ns but for chemiluminescence measurement, the gate time is set as high as 200ms.

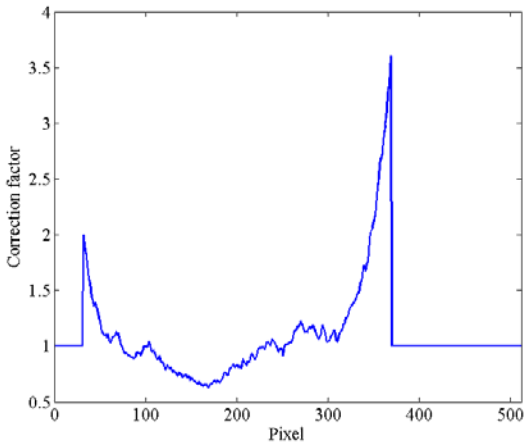

Figure 3.7 Correction factor along the center line

Ideally the laser beam sheet is uniform after expansion. But it is hard to be uniform in reality. Beam intensity is measured before the experiment with a special card which can give the fluorescence signal. According to the measured beam distribution, the correction matrix can be calculated. Figure 3.7 is the correction factor distribution along the center line of the flame.

3.2 OH-PLIF

3.2.1 General description of PLIF

The basic principal of the laser-induced fluorescence technique is that laser radiation is used to selectively excite an atomic or molecular species of interest to an upper-electronic state via a laser-absorption process (Eckbreth, 1996; Hassel and Linow, 2000). The excitation process is followed by the spontaneous emission of a photon when the excited atom or molecule decays back to a lower-energy level. The spontaneous

emission is referred to as fluorescence. Laser-induced fluorescence (LIF) can be used to make point measurements where a photomultiplier can be used as a detector, or it can be planar laser induced fluorescence (PLIF) where it provides spatial resolution by using laser beam sheet and ICCD camera.

OH planar laser-induced fluorescence is commonly used for imaging and characterizing combustion processes. There is good separation between its rovibronic lines and little spectral interference has been encountered for most of the combustion environments in which OH PLIF has been applied. OH PLIF has been shown to be a very effective two-dimensional visualization tool for examining flow uniformity and mixing.

Excitation of the OH radical is usually done via a weak transition of the A–X (1–0) band to avoid saturation and one monitors the combined fluorescence of A–X (0–0) and (1–1) bands at 305–330 nm. The process is well understood, the data evaluation is relatively straightforward and all of the spectral information needed is available.

Figure 3.8 is the OH spectrum from Hult et al. (2005). It shows that the excitation is quite narrow and has multiple peaks. The sharp response in the OH spectrum shows that choosing a right laser beam for excitation is critical. In reality, if the dye solution is too old, then the wavelength may be off and it affects the fluorescence signal. Figure 3.9 is the OH spectrum obtained in our experiment. Due to the operation range of the dye laser, only a small range of the wavelength was examined. It verifies that the OH fluorescence signal is sensitive to the UV beam wavelength.

When pressurized experiments are involved, the effect of pressure on OH PLIF signal has to be considered. Quantitative interpretations of linear laser induced fluorescence require accurate accounting of collision-induced phenomena. These phenomena, which include absorption line shape broadening, radiative trapping and collisional deactivation or quenching, can be severe at elevated pressure (Allen, 1995; Battles, 1995). Figure 3.10 is the measured OH fluorescence intensity of methane/air flame at various pressures and two locations above the burner by Katharina et al (1990).

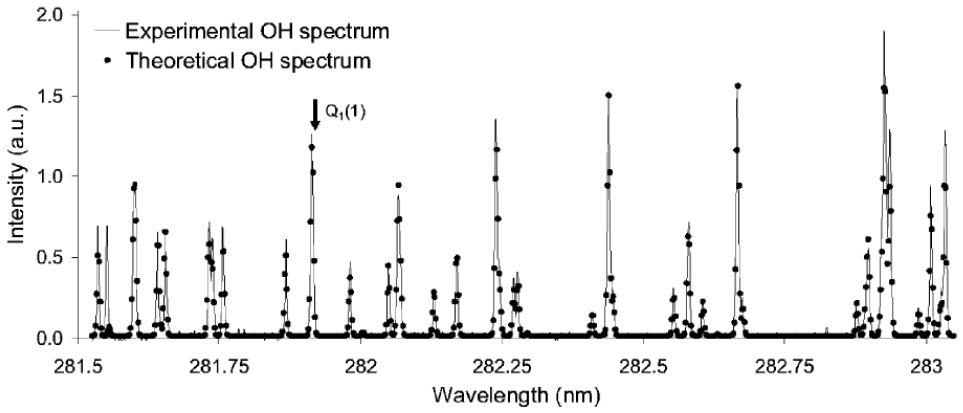

Figure 3.8 OH spectrum

Source: Hult, 2005

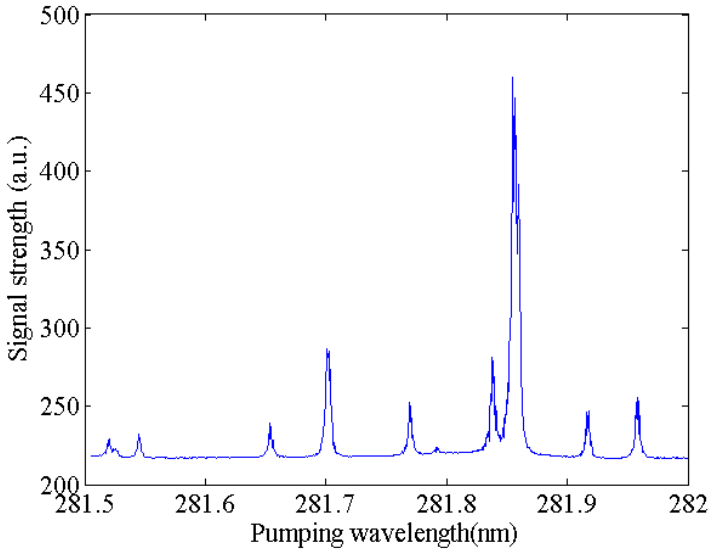

Figure 3.9 Measured OH spectrum

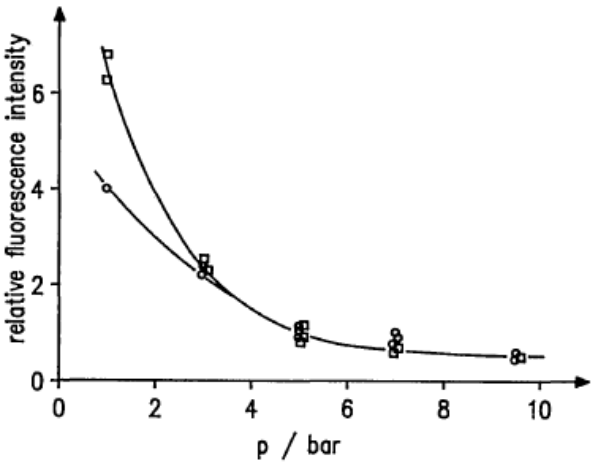

Figure 3.10 OH fluorescence intensity S_{21} vs pressure at 3mm (squares) and 6 mm (circles) above the burner surface

Source: Katharina et al., 1990

The OH fluorescence intensity is not linearly related with pressure. In addition, it changes at different locations in the flame region. In a word, OH fluorescence at higher pressures tends to be difficult and quantitative calibration of its relation to pressure is not available yet.

3.3 Experiment Procedure and Data Acquisition

The following steps outline the general procedures in conducting the combustion dynamics experiments.

1. Laser system check up

   Enable the water for laser cooling—turn on the power of the laser—turn on the dye pump—turn on the key switch when the LED changes from red to

green—operate the control box –shoot the laser and set it to program 1 to warm up for about 20 minutes

Measure the beam power from the Nd:YAG, Dye laser and the final UV beam

2. Optics alignment

   Maximize the power of the UV beam

   Check the pass of the beam and have it pass through the center of the burner

3. Setup gas flows

   Open the electric valve at the door. This valve controls all the electro-magnetic valves for the cylinders.

   Open the valves for the gas supply (Fuel, Oxidizer, co-flow, nitrogen for Camera, and cooling nitrogen for speakers).

   Set flow meters for the air and fuel to the right flow rates.

   Make sure the valves for air, nitrogen, and coflow are open and correctly connected. This experiment shares some lines with other experiment. It is important to check.

   Make sure the exhaust valves are open.

4. Turn on all the measurement equipments

   Pressure monitor: Oscilloscope, pressure transducer power supply

   Acoustic system: set the function generator to the right frequency, turn on the amplifier and the data box.

5. Beam profile calibration

   Use low power laser. Set delay time as 85μs

   Set camera gain to 250, and gate width to 100ns.

   Turn off the room light

   Allow laser sheet to impinge on fluorescent card and acquire the beam profile.

   Finally, cap the camera, turn on the room light, take the card out of the chamber and seal the window

6. Ignite the flame

   Have the fuel ignition valve closed. This is the valve on the chamber table.

   Loosen one of the small flanges on the combustion chamber which are close to the burner. And practice to stick the igniter into the chamber from the flange.

   Set the air flow rate by turning the knob. The reading from the meter has to be converted to slpm according to the table. Similarly set the fuel meter.

   Open the fuel valve on the chamber table and watch the readings of the fuel meter. Once the reading hits the required number, quickly open the flange on the chamber, stick the igniter in, and ignite. Waiting too long before igniting can be dangerous since too much fuel can accumulate in the chamber.

   If a flame could not be achieved with a couple of sparks, take out the igniter, shut off the fuel supply value, and turn on the exhaust fan to completely remove the fuel from the combustion chamber. Repeat the entire process until a flame is established.
7. Open the Nitrogen co-flow slowly.
8. Enforce acoustic perturbation
9. Turn off the light of the room
10. Shoot the laser and take the data

    Change the frequency of the acoustic forcing and repeat
11. End experiment

    Stop the laser.

    Turn off the camera and turn on the light

    Shut off the fuel supply once the flame is extinguished. Cut off the oxidizer supply followed by the other gases.

    Turn off all the measurement equipments and the valves.

    Cover the optics.

For each frequency, three to six sets of images are collected. The pressure signal is then extracted according to the image gating signal so that the corresponding pressure for each image is known. This enables the calculation of Rayleigh index maps of the flame.

Summary

This chapter gives a detailed description of the experimental system, including features of the unique acoustic chamber, the low swirl burner and the laser system. Acoustic field around the flame region was examined and the thermoacoustic method-transfer matrix was constructed. It qualifies our installation of the pressure transducer. The second section introduces the OH-PLIF diagnostic method which is the major tool for this work. Lastly it details the procedure for the experiment.

CHAPTER 4

RAYLEIGH INDEX MAP OF THE FLAME

This chapter builds on the work laid out in chapter 2 to extract new insights into the flame-acoustic coupling and the behavior of the underlying flow field. Rayleigh index is the primary indicator of interest and this chapter lays out the methodology for constructing the Rayleigh index map of the flame and assess the resulting data. The objective of this chapter is to study the structures observed in the Rayleigh index map.

4.1 Measurement and Calculation of Rayleigh Index Map

4.1.1 Pressure Signal and Flame Images

In the current experimental setup, there are no self-induced acoustics. Figure 4.1 shows the natural pressure oscillations in the chamber with combustion; the plot shows that there is only broad band noise and this only occurs at frequencies near zero. The lack of self-induced oscillations may be attributed to two reasons. First, the chamber is relatively big and has significant area for dissipation. As is known for thermoacoustic engines where oscillations are desired, there must be enough of a temperature gradient and appropriate geometry to produce resonance. Here the combustion process (most likely) does not release enough energy to create a large enough temperature gradient across the chamber to induce the thermoacoustic oscillation. The other possible reason is that the low swirl burner stabilizes the flame through flow divergence rather than through recirculation. Naturally induced oscillations are often observed in dump combustors or confined geometries which have strong recirculation zones.

As no natural acoustic resonance is present, the acoustics studied in this work are all imposed with speakers located at the far end of the chamber. Because of this, the frequency and the amplitude can be adjusted as desired. Figure 4.2 shows a pressure trace

with excitation. The imposed frequency is easily visible, as is the low frequency combustion-induced noise.

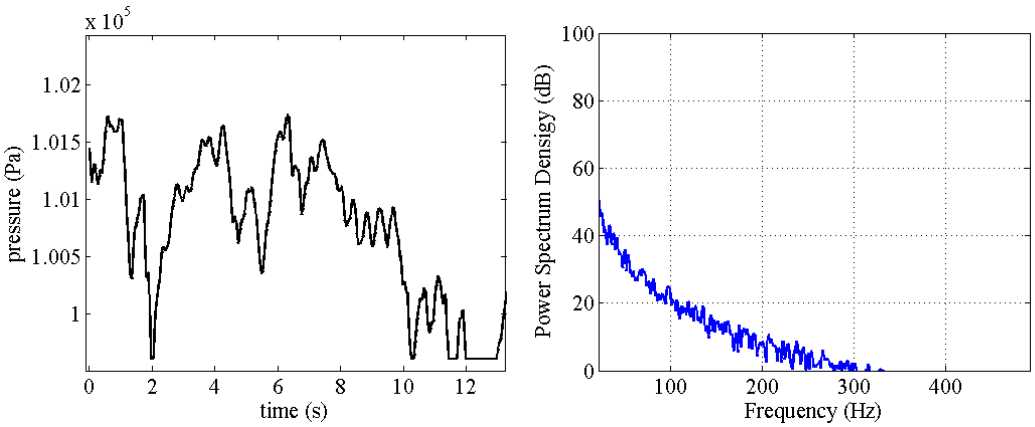

Figure 4.1 Pressure fluctuations and the power spectrum density without acoustic excitation

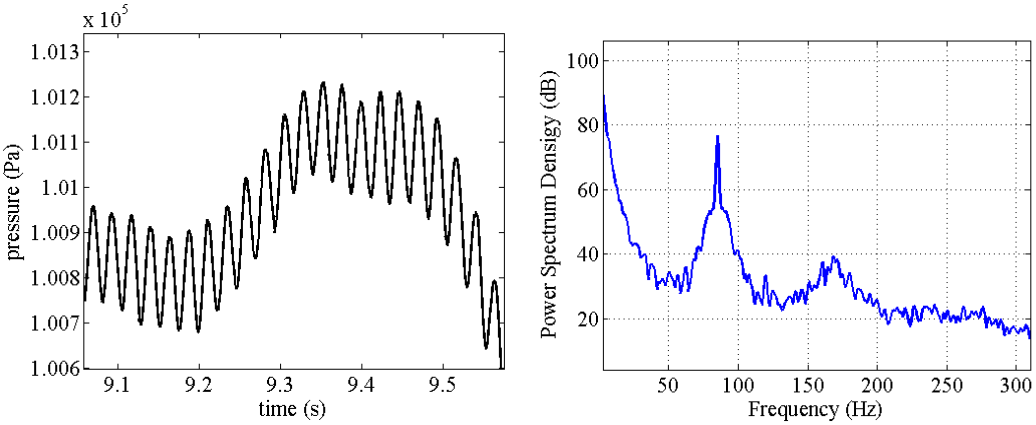

Figure 4.2 Pressure signal and power spectrum density at 85Hz excitation

Flame photography and imaging has been an important technique for the study of flame dynamics and provides significant information. In the experiment, different views of the lean premixed methane-air flame are captured with various imaging techniques. Figure 4.3(a) is the visible flame without any light filtering or laser excitation (as obtained by a normal camera). The blue flame is bowl shaped with a skewed bottom. It is blue because lean methane-air combustion produces no significant soot and only the 432 nm C-H swan band releases light (which is blue). The bowl shape is characteristic of the low swirl burner. Figure 4.3(b) is the instantaneous OH planar laser induced fluorescence image. The flame is highly curved and there are occasional pockets or islands in the flame front due to turbulence. Intense OH is present at the flame leading edge with lesser amounts in the product zone. Figure 4.3(c) is an image of the mean OH field, based on 900 instantaneous OH-PLIF images. The PLIF images are corrected for the span-wise variation in laser beam intensity. The mean OH-PLIF images are basically identical at all excitation frequencies for a given flow rate.

Figure 4.3(d) is the chemiluminescence image of the flame. Chemiluminescence is the natural radiation from the flame without laser excitation. To take a chemiluminescence image, the laser beam has to be blocked and the gate time of the camera is extended as the signal is much weaker than the fluorescence signal. Because of the elongated gate time, the chemiluminescence image is closer in appearance to the PLIF average image (c) rather than the instantaneous PLIF image (b). The chemiluminescence image doesn't show the small-scale turbulence structures, and this is one of the reasons that PLIF is becoming more and more popular for this type of measurement.

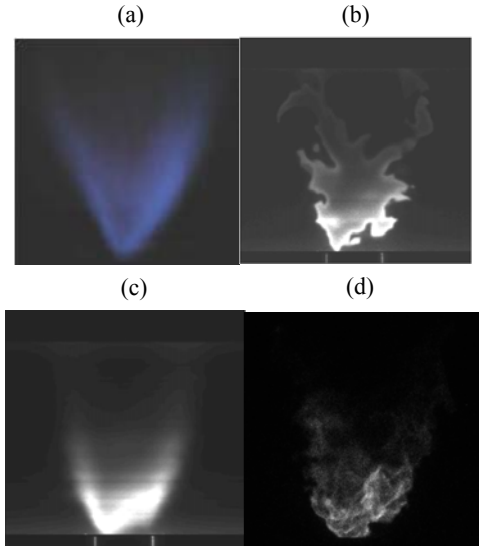

Figure 4.3 Different views of the flame: (a) visible flame, (b) instantaneous OH-PLIF, (c) average PLIF, (d) OH chemiluminescence

4.1.2 Procedure to Calculate Rayleigh Index Map

Different Rayleigh criterion formulations have been derived by various researchers. The principle underlying all of these remains the same, which is to show the phase relation between the pressure fluctuation and the heat release fluctuation. In this work, the simplified Rayleigh index is formulated as Eq. 4.1. It follows the mathematical work of Culick (1976), the measurement by Pun (2003), and the measurement by Kang (2006).

$$R_f = \int_0^1 \frac{p'q'}{p_{rms}\bar{q}}\,dt \tag{4.1}$$

where p' is the pressure oscillation, p_{rms} is the root mean square of the pressure oscillation for each set of images, q' is the oscillation of the heat release, $\bar{q}$ is the mean heat release, and dt indicates an integral over time.

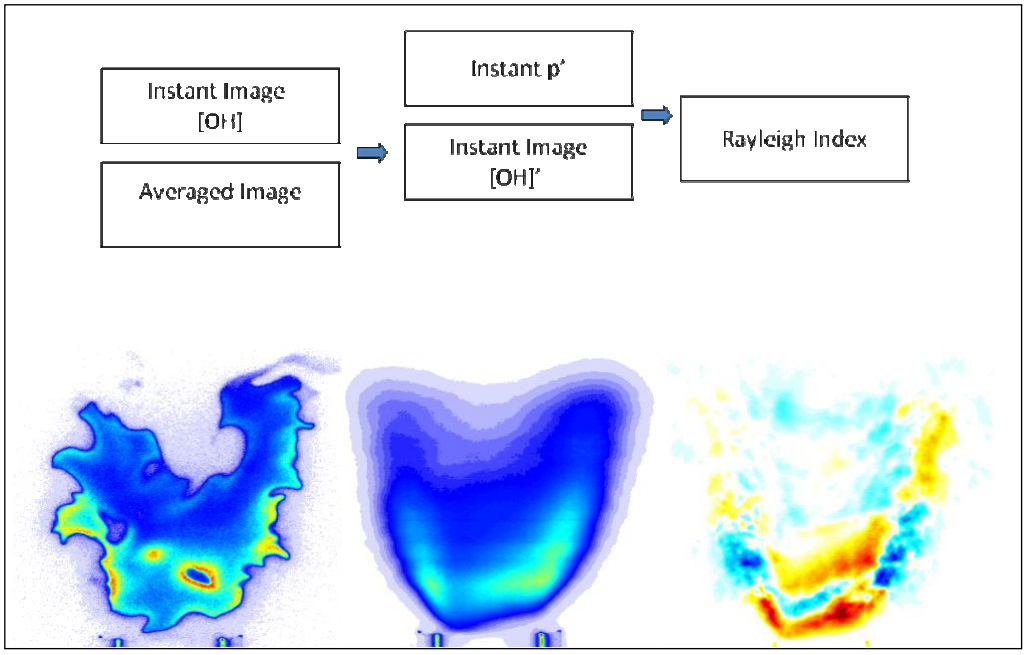

Figure 4.4 Calculation of Rayleigh index

Figure 4.4 has both a graphical description of the procedure to calculate the Rayleigh index and images showing the results at intermediate stages of the process. First, the mean OH image is computed based upon averaging a series of instantaneous images. The fluctuation value field is the instantaneous image minus the mean image. Next, the corresponding pressure for each image is extracted from the pressure signal with aid of the camera gate signal. Finally, summation of the p′q′ yields the Rayleigh Index map.

4.1.3 Typical Rayleigh Index Maps

Some typical Rayleigh index maps are shown in Figures 4.5 to 4.8. One set has a Reynolds number of 5865 and an equivalence ratio 0.51 while the second set has Re 8547 and equivalence ratio 0.59. The Reynolds number is based on the inner diameter of the burner and the mean velocity at its exit. These two sets of data represent the lowest and

the highest Reynolds numbers obtained in current experiment. The operating conditions of the experiments are tabulated in Table 4.1. These conditions are chosen according the operation range of the low swirl burner and the directions from the designer. In general, distinguishable structures were observed in the Rayleigh Index distribution although few differences were observable in the OH images.

For the set of experiments which have Re=5865 (Fig. 4.5 and Fig. 4.6), the acoustic excitation was from 13Hz to 208Hz. At 13Hz, very fine structures are visible in Rayleigh index plots. These pockets of positive or negative regions are not coherent and are less than 3mm. The 208Hz case shows similar structure; but between 55Hz and 130Hz, large scale coherent structures are evident. These were referred to by Kang et al. (2007) as toroidal structures.

For this higher Reynolds number set of experiments (Re=8547), the acoustic excitation is from 22Hz to 270Hz. At 22Hz, there are fine structures (e.g. less than 1cm) in the Rayleigh index. Pockets of positive or negative regions are mixed together and no large-scale pattern is observed. Such characteristics are also of the 160Hz and 270Hz cases. But again, between 32Hz to 125Hz, the large coherent structures exist in the Rayleigh index distribution.

Table 4.1 Experiment conditions

Re	Φ	CH_4(SLPM)	Air(SLPM)	Q(kW)
5865	0.51	5.38	100.63	3.21
6636	0.63	7.43	112.5	4.45
8547	0.59	9.01	145.47	5.39

A) Rayleigh index maps for Re=5865, Φ=0.51

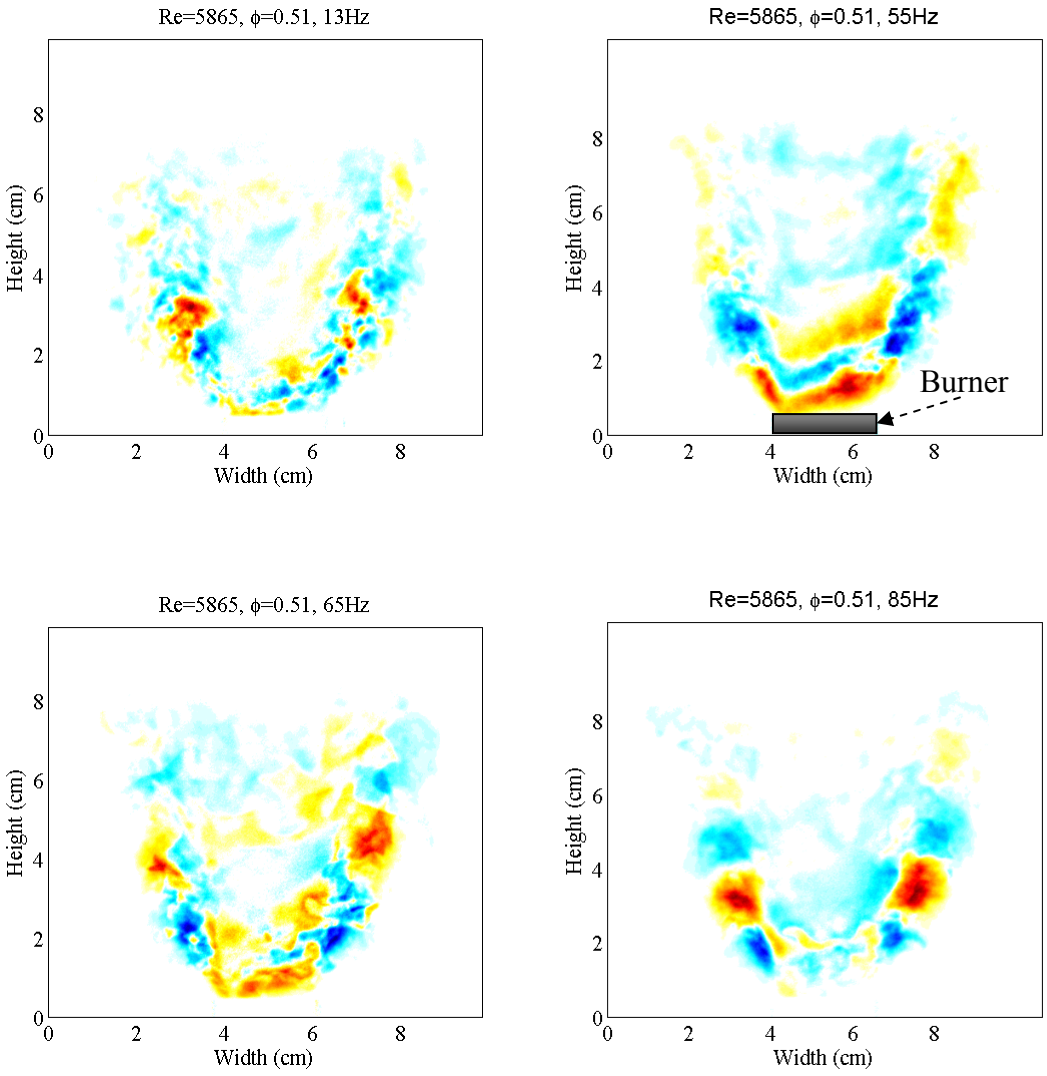

Figure 4.5 Rayleigh index maps for Re=5865 (f=13, 55, 65, 85 Hz)

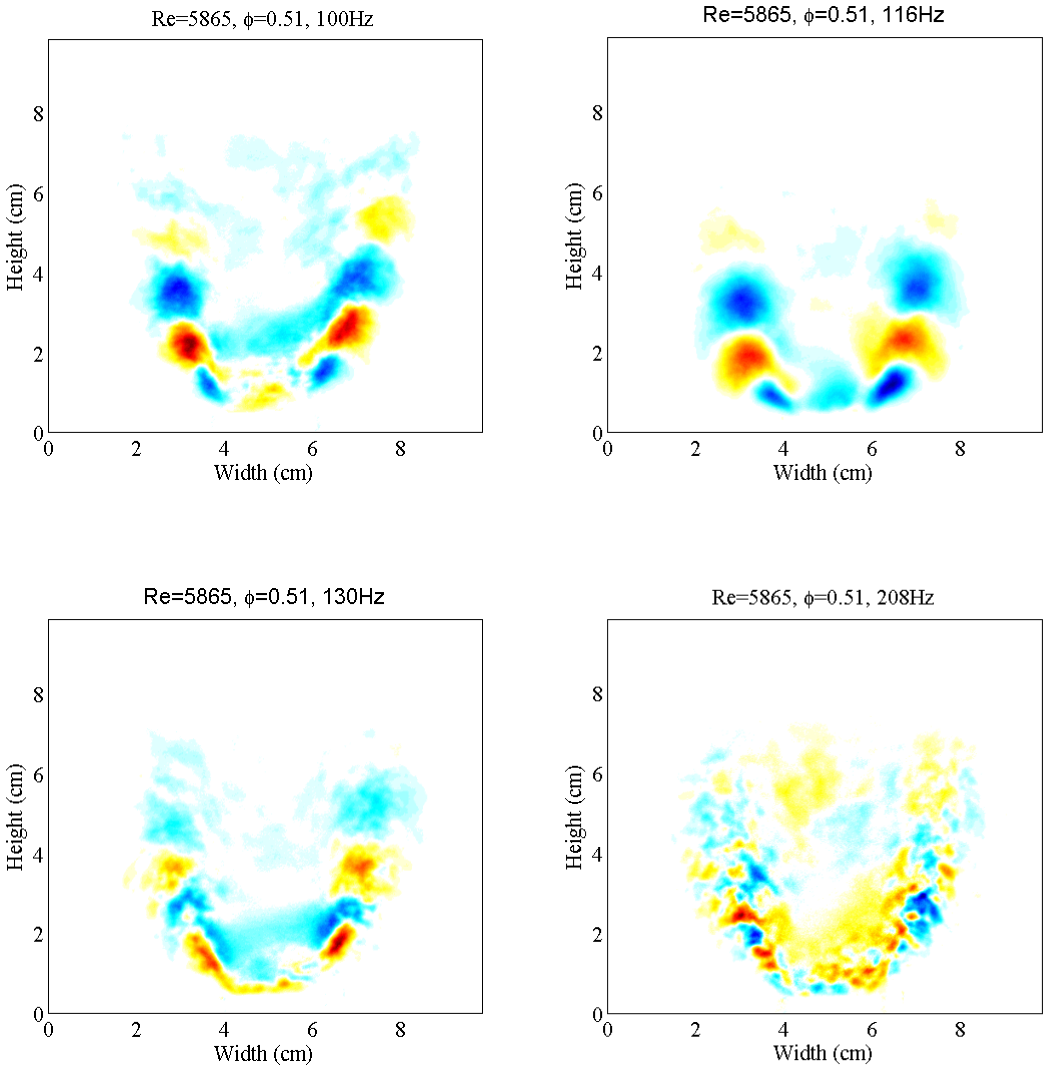

Figure 4.6 Rayleigh index maps for Re=5865 (f=100, 116, 130, 208Hz)

B) Rayleigh index maps for Re=8547, Φ=0.59

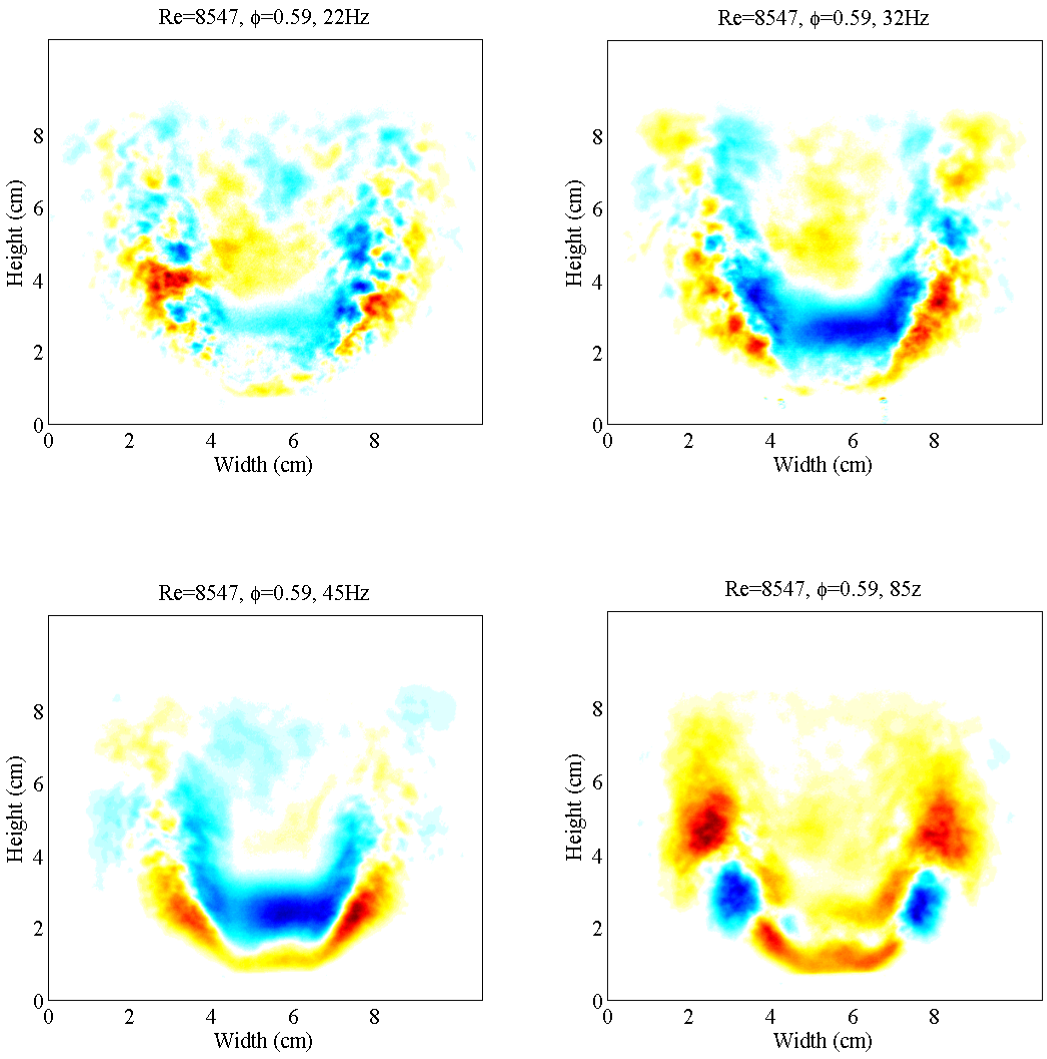

Figure 4. 7 Rayleigh Index Maps for Re=8547 (f=22,32,45,85Hz)

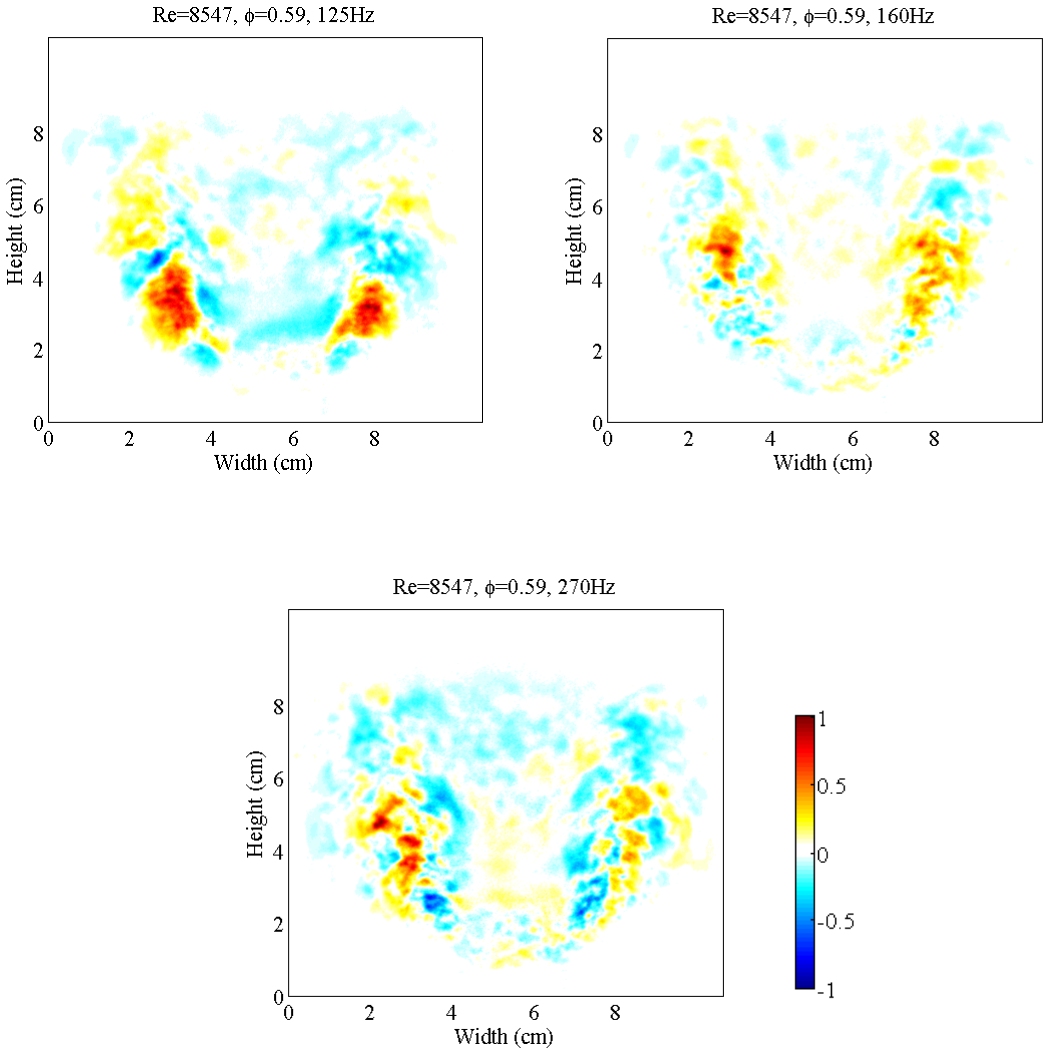

Figure 4.8 Rayleigh Index Maps for Re=8547 (f=125,160,270Hz)

4.2 Characteristics of the Rayleigh Index Map

In the above two sets of experiment, positive-negative structures in the Rayleigh index maps are observed at certain excitation frequencies. These appear to show cross-sections of a series of positive-negative toroidal structures. According to Rayleigh criterion, the positive regions are where the heat release and pressure oscillation are coupled and instability tends to grow; the negative regions are where the heat release and pressure oscillations are out of phase and the instability is inhibited. So how these structures are formed and what do they indicate? In the following sections, these structures will be examined to help answer these questions and understand the mechanism behind the phenomena.

4.2.1 The Toroidal Structure

Examining the Rayleigh index maps where large coherent structures appear (Figure 4.5 to Figure 4.8), the Rayleigh value is decreasing along the axial direction and the size of the vortices changes with frequency. It is needed to examine the value along the centerlines of the bulb structure. First, the centers are manually located in the Rayleigh index map. Then a 3 order polynomial curve is fitted using the tool box in Matlab. Figure 4.9 is the extracted Rayleigh indices along the centerlines for Re=5865 case. First, the absolute value of Rayleigh index at 85Hz, 100Hz, and 116Hz are higher than those at 55Hz, 65Hz and 130Hz. This means that the flame was more sensitive to the perturbations from 85Hz to 116Hz. Secondly, the Rayleigh index along the centerlines are weakly decreasing sinusoidal functions. Also, the wave numbers of the structures decrease when the frequency increases from 85Hz to 116Hz. Figure 4.10 extracts the Rayleigh index at Re=8547, and shows similar trends.

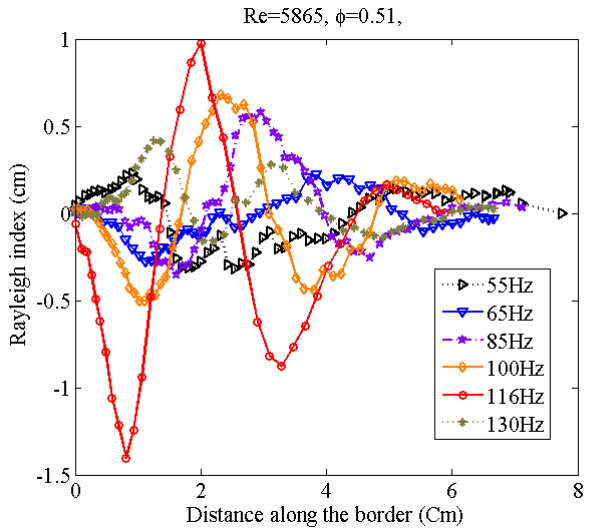

Figure 4.9 Rayleigh Indices along the vortex centerlines, Re=5865

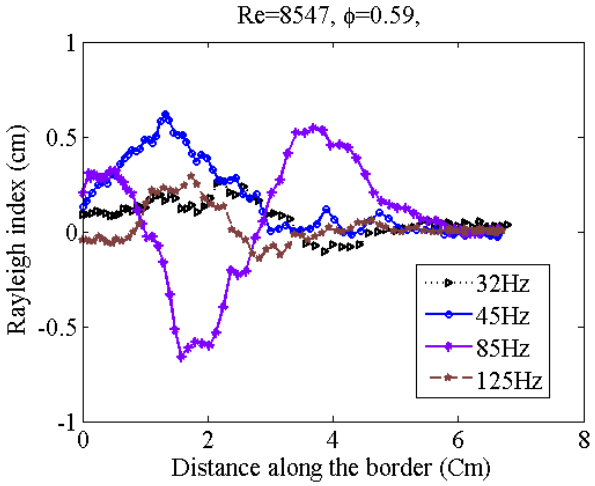

Figure 4.10 Rayleigh Index along the vortex centerline, Re=8547

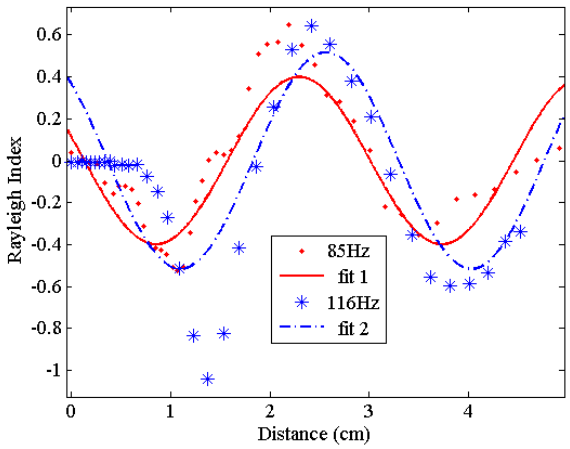

Figure 4.11 Rayleigh Index along the centerline of the vortex rings

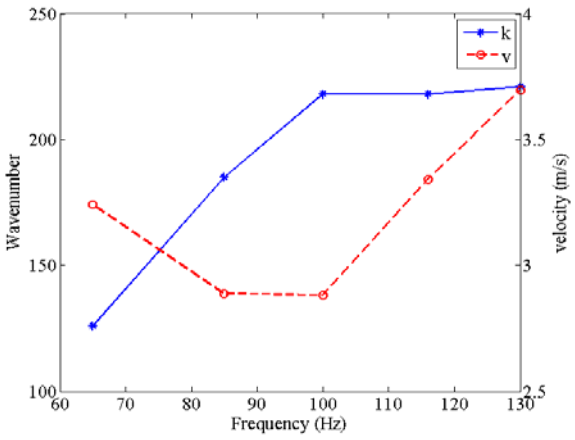

Figure 4.12 Wave number and convective velocity

Sine functions seem to match the distribution of the Rayleigh index along the centerlines (Figure 4.11). For example, for 85Hz case, the wave number is approximately k = 190. With this wave-number, and the enforced frequency, the convective velocity of the structure can be calculated: It is significant to notice that this convective velocity is of the same magnitude of the flow velocity.

$$v = {2\pi f}/{k} = 2.81\, m/s$$

All the wave numbers and calculated velocities are summarized in Figure 4.12. It shows that while the wave number increases with the frequency, the convective velocity of the structures in Rayleigh Index stays relatively constant. It is about 80% of the burner exit velocity (3.48 m/s).

This convective velocity analysis shows that the toroidal structures move with the shear layer but they are frequency locked onto the frequency of the sound field. Then the question is to find the relative location of the structures in the combustion field or the underlying flow field. Figure 4.13 gives a combination of the mean OH-PLIF flame and the corresponding centerline of the vortex structures seen in Rayleigh Index distribution (Re=5865, f=116Hz, Φ=0.51). The shear-layer/vortex centerline was estimated from both the Rayleigh images and the previously mentioned PIV results, and the Rayleigh values along this line were then manually extracted and curve fit. The centerline of the structure appears to be between the flame (hot products) and the surrounding co-flow.

In combustion, premixed reactants pass through the swirler inside the burner and then exit the burner as a free jet; above the burner (post combustion) are hot products surrounded by nitrogen co-flow. The natural buoyancy of the flame interacts with the low swirl jet and creates a modified buoyant jet type flow-field. The difference in flow density, velocity, and temperature put the interface (shear layer) into a regime where it is susceptible to perturbations. In the acoustic excitation experiment, the acoustic

perturbation trigs this shear layer which produces vortex shedding phenomena like in non-reacting flow field.

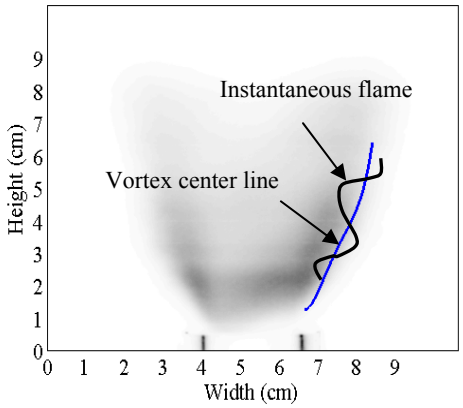

Figure 4.13 Vortex Centerline

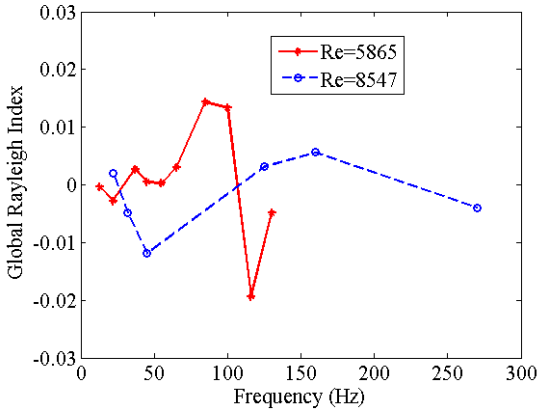

Figure 4.14 Global Rayleigh Index

4.2.2. Global Rayleigh Index

If we examine the Rayleigh index maps, another interesting point is that although these positive (unstable) or negative (stable) structures are seen in the local Rayleigh index distribution, the global Rayleigh Indices (Figure 4.14) are close to zero despite the different spatial distributions (global means the whole image region). So, in global sense, the flame is still stable. In addition, the structure doesn't appear without the excitation and the oscillation or the structure doesn't grow with time. These lead to the conclusion that the shear layer is convectively unstable for a sub-range of acoustic excitation frequencies.

4.2.3. Phase Resolved Variations

As we know that Rayleigh index is not a direct marker of a flow field like velocity, but its characteristics show the underlying flow field above the burner. In this section, phase resolved Rayleigh index and OH flame maps are given to check how they evolve in a cycle of the excitation.

Figure 4.15 illustrates a typical excitation at 116Hz when a clear structure in Rayleigh index was observed. For comparison, both the Rayleigh index and the OH intensity are normalized by their respective rms amplitude over a cycle. Figure (a) shows the Rayleigh index and (b) is the OH intensity. On comparing Rayleigh index and OH images, we can see that the general structure of Rayleigh Index doesn't change much within different phase segments, but the OH intensity distribution varies in a cycle. The most distinguishing feature of the OH maps is that the positive and negative regions switched between the first half and the second half of the period. There are also variations in local peak values. Figure 4.16 illustrates another excitation (208Hz) when no clear vortex structures are observed. Because the acoustic field and the shear layer are not coupled at this frequency, there is no clear structure in the OH intensity maps and therefore no structures in Rayleigh Index either.

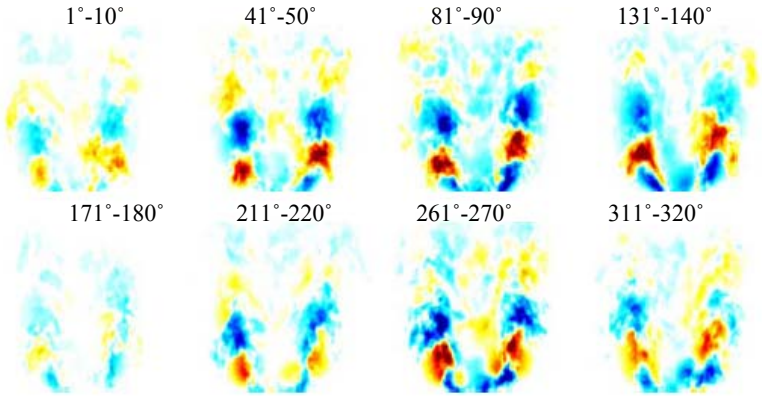

(a)

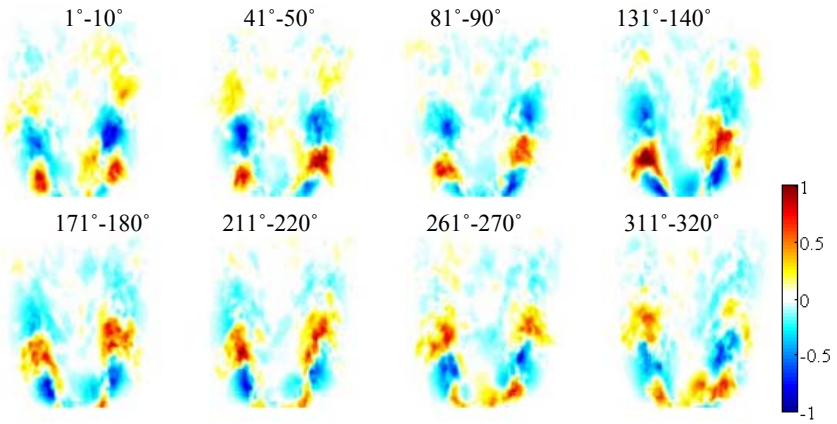

(b)

Figure 4.15 Phase resolved properties at 116Hz:
(a) Rayleigh Index, (b) OH intensity

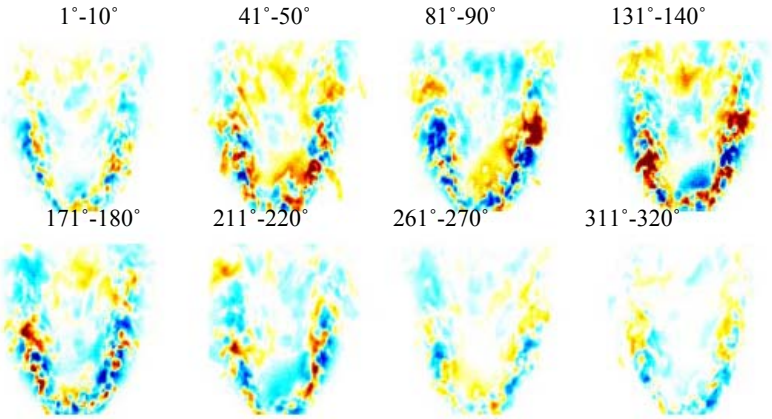

(a)

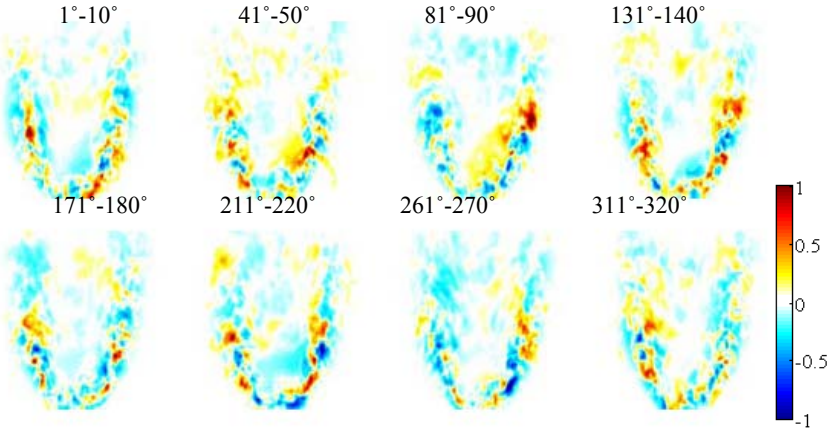

(b)

Figure 4.16 Phase resolved properties at 208Hz:
(a) Rayleigh Index, (b) OH intensity.

Phase resolved analysis shows that it is the OH intensity distribution that creates the positive-negative structure in Rayleigh index maps. When acoustic perturbation is enforced, the shear layer between the hot products and the surrounding cold flow becomes unstable and vortex structures are generated. The OH radical marks the underlying flow field and is captured by the fluorescence signals. Since mass is conserved, the overall OH variation in a cycle should be zero. This also explains why the global Rayleigh index is close to zero. For each instant flame, the spatial overall OH fluctuation is zero. As the pressure is assumed uniform across the whole field, the summation of the product of pressure and OH is also zero.

The influence of the acoustics or vortices on combustion has been previously investigated for a range of scenarios (Renard et al., 2000; Gutmark et al., 1989). Examining this as a driving mechanism for combustion instability, the general conclusion was that the frequency of vortex rollup can lock onto the frequency of a sound field if the amplitude of the acoustic oscillation is large enough and its frequency is sufficiently close to the natural frequency of vortex shedding. Lock-on phenomena was observed for Strouhal number of the order of unity, such as St=0.1-0.2 for a premixed propane air flame in a side-dump combustor (Samaniego et al, 1993) and St=0.58 for a premixed swirl stabilized flame (Paschereit et al., 1999).

The Reynolds and Strouhal numbers of this work are summarized in Table 4.2. The Strouhal number is based on the imposed acoustic frequencies. When Re = 5865, the coupling occurs from 55Hz to 120Hz and the corresponding Strouhal number ranges from 0.27 to 0.87. When the Reynolds number is 8547, the coupling started at St = 0.11.

Strouhal Number: $$St = \frac{fD}{U} \quad (4.2)$$

Reynolds Number: $$\mathrm{Re} = \frac{UD}{\nu} \quad (4.3)$$

Table 4.2 Summary of Strouhal numbers

Re=5865 (Φ=0.50)	f*(Hz)*	13	22	37	45	55	65	85	100	120	208
	St	0.09	0.16	0.27	0.33	0.40	0.47	0.62	0.73	0.88	1.51
Re=6186 (Φ=0.63)	f*(Hz)*	37	45	55	65	85	100	110			
	St	0.24	0.29	0.35	0.42	0.55	0.64	0.71			
Re=8547 (Φ=0.59)	St	22	32	45	85	125	160	270			
	St	0.11	0.16	0.23	0.43	0.63	0.8	1.35			

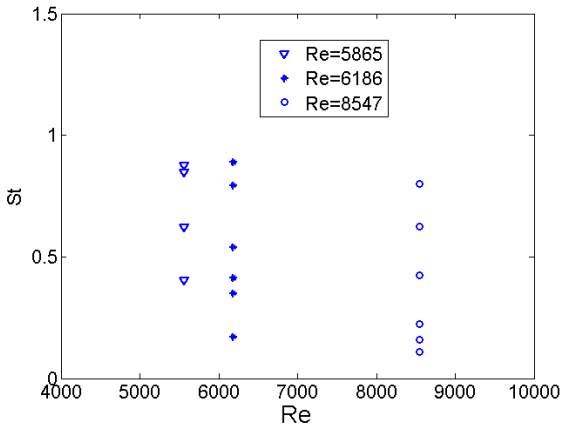

Figure 4. 17 Convectively unstable region

Experimental work on this low swirl stabilized lean premixed methane-air flame shows a coupling which is stronger than non-reacting flow but weaker than non swirling hot jet. This could be due to the combined effects of combustion and flow swirling. Combustion promotes instability while swirl in the azimuthal direction prohibits it. The coupling range is estimated and shown in Figure 4.17. Previous instability studies on jets and shear layers show that the cut-off frequency, which is close to that of the preferred mode of jet, is in the range of St=fD/U=0.25-0.5. Also according to early studies, reacting jet is absolutely unstable to varicose instability modes.

This experiment is unique in that a broad frequency lock-on was observed. The work suggests that the range of St when combustion will respond to acoustic excitation increases with Reynolds number. This gives us a guideline to judge if a system is susceptible to acoustic perturbation.

4.3 Flame Surface Analysis

One remaining question is whether Rayleigh Index variation is induced by combustion intensity changes, flame surface density (FSD) changes, or combination of both. Detecting flame surface with OH PLIF images was applied in several studies (Balachandran et al., 2005; Ayoola, et al., 2006; Roberts et al., 1993).

In current work, the edge detection was made with the Matlab® Canny Edge Detector. An appropriate critical value based on the heat release and beam quality must be chosen to ensure efficient surface detection. Figure 4.18 shows an example of the detection. In this work, flame surface density is defined as FSD = total flame length/area, since measurement in current work is 2 dimensional (2D). In the previous analysis, the Rayleigh index maps and the OH PLIF images are all in 2D. Hence 3D estimation is not carried out here. The flame surface density in 3 dimensional can be obtained by assuming a symmetric inverted conical flame shape. The image size of the flame and top of the

burner is of 10cm ×10cm and the pixel is 512×512. Therefore, the uncertainty of the detection is 0.2mm.

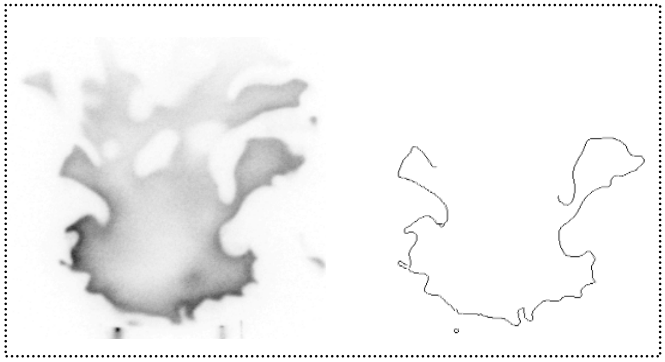

Figure 4.18 Flame surface detection with Matlab

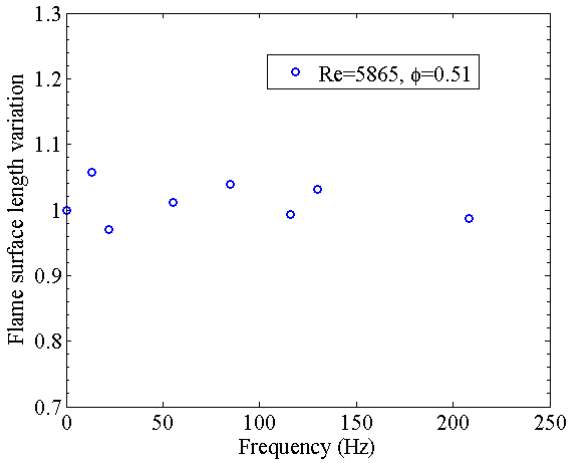

Figure 4.19 Flame surface vs perturbation frequency

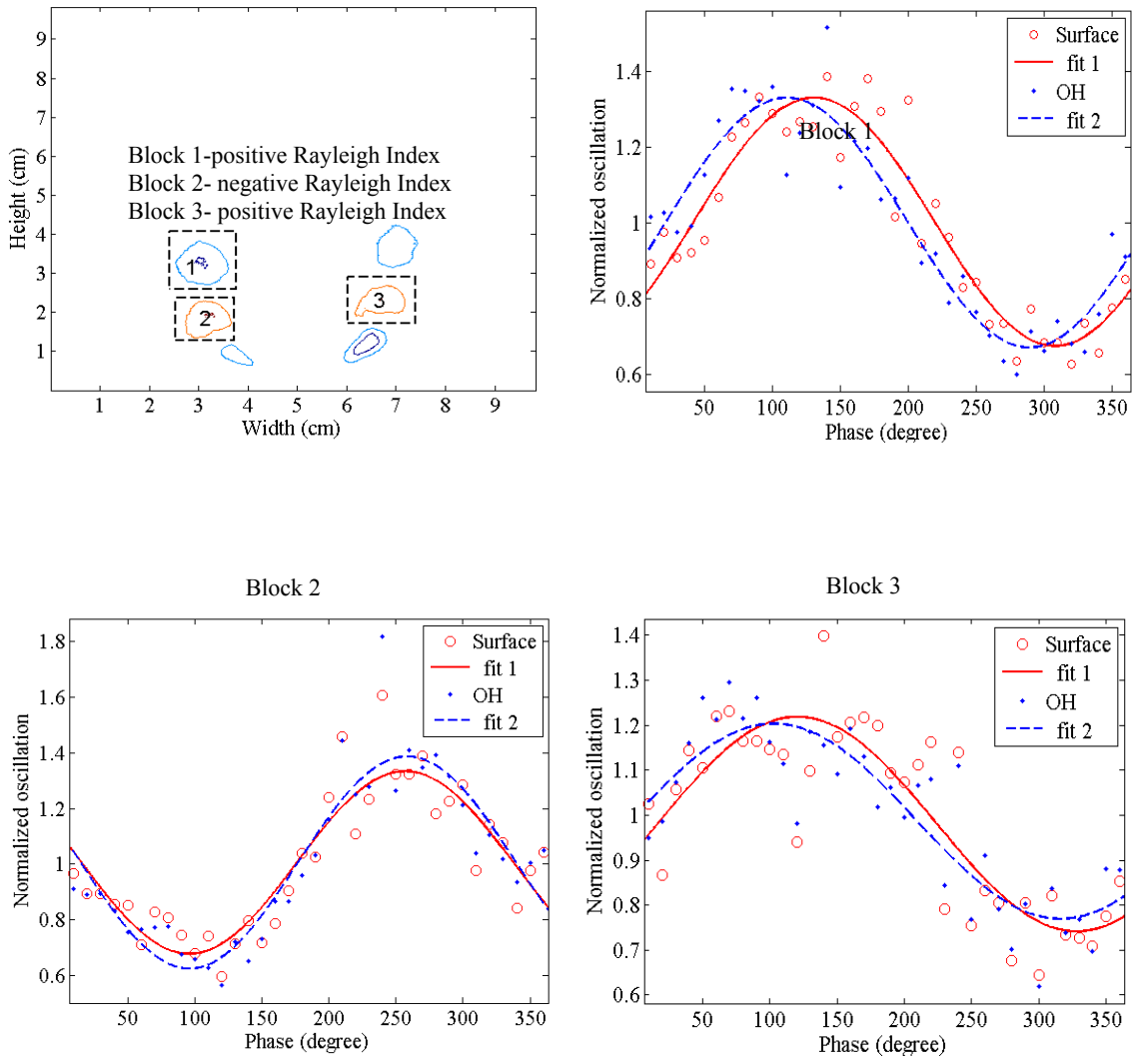

Figure 4.20 Local FSD and OH intensity variations over a cycle (Φ=0.5, f=116Hz)

Firstly, the flame surface length of the whole flame is computed and compared among various frequencies in Figure 4.19. The flame lengths are normalized by the values under no perturbation condition. The variations are less than 5% for all the frequencies except at 22Hz which is 6%. It implies that the low perturbations didn't cause significant change in combustion physics. The flame surface density is nearly constant as the mass flow rates of the methane and air are fixed across the various frequencies tested.

Then a more interesting thing is to examine the FSD of certain areas in the flame. Like in the phase resolved analysis, the flame surface detection and calculations are performed for each 10 degrees of phase and then the results are normalized by their respective means to show the variation within the cycle. Figure 4.20(a) shows the regions of interest which are selected according to strong Rayleigh index response. 4.20(b), 4.20(c) and 4.20(d) are the graphs for area 1, 2 and 3, respectively. Results show good correlation between the flame surface density and OH intensity. The correlation coefficients between these two parameters are 0.90, 0.96 and 0.92 for the three blocks, respectively. The correlation coefficient represents the normalized measure of the strength of linear relationship between variables (Matlab®, curve fitting toolbox). It is clear that OH variation follows the FSD variation in a period, which implies that the OH intensity variation is caused by the distortion of flame surface rather than through local intensity changes.

As an explanation of this periodic FSD variation in the shear-layer, it seems clear that acoustic-flow coupling causes the neutrally stable shear layer to produce strong vortices at the acoustic forcing frequency. These vortices then deform the flame and create zones of high FSD between them (as the vortices roll-up reactants ahead of the flame) and low FSD next to them (as the vortices pass and strain the flame into more of a flat surface). This variation in flame surface causes a net change in reactant consumption and a similar variation in the resulting heat release. This whole process transforms the coupling (phase-locked) between the acoustic oscillation and the fluid mechanics into a heat release variation that induces the structures seen in the Rayleigh index.

The type of flame surface distortion is different from other systems where flame vortex interaction has been studied and mathematical models constructed for predicting the flame response. The existing models fall into several categories like laminar flame disturbed by a vortex, anchored (and non-wrinkled) turbulent flames (Birbaud, et al., 2006), and mildly turbulent flames that are engulfed and rolled into large vortices

(Balachandran, et al., 2005). The behavior encountered here with the LSB involves a highly wrinkled flame surface (as is evident from Fig. 4.3) that is compacted or elongated, depending on location, by the passage of vortices. The resulting change in local FSD is approximately a 30% increase in front of the vortex and a 30% decrease as the vortex passes by, with the total FSD remaining unchanged. This is again very different from configurations where the flame surface is initially smooth and the vortex passage creates a smooth curve deformation. Also all the other studies involve local acoustic driving which creates a companion mass flow oscillation which would induce a variation in the total FSD.

The FSD analysis also shows, as expected, that products zones that have slowly varying OH concentrations are filtered out by the analysis process and do not significantly contribute to the resulting data. This validates the methodology and indicates its broad applicability for providing significant insight into a range of turbulent or fluctuating flames.

4.4 Conclusion

This chapter detailed the study of Rayleigh index maps measured in the experiment. Rayleigh index is an important indicator of the coupling between heat release and pressure oscillation in combustion. Toroidal structures were observed when the acoustic excitation is around the middle of the range (f=55Hz to 120Hz at Re=5865). No clear positive-negative structures were observed at the low or high ends. It showed that the coupling behavior is frequency selective.

The structure was examined in different views. Along the centerlines of the structures, the Rayleigh index featured a damping sinusoidal function. The convection velocity of the structure matched with the underlying flow field. Examining the OH fluorescence intensity evolution in a cycle, it showed that OH radical was relocated by

the vortices forming positive-negative structures as vortex shedding. Rayleigh index inherits the structure from OH intensity but its positive-negative structure is fixed in the cycle since it is the product of OH intensity and the fluctuating pressure.

The condition when the acoustic perturbation may couple with combustion was attributed to the Reynolds and Strouhal numbers. When the Strouhal number is of the order of unity (0.11 to 0.88), the acoustic perturbation is likely to induce vortex shedding in the shear layer. This analysis may give guideline for the real gas turbine industry.

CHAPTER 5
THE INFLUENCE OF CHAMBER PRESSURE ON THERMOACOUSTIC INSTABILITY

This chapter expands the examination of lean premixed low-swirl-stabilized flames to elevated mean chamber pressures. The experiments were achieved with pressures up to 0.34MPa. The emphasis is to characterize how the flame behavior responds to pressure increases, and to examine the effect of elevated pressure on thermoacoustic coupling.

5.1 Introduction

There is a significant amount of work comparing the combustion behavior at one atmosphere with that at high pressures. A range of research exists assessing the influence of pressure on laminar and turbulent flame speed, flame thickness, blowout limits, etc. (Law, 2006). Experiments by Boschek et al. (2005) showed that for pure methane and methane-hydrogen mixtures, lean blowout occurs at higher equivalence ratios as the pressure is increased. This effect was attributed to a reduction in the flame radical pool concentrations at higher pressures. The flame temperature itself is nearly insensitive to pressure variations (for pressures from 0.5 to 3.0 atm) for a swirling tubular flame, but the pressure variations change the Damkohler number (Zhang et al., 2009). Griebel et al. (2007) measured the turbulent lean methane-air flame speed up to 1.44MPa; the turbulent flame speed, S_T, was found to be independent of pressure.

The study of high pressure combustion is important both in terms of fundamental understanding and practical applications. Most industrial turbine combustors operate at high pressures for enhanced efficiency and greater power output, with pressures as high as 2 to 3 MPa. The existence of ongoing practical problems in spite of previous research work makes clear that the study of combustion dynamics at elevated pressure, above and

beyond the basic flame speed characterizations that have been previously carried out, is important and necessary.

5.2 The Influence of Pressure on Combustion Physics

Combustor operating pressure has a significant impact on combustion. It changes the flame speed, the reactant flow path, and so on. Even at relatively low pressure, the effect of pressure on chemical reactions is important (Law, 2006). For methane-air combustion, several flame characteristics change dramatically when the mean pressure is increased from 0.1 to 0.5MPa. For example, the overall reaction order (n) first decreases and then (above 0.5MPa for lean methane-air combustion) increases with pressure. The region of 0.1 to 0.5 MPa is the focus of interest for the current study.

For a lean premixed laminar flame, the influence of pressure and temperature on the flame speed is as described by Eq. 5.1 (Turns, 2000) where S_L is the laminar flame speed, P is the pressure, T_u is unburned gas temperature, T_b is burned gas temperature, E_A is the activation energy and n is the global reaction order. Flame speed is the speed at which the unburned mixture approaching the flame front (Turns, 2000). Experimental measurements generally show a negative dependence to pressure.

$$S_L \propto \overline{T}^{0.375} T_u T_b^{-n/2} \exp\left(-E_A / 2R_u T_b\right) P^{(n-2)/2} \tag{5.1}$$

For n= 1, as is the case for methane-air combustion, $S_L \propto P^{-0.5}$. Table 5.1 lists the laminar flame speeds extrapolated from Law (2006). The turbulent flame speed S_T exhibits a large degree of scatter and appears to be system dependent, hence reliable correlations are difficult to formulate. Shepherd and Cheng (2001) presented a validation for various turbulent flame speed models with the low swirl burner. They constructed a general empirical formula for S_T, Eq.5.2, which is based on two constants, C and n, and the turbulent fluctuating velocity, u'.

$$\frac{S_T}{S_L} = \left(1 + C\left(\frac{u'}{S_L}\right)^n\right)^{1/n} \tag{5.2}$$

This equation shows that the turbulent flame speed has a linear dependence on u'/S_L (for values up to u'/S_L ~7.3). Thus, the turbulent flame speed must decrease with pressure in pace with the laminar flame speed. For a real system, flame speed change implies that the supply speed must be adjusted accordingly.

From this analysis, it is evident that the flame would blow out with increasing pressure if the velocity remains unchanged. Conversely, the increase in density causes a corresponding decrease in the velocity field and this decrease is greater than the pressure-induced increase in flame speed. Consequently, the flame stabilizes at a lower position than that observed at one atmosphere.

The turbulence intensity of the burner is typically 10% of the mean flow for stable flame operation. With an equivalence ratio of Φ=0.59 and Reynolds Number of Re=8547, the mean velocity at the burner exit is 5.1m/s while the turbulent velocity u′ is nearly 0.51m/s (at one atmosphere). These values, for the atmospheric pressure conditions, put the low swirl flame in the Corrugated Flamelets region of the Borghi/Peters diagram shown in Figure 5.1 (Shepherd and Cheng, 2001).

From the ideal gas law, the mean velocity decreases linearly (P^{-1}) when the mass flow rates are fixed (Eq. 5.3). Consequently, u'/S_L varies from 4.6 to 2.55 as pressure increases to 0.5MPa. The transition that this induces in the flame structure is shown (with an arrow) in Figure 5.1.

$$U = \frac{\dot{m}}{\rho A} = \frac{\dot{m}RT}{PA} \tag{5.3}$$

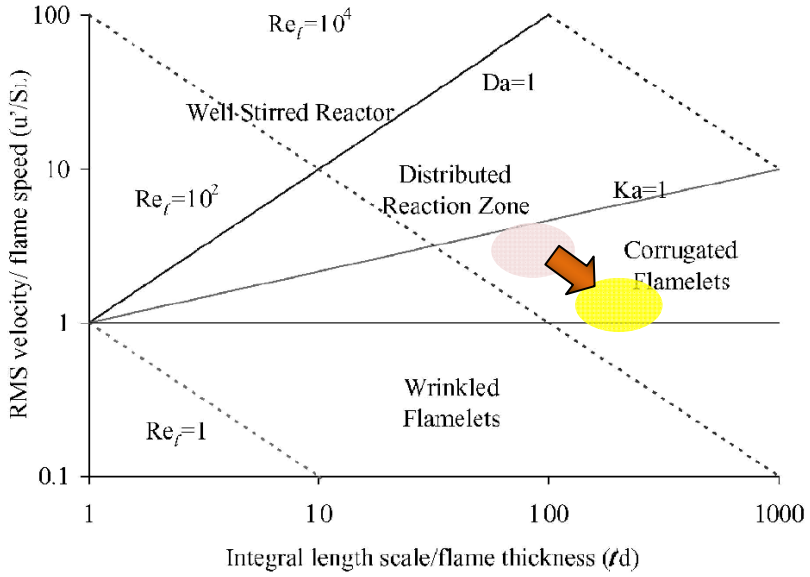

Figure 5.1 Regime diagram for premixed turbulent combustion

Flame-acoustic interaction requires the study of how the pressure changes the flame thickness and flame structure, and how the pressure influences the interaction of acoustic perturbations with the flame surface. While there are still debates about the exact value of methane-air flame thickness, the value is of the order of a millimeter. Table 5.1 lists values that are extrapolated from Law (2006) to enable basic analysis of the low swirl flame under pressurized conditions. Different from the laminar flame speed, which decreases gradually, the flame thickness drops sharply with pressure from 0.1MPa to 0.5MPa.

Table 5.1 Laminar flame of Methane-air Mixture (Φ=0.6, T=300K)

P(MPa)	0.1	0.2	0.3	0.4	0.5
S_L(cm/s)	11	9	8	6	4
δ (mm)	0.4	0.3	0.2	0.16	0.15

The acoustic properties of the chamber at elevated pressures should be assessed as well. Fortunately, the sound speed is only slightly affected by pressure; primarily, the sound speed varies with temperature. Due to combustion in the chamber, the gases present are markedly hotter than the outside air. Under pressurized conditions, the temperature increases even more due to the flow restriction at the system exhaust. In assessing these effects, the surface of the burner has been measured to often reach 373K and the chamber walls reach 340K or higher. If the mean temperature is assumed to be 330K, then the sound speed in the chamber will be approximately 360m/s (Table 5.2 shows the variation in sound speed with temperature). This corresponds to about a 6.6% increase in the sound speed, while results from section 5.3.1 show only a ~2% speed increase. This supports the idea that there is only a moderate increase in bulk gas temperature.

Table 5.2 The speed of sound in air

T(K)	290	300	320	350	380
c(m/s)	341.5	347.4	358.8	375.2	390.9

Table 5.3 The acoustic wavelength (c=360m/s)

f(Hz)	55	100	200	300	400
λ(m)	6.55	3.6	1.8	1.2	0.9

Table 5.3 lists the acoustic wavelength at different frequencies based on the 330K mean temperature assumption. If these values are compared with the flame thickness, it is clear that the flame thickness, even at frequency up to 400Hz, is 3 orders of magnitude

smaller than the acoustic wavelength. With these conditions, the assumption of a compact flame is clearly valid at atmospheric pressure. Since the flame thickness decreases with pressure (as will the acoustic wavelength), the compact flame assumption in chapter 3 remain valid at elevated pressures.

$$c = \sqrt{\gamma RT} = \sqrt{\frac{kP}{\rho}} \tag{5.4}$$

5.3 Results and Discussion

Experiments examining combustion instability at elevated pressures turned out to be challenging to perform. There are several key factors that make it so. First, the system was designed to have the flame ignited with the chamber open and the pressurization process to be performed after ignition and with a stable flame present. Unfortunately, the flame may blow out or flash back during the pressurization process since the stabilization zone changes with pressure. Secondly, pressurized experiments require a larger supply of air, fuel, and cooling gas. In the current system, the gases are supplied from compressed gas cylinders which only last a short time at the higher flow-rates required at higher pressures. Third, the chamber temperature rises even faster at elevated pressures (due to the greater heat release resulting from the higher flow-rates) than at one atmosphere. When the exterior of the chamber approaches 373K, it becomes difficult to work with. Fortunately, even through these difficulties, some experiments were successful.

The following sections present experimental results and analysis including behavior of the chamber pressure frequency spectrum, the stabilized flame position, the flame front structure, the Rayleigh index map, and the computed flame transfer function.

5.3.1 Chamber Pressure Spectrum

The chamber pressure acoustic spectrum measured with no external acoustic excitation, shown in Figure 5.2, shows the natural acoustic modes of the chamber. The wideband noise generated by combustion is present at all pressures (compare to Figure 5.3). The chamber resonance, seen at 100 and 125 Hz at 0.1MPa, shifts slightly to 102 and 127 Hz at 0.34MPa. As the geometry is fixed, the increase in frequency represents a 2% increase in sound speed (f=c/L).

Figures 5.4 and 5.5 show the frequency response of the system to 85 Hz forcing at 0.1MPa and 0.34MPa. Amplifier noise is evident in the secondary peaks that are seen to occur with ~10 Hz spacing while chamber modes are evident as the peaks with ~85 Hz spacing. The greatest of these are more than 50 db below the main peak and are inconsequential.

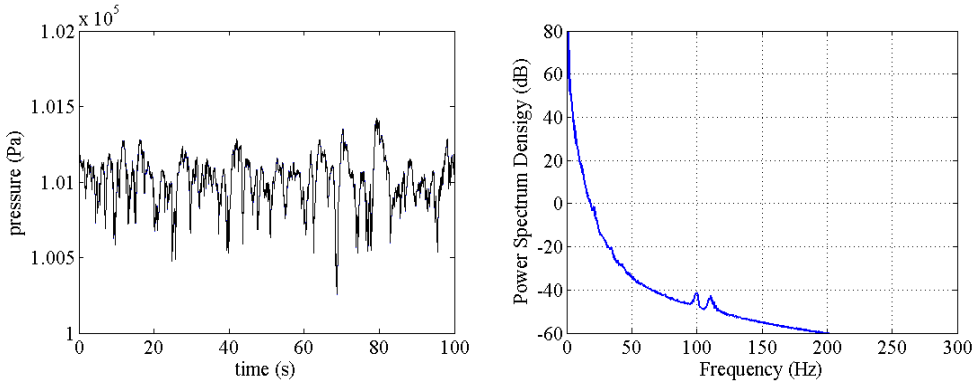

Figure 5.2 The pressure fluctuation and spectrum at 0.1MPa (No perturbation, Reacting flow)

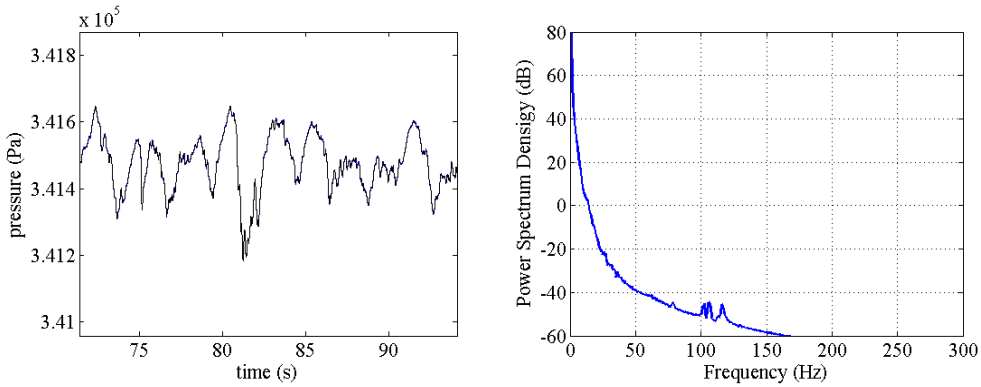

Figure 5.3 The pressure fluctuation and spectrum at 0.34MPa (No perturbation, Reacting flow)

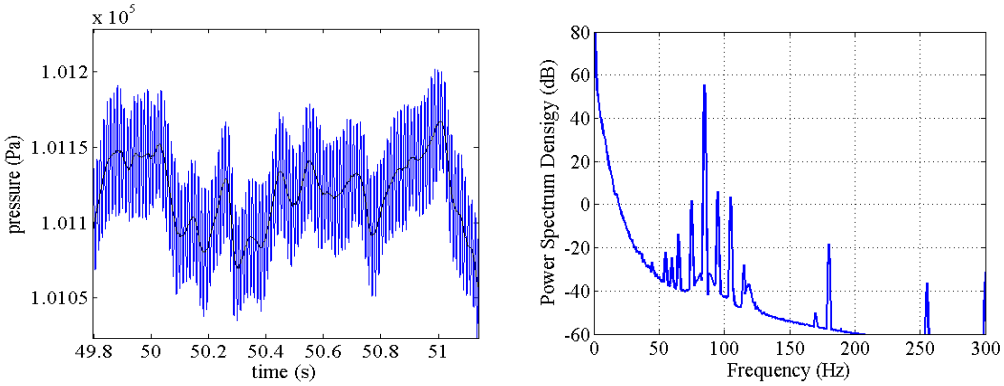

Figure 5.4 The pressure fluctuation and spectrum at 0.1MPa (f=85Hz, Reacting flow)

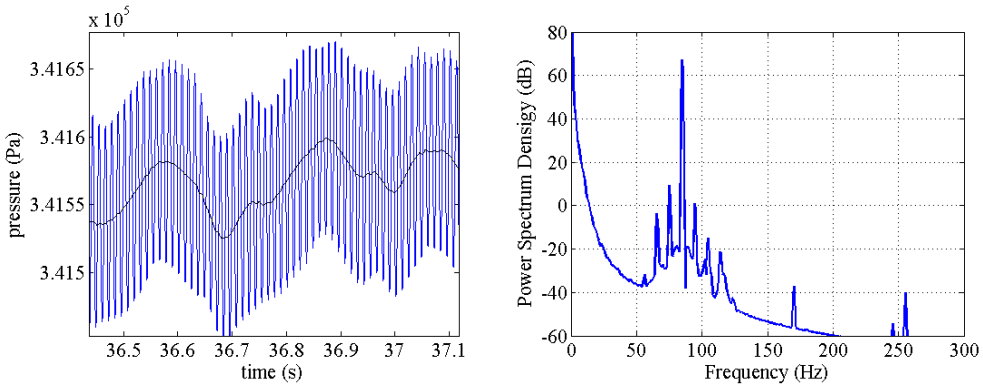

Figure 5.5 The pressure fluctuation and spectrum at 0.34MPa (f=85Hz, Reacting flow)

5.3.2 Flame Structure

Since the flame speed doesn't decrease as fast as the decrease in the flow velocity when pressure increases, the flame will propagate back towards the burner and can flash back inside the burner if the mass flux is low enough. This necessitates that the mass flow rates of both methane and air gradually increase to keep the flame lifted above the burner.

Figure 5.6 compares the mean flames at 0.1MPa and 0.15MPa with the same mass flowrate of methane and air ($\dot{m}_f$ =0.11mg/s, $\dot{m}_a$=3.1g/s). It is evident that the bottom part of the flame is closer to the burner exit at 0.15 MPa.

Also evident is a significant decrease in the averaged image intensity when pressure increases, as shown in Figure 5.7, for both OH-PLIF and OH chemiluminescence signals. The chemiluminescence signal dropped 11% from 0.1 to 0.2 MPa while the PLIF signal dropped 15% from 0.22 to 0.34MPa. In general, the fluorescence signal of a radical is affected by temperature, pressure and the mixture composition. Increasing pressure usually causes increased collisional quenching and a reduction in the strength of the signal. In addition, the equilibrium OH concentration decreases with pressure for methane-air flames (Battles, 1995). It has been shown, both theoretically and experimentally, that OH fluorescence levels were similar for many hydrocarbon flames and decreases by approximately a factor of 5 in strength for pressure changing from 0.1 to 1.0MPa (Allen, 1995).

Without the chemiluminescence measurement, it seems clear that high-pressure-induced quenching was the main factor in reducing signal levels. Figure 3.10, by Katharina et al. (1990), shows a more than 20% decrease in OH signal for a pressure change of 0.1MPa to 0.2MPa, followed by a slight decrease, and then the signal holding fairly constant above 0.4MPa. The OH chemiluminescence allows a cross check on these ideas as it has been extensively used as an indicator of heat release (Lee et al., 2000; Lee and Santavica, 2003; Ghoniem et al., 2005; Durox et al., 1998; Durox et al., 2005) and is well characterized in terms of pressure dependence.

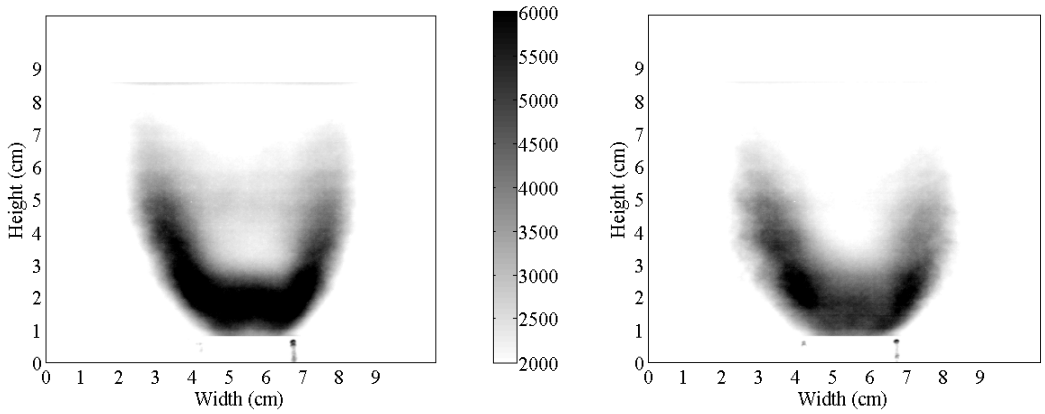

Figure 5.6 Flames at 0.1 MPa (left) and 0.15 MPa (right)

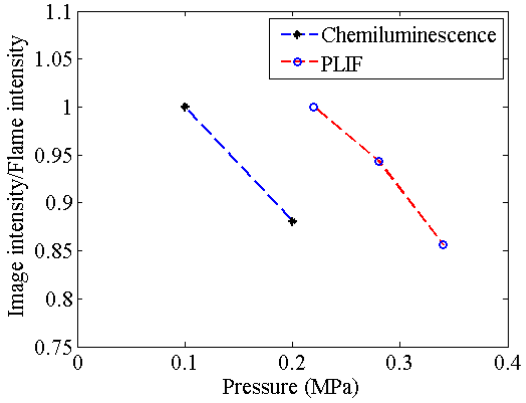

Figure 5.7 Pressure influence on heat release

A more than 50% decrease in OH* luminous intensity with a pressure change from 1 atm to 2 atm was observed by Docquier et al. (2000). While collisional quenching has typically been considered the main factor for this, it is also possible that not all of the fuel is combusted at elevated pressures. For hydrocarbon flames, the ignition temperature lies between 1300K and 1500K at ambient pressure. This temperature increases with pressure (Peters, 2000).

The general conclusion is that to have a precise indicator of the heat release, more than one radical should be used (Ayoola, 2006; Wangher et al., 2008). Because of this, the current work focuses on the flame response and structural change derived from OH radical fluorescence measurement, and not on an absolute measurement of the heat release.

Figures 5.8-5.11 show the instantaneous OH-PLIF images of the flames and their corresponding flame surface contours, for various mean pressures and perturbation frequencies. As discussed in the first part of this chapter, the flame stays in the corrugated flame region and is highly curved. Due to the turbulence present, no obvious differences in the flame structure are evident.

5.3.3 Rayleigh Maps

Measuring the Rayleigh index distribution was shown to be an effective way to examine the coupling between the flame front and the acoustic perturbation in chapter 4. When the Strouhal number is of the order of unity, the acoustic perturbation is likely to induce vortex shedding in the shear layer and this creates toroidal structure in Rayleigh index maps. This section focuses on computing the Rayleigh index maps for elevated pressure test cases.

Figure 5.12 shows the Rayleigh Index distributions at acoustic excitation frequencies from 22Hz to 370Hz at a mean chamber pressure of 0.19MPa. At low frequencies, especially when the enforced acoustic oscillation is between 45 and 140 Hz, the structures are clear. At high frequencies, the structures disappear. The pattern and the structure of the Rayleigh index map are similar to that of the one atmosphere experiment.

Stable flames were achieved with pressures up to 0.29MPa and 0.34MPa. However, the laser beam quality was insufficient for quantitatively accurate PLIF measurements. Yet, the result qualitatively shows that the large scale structures in the Rayleigh index maps are still present as shown in Figure 5.13.

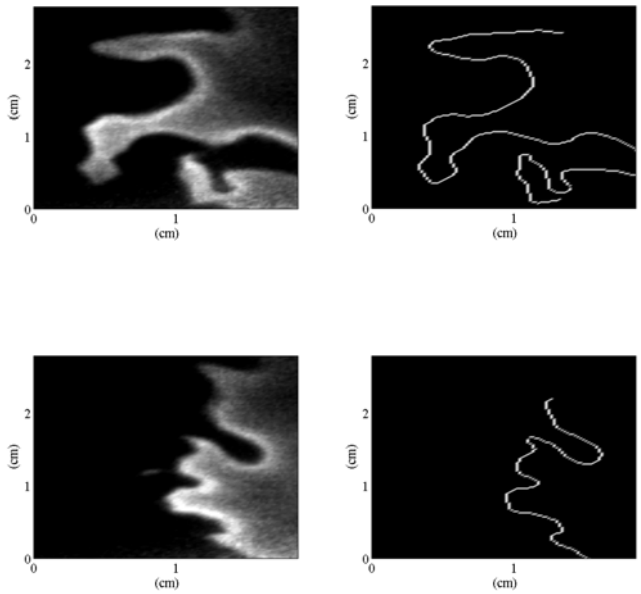

Figure 5.8 Flame structure at 0.22MPa, no perturbation

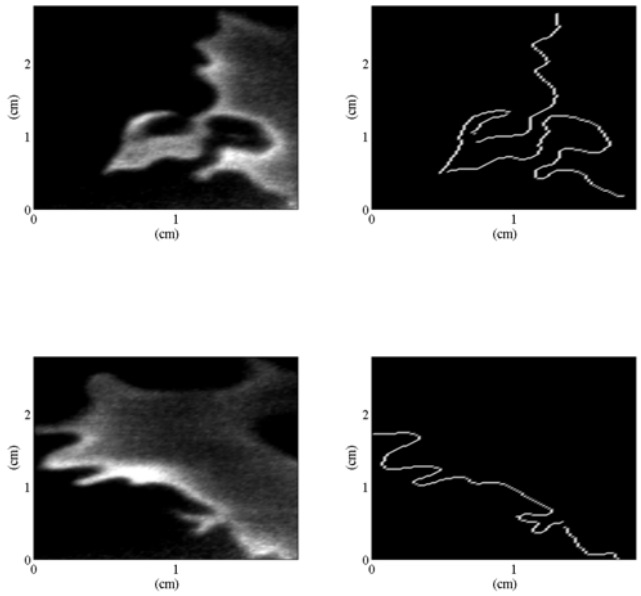

Figure 5.9 Flame structure at 0.22MPa, f=85Hz

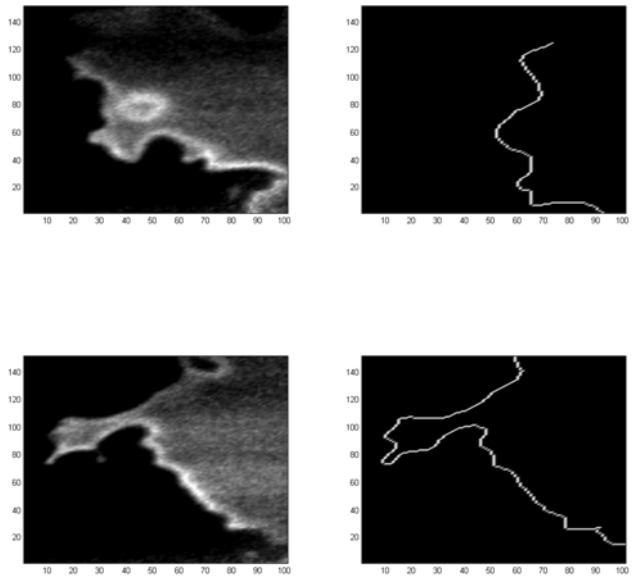

Figure 5.10 Flame structure at 0.34MPa, no perturbation

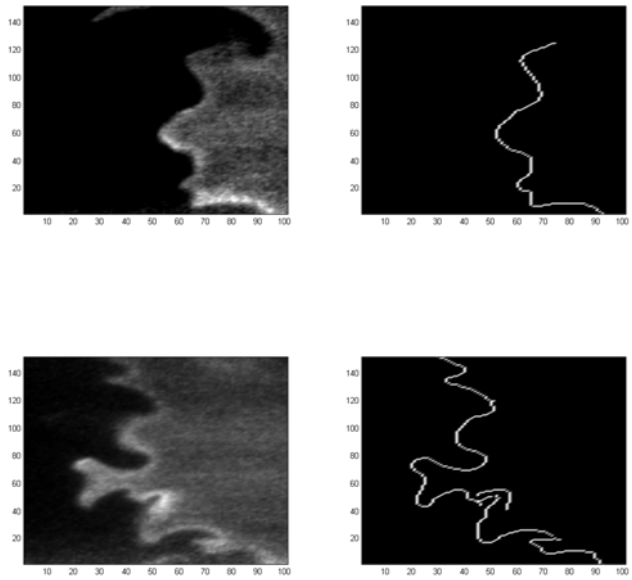

Figure 5.11 Flame structure at 0.34MPa, f=85Hz

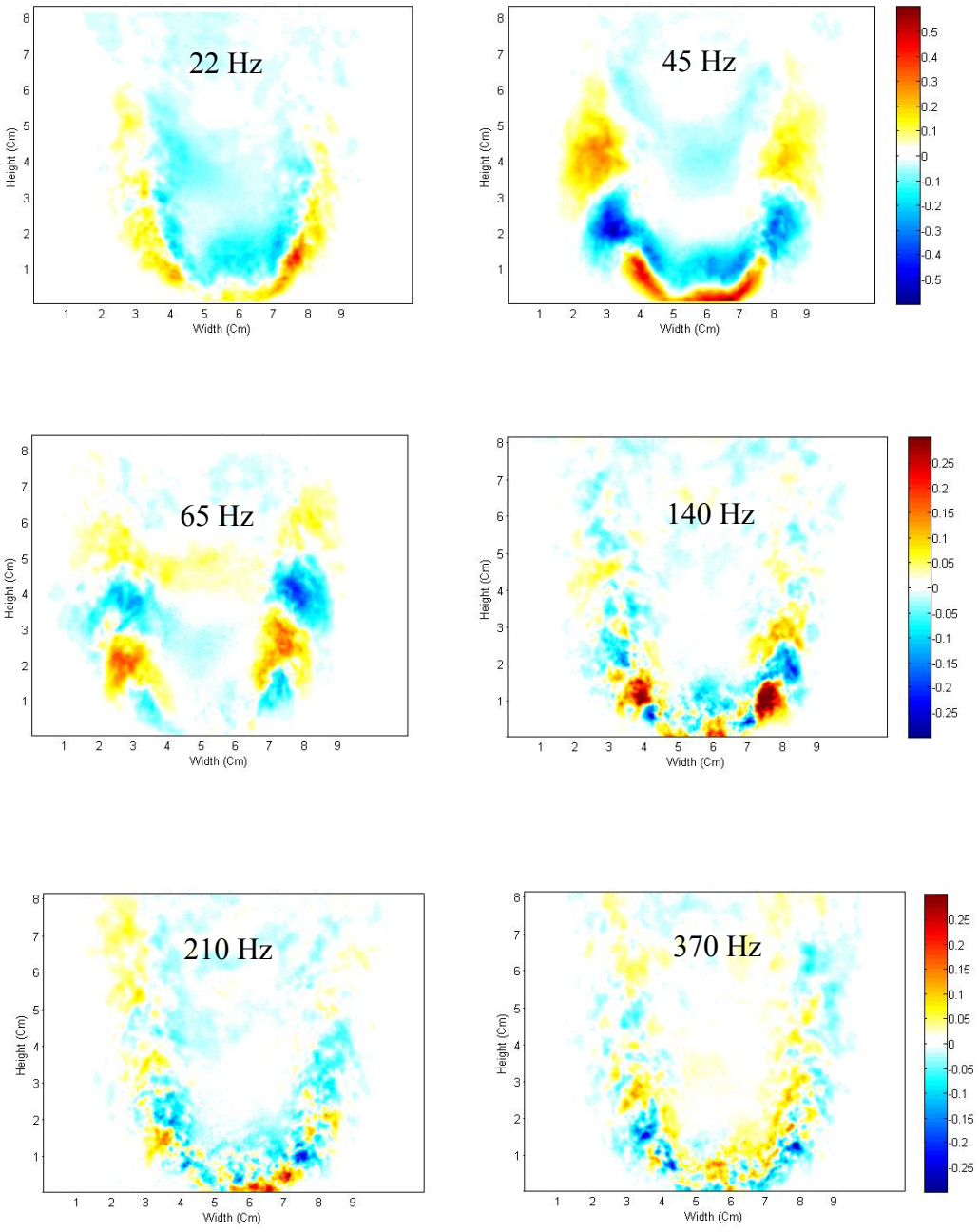

Figure 5.12 Rayleigh Index at 0.19MPa
(f=22, 45, 65, 140, 210, 370Hz)

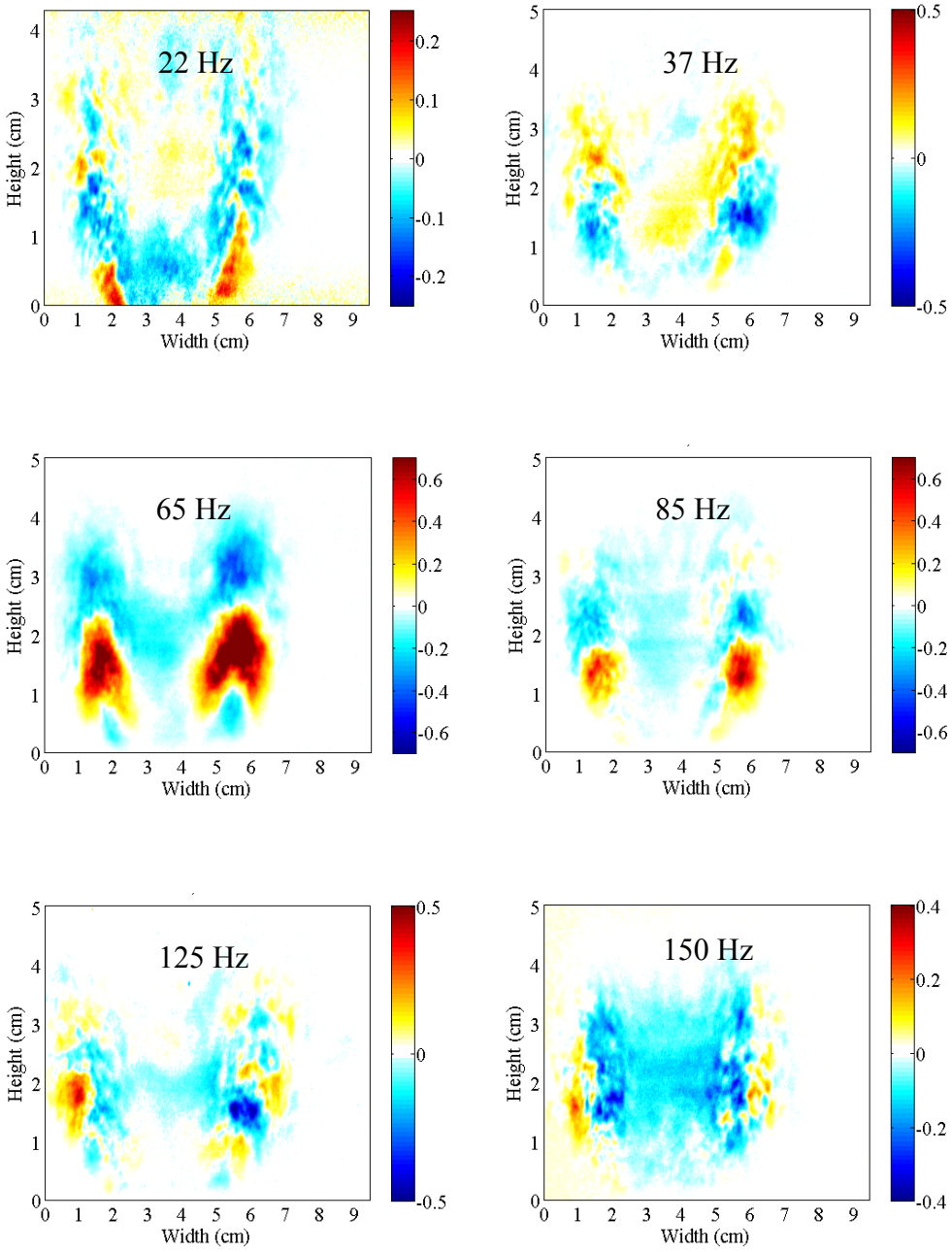

Figure 5.13 Rayleigh index maps at 0.29MPa

Test cases for a range of pressures, all acoustically driven at 85Hz, are compared in Figure 5.14. The large positive-negative structures in the Rayleigh index are observed at all pressure conditions. From 0.1MPa to 0.15MPa, there are three large regions along the shear layer, but a fourth region appears when the pressure reaches 0.22MPa. This is most likely due to a decrease in vortex size.

Figure 5.15 summarizes the Rayleigh Index along the centerline of the structure and the Fourier fitting at various pressures and frequencies. The fitting is intended to approximately show the wave number k of the structure. The wave numbers are 137, 172, 172, 182, and 222 respectively at each pressure. The fitting is consistent with the previous figures which show the vortex structures getting smaller. The 0.22MPa case deviates from the general trend in that at least one of the vortices appears to be located in the flame products region. The computed speeds of the vortices is 3.90m/s, 3.11m/s, 3.11m/s, 2.93m/s, and 2.4m/s respectively. This shows that the speed of the shedding at 0.1MPa is about thirty percent higher than that of 0.15MPa, and 63% higher than at 0.34MPa. If the mixture is a perfect gas, when the pressure increases from 0.1MPa to 0.34MPa, the density increases 70%, and therefore the velocity should decrease by about the same amount.

A summary of the perturbation frequencies and Strouhal numbers is listed in Tables 5.4-5.6. The flame acoustic coupling causes structures to exist for cases with a Strouhal number less than 2. For the 0.19MPa experiments, the Strouhal number ranges from 0.23 to 3.39 while the coupling occurs only for values of 0.23 to 1.48. The coupling is observed to shift slightly to 0.32-1.81 at 0.29MPa. More experiments are needed to make a complete chart of the coupling range.

The previous experiments also showed that the flame acoustic coupling is Reynolds number dependent, which appears to conflict with the classical Reynolds number independence of free shear flows (Pope, 2000). However, the Reynolds number independence typically invoked requires a higher value than that seen here. The mass

flow rates are fixed in the experiment in this chapter to keep the Reynolds number constant in an attempt to remove Reynolds number changes as a source of variability. The Reynolds number is not affected by pressure since the viscosity is relatively independent from pressure over the range tested.

$$\mathrm{Re} = \frac{UD}{\nu} = \frac{\rho UD}{\mu} = \frac{4\dot{m}}{\pi D}\frac{1}{\mu} \tag{5.5}$$

The Strouhal number and pressure variation is computed in Figure 5.16 and the area where flame is sensitive to thermoacoustic instability is marked. The frequency range shows change with pressure. For example, 10Hz at 0.4MPa falls in the area, but not at 0.1MPa. Therefore, the flame is more sensitive to low frequency perturbation at high pressure. As the convective time is longer for cases with a reduced convection velocity, the flame front may couple with low frequency perturbations in those cases.

Comparing the results at elevated pressures with the atmospheric pressure experiments, similar characteristics are observed. The toroidal structure still exists in the shear layer, the structures are clear in a certain frequency range, and the global Rayleigh indices are all close to zero. This appears that the coupling inherits the same characteristic as seen at one atmosphere, except that the flame shear layer will be sensitive to different frequency perturbations.

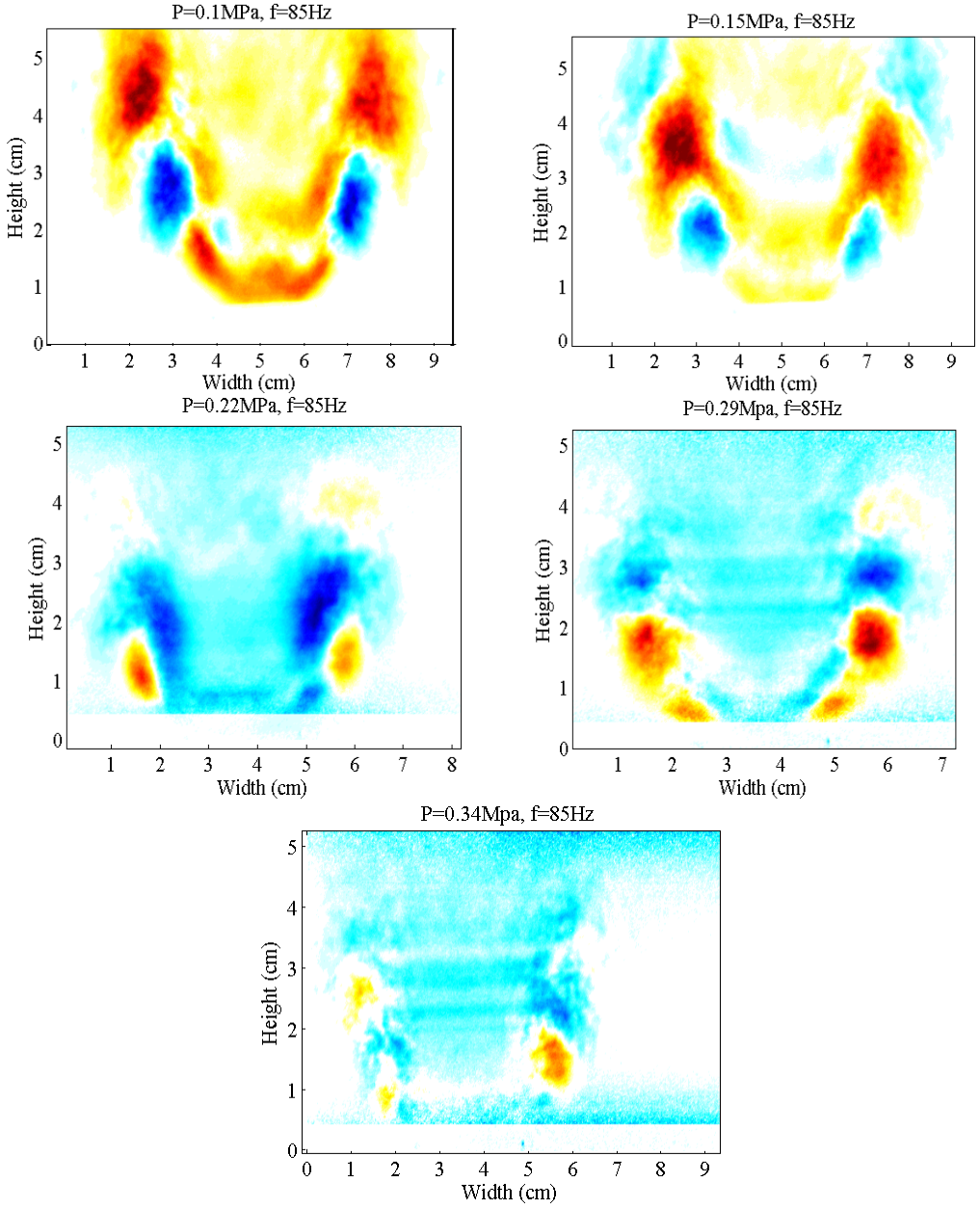

Figure 5.14 Rayleigh Index distribution at 85Hz (Re=8547, Φ=0.6)

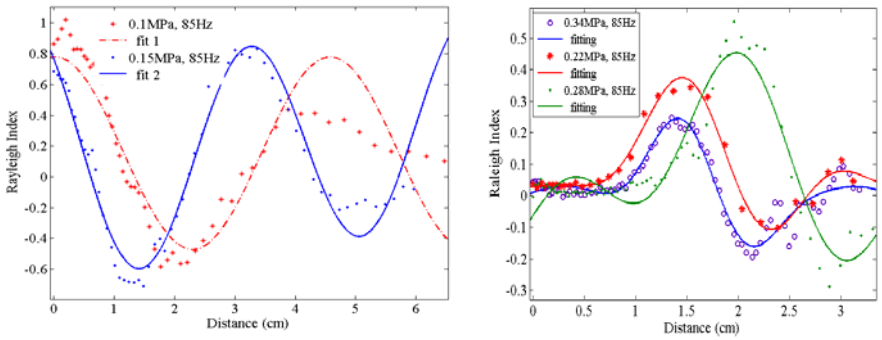

Figure 5.15 Rayleigh Index along the vortex centerline (Re =8547, Φ=0.6)

Table 5.4 Strouhal number (0.19MPa)

f(Hz)	22	45	65	140	210	370
St	0.21	0.43	0.62	1.33	1.99	3.51

Table 5.5 Strouhal number (0.29MPa)

f(Hz)	22	37	65	85	125	150
St	0.32	0.54	0.94	1.23	1.81	2.18

Table 5.6 Strouhal number (0.34MPa)

f(Hz)	85	150
St	1.44	2.55

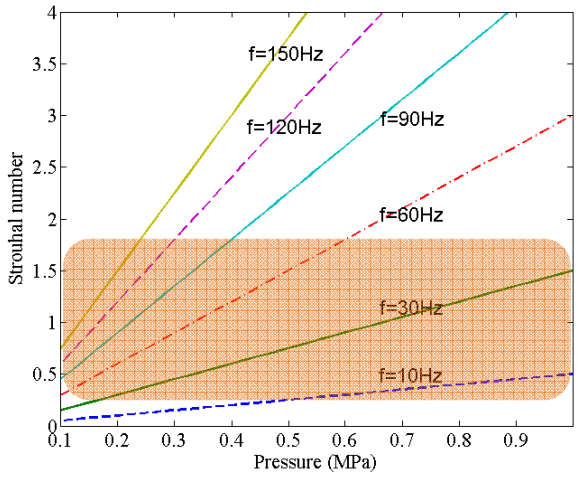

Figure 5.16 Strouhal number vs pressure

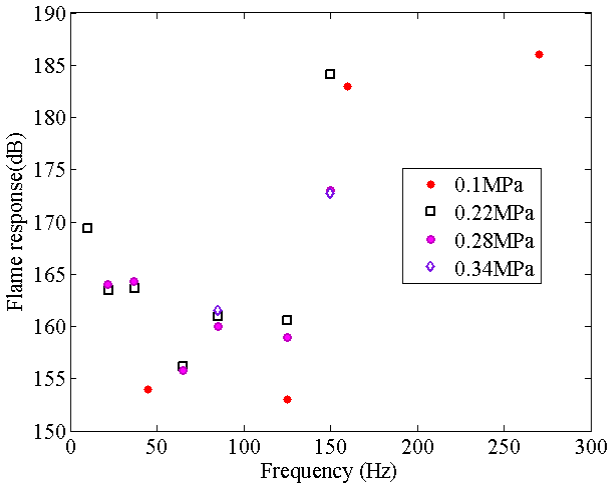

Figure 5.17 Flame response (Re=8547, Φ=0.6)

5.3.4 Flame Transfer Function

Prediction of combustion instability requires a description of the flame response to external perturbations, namely transfer function. Such information will help to predict and control the combustion dynamics in a real engine, and it gives validation to computational simulation. A typical transfer function for experimental thermoacoustic instability study links heat release rate fluctuations to the pressure perturbation as given by Eq.5.6.

$$F = \frac{q'/Q}{p'/P} \tag{5.6}$$

The flame response of the low swirl stabilized lean premixed methane-air flame is measured in Figure 5.17. The y-axis is in units of dB and it is defined as 20*log(F) as per convention. In general, the flame shows higher response above 125Hz, while it is relatively constant between 37Hz to 125Hz. Apparently the flame resoponds to fast perturbation. The flame also reports higher response at elevated pressures.

Clavin et al. (1990) and McIntosh (1991) seperately analyzied the instability of a laminar planar flame. The flame response was computed based on the assumption of one-step Arrhenius chemical kinetics. The flame response was given as a function of reduced frequency, $\omega\tau_t$, where ω is the perturbation frequency, and $\tau_t=\delta/S_L$ is the flame transit time. The flame response amplitude and phase both show a continuous increase for moderate frequencies. Wangher et al. (2008) examined the model with a laminar flame maintained stationary in a tube. The flame response showed relativley constant behavior for 0.4-0.9 relative frequencies. Durox et al. (2009) measured the transfer function of four types of flames- the conical flame, 'V' shape flame, 'M' shape flame, and a collection of small conical flames. The conical flame showed a decreasing response with increasing frequency. But the 'V' shaped flame first showed an increse then decrese in response.

At low and intermediate frequencies, the flame response of the low swirl burner showe a trend similar to the 'V' shape flame of Durox et al., and the theroretical work of Clavin. The low swirl stabilized flame doesn't attach to the burner. In addition, the flame has an open end. The characteristic of the bowl-shaped flame deliminates factors which are difficult for similified analysis such as heat transfer to the wall.

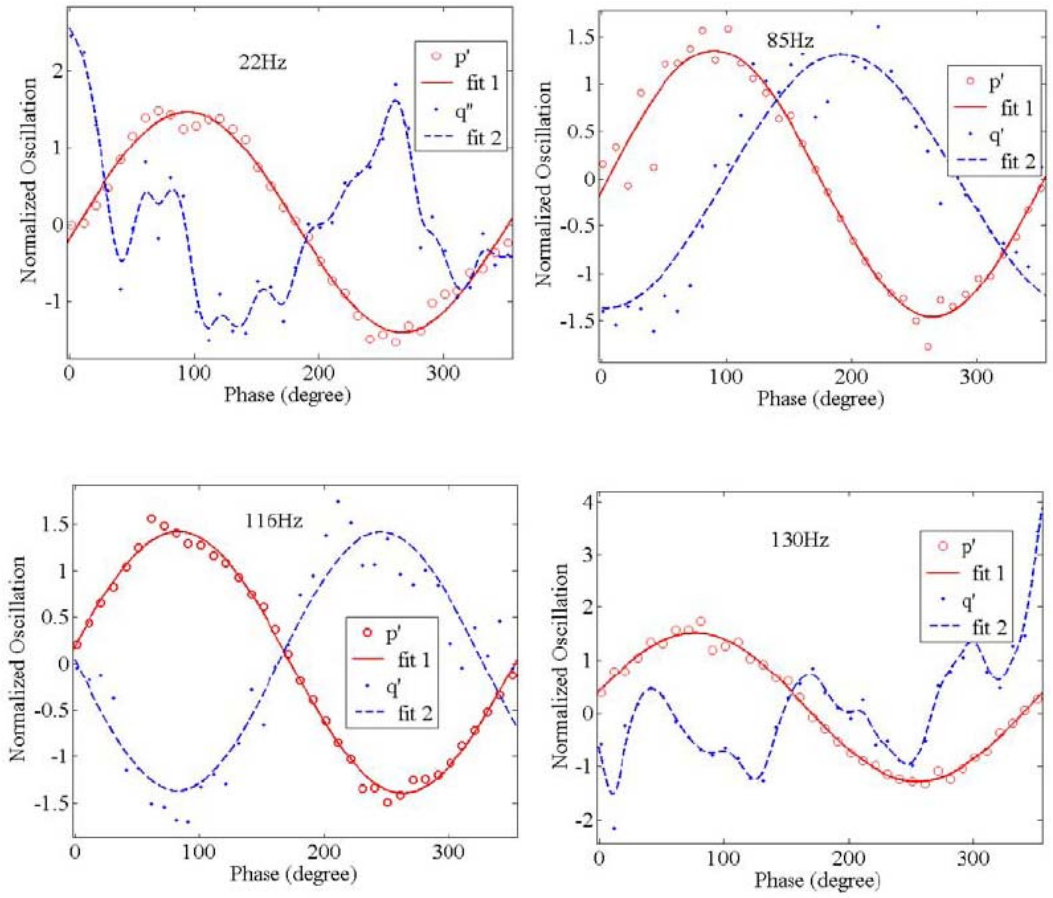

Figure 5.18 The phase of the flame response

Figure 5.18 lists the heat release (OH fluorescence) and pressure oscillation for a specific frequency. For some frequencies, the heat release follows the sinusoidal pattern

of the pressure oscillation. But for other conditions, especially lower end and higher end frequencies, the heat release appears turbulent. As emphasized in the early part of the thesis, our system introduces weak perturbation, less than 0.1%, to the flame from downstream of the chamber. The other work, represented by Candel group, imposes large oscillations to the fuel supply line (typically 10%), and produces heat release oscillations in all perturbations. The measurement of phase information of the low swirl flame response remains incomplete. Much work is in progress to make it complete.

5.5 Conclusion

The influence of pressure on the lean premixed low swirl stabilized flame was examined. We know from literature that Flame characteristics, including the laminar flame thickness and the laminar flame speed, change dramatically when the pressure increases from 0.1MPa to 0.5MPa. Conversely, these changes did not significantly change the flame acoustic interactions that were observed in our experiments. Pressurizing the chamber changed the position of the flame with fixed mass flow and higher flow rates were required at elevated pressures to keep the flame lifted.

In general, the flame is stable at elevated pressures. The shear layer of the flame front keeps its sensitivity to perturbation at frequencies of 50-150 Hz. The toroidal structures of Rayleigh Index seen at one atmosphere persisted through all the pressures tested. The acoustic perturbation forces the shear layer to develop vortices at the same (acoustically driven) pace.

The flame response study shows that the low swirl stabilized flame has a stronger response to high frequency perturbations, and this will require continuing study.

CHAPTER 6

VARIATIONS IN EXAMINING THE THERMOACOUSTIC COUPLING

This chapter expands the examination of lean premixed low-swirl-stabilized flames to a wider range of conditions. Of primary interest are the effects of swirl, acoustic forcing amplitude, and natural system instability. The effect of swirl is assessed by performing a comparison of the flow structure and flame stability between two burners with swirl numbers of 0.5 and 0.2. The amplitude sensitivity and natural resonance are assessed by changing how the acoustic forcing amplitude is controlled.

6.1 Swirl Effects

Swirling flows are extensively used in gas turbines, gasoline and diesel engines, industrial furnaces, utility boilers, and many other practical heating devices. Swirl flows general are produced by three methods, tangential entry, guided vanes, and direct rotation. The definition of swirl is (Gupta, 1984)

$$S = \frac{G_\theta}{G_x (d/2)} \tag{6.1}$$

where G_θ is the axial flux of rotational (swirl) momentum, G_x is the axial flux of axial momentum, and d/2 is the nozzle radius.

The swirl number can be directly computed from the measured nozzle thrust and torque, or by the angle of spread in the flow downstream of the nozzle, or by other, similar means. Alternatively, the swirl number may be characterized in terms of the vane swirl angle and nozzle geometry. The swirl number for the low swirl burner used in the current research is

$$S = \frac{2}{3}\tan\alpha \frac{1-R^3}{1-R^2+\left[m^2\left(1/R^2-1\right)^2\right]R^2} \tag{6.2}$$

Where α is the vane angle, R is the ratio between the radius of the un-swirled passage to the radius of the total flow opening, and m is the ratio of the mass fluxes of the unswirled and the swirled flows.

6.1.1 Burner Geometry and Flame Shape

The two swirl burners tested are shown in Figure 6.1. Swirl burner A has a swirl number of about 0.5 and is the swirler used in the studies conducted in chapters 4 and 5. Swirl burner B has a swirl number of approximately 0.2. The swirl numbers here are provided by the designers and have an uncertainty of no more than 20%. The outside diameters of both burners are 2.54cm and the height is 2.0cm, but the ratio of the center portion (R_c) to the entire diameter (R_i) and the angle of the vanes (α) are different between the burners. Swirler A has an R_c/R_i=0.5 and a vane angle of 37 degrees while Swirler B has R_c/R_i=0.8 and a vane angle of 60 degrees.

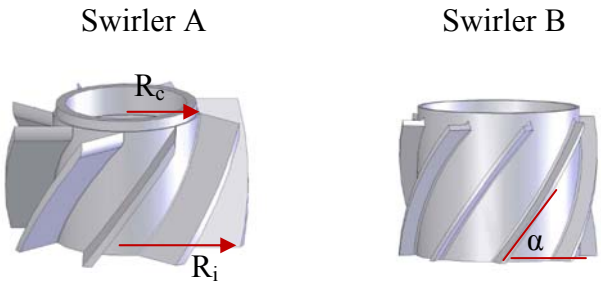

Figure 6.1 Images of the two burners

The instantaneous and mean OH-PLIF images of the flames from the two swirlers are compared in Fig. 6.2. It is evident that both flames are turbulent and that flame A is more uniform than flame B. Examining a series of images for both flames, it appears that one side of flame B is nearly anchored on the burner while the other side of the flame, which is lifted, vibrates. However, both sides of flame A are lifted and stable. Therefore, in the mean image, flame B is asymmetric and appears wide, while flame A is more narrow and symmetric. The asymmetry of flame B can be attributed to the upstream swirler. A higher percentage of the swirled exit flow in A makes the flow field more uniform. With flame B having a very low swirl number, a small non-uniformity in the swirler can manifest as a flow defect and be transported downstream, and result in flame anchoring and asymmetry.

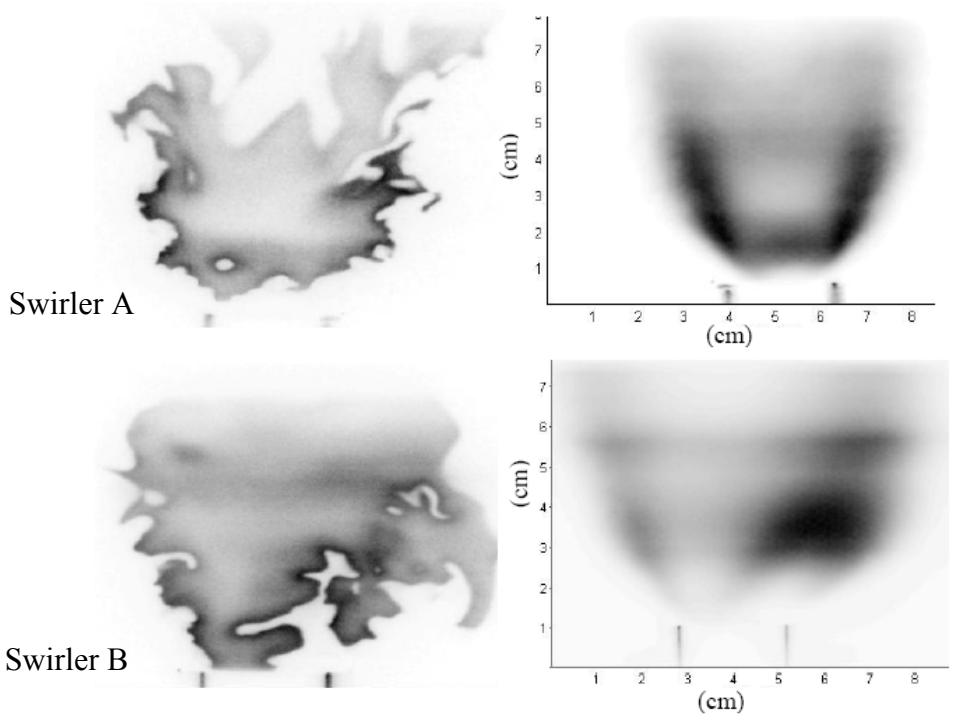

Figure 6.2 Instantaneous and mean OH-PLIF images of the turbulent flames

6.1.2 Rayleigh Maps

Each burner was tested under various acoustic excitation frequencies: 37, 45, 55, 65, 85, and 110Hz. Figure 6.3 shows two typical Rayleigh Index maps with excitation frequencies of 37Hz and 110Hz. The maps are all normalized according to their maximum and minimum values for comparison. At 37Hz, the perturbation does not affect the shear layer and no clear vortex structure is induced, while at 110Hz the shear layer and the acoustics are coupled. In general, flame B has similar characteristics as Flame A. Toroidal structures are observed in particular ranges, for example, no structures are seen between 37Hz to 65Hz excitation, but clear vortex formations show up from 85Hz to 110Hz for both swirlers. The corresponding Strouhal number for the vortex cases is 0.50 to 0.65, but the range in which the acoustic perturbation triggers the vortex shedding is different from that of swirl burner A. As shown in previous work, for Swirler A with a Reynolds number of around 7000, the coupling range starts from a Strouhal number of 0.3.

One distinguishing feature of Flame B is that only the left side of the flame shows clear structure. The other side does not exhibit a clear vortex structure. As shown in Figure 6.2, the right side of the flame vibrates and has a wide flame brush. Possibly, the positive-negative spots in Rayleigh index overlap each other and the clear structure is smeared out. Comparison of the two flames, A and B, reveals that the vortex structure in Rayleigh Index can only be seen when the flame is relatively ‘stable’. The flame is convectively unstable as it couples with the acoustic perturbation, but not absolutely unstable. If the flame has a wide brush, as is seen in the right side of flame B, the clear structures are eliminated or hidden.

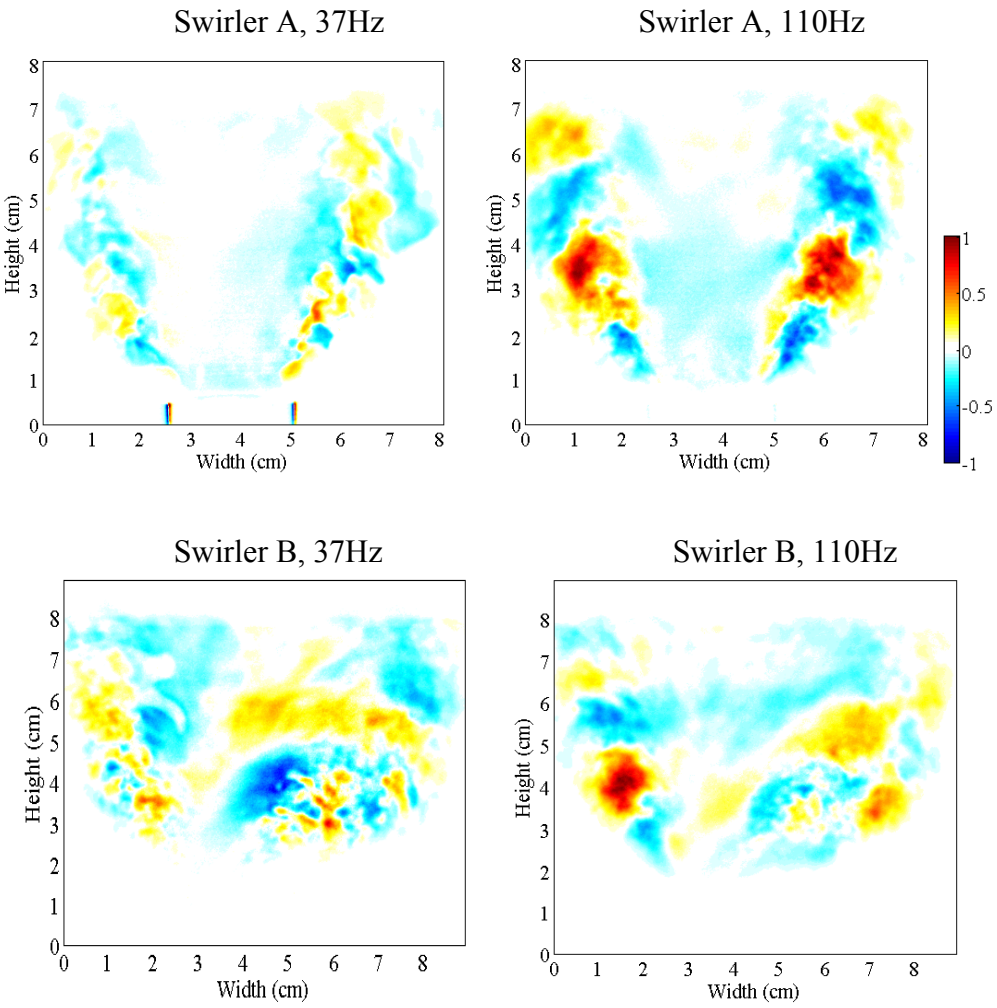

Figure 6.3 Local Rayleigh Index distributions at 0.1 MPa

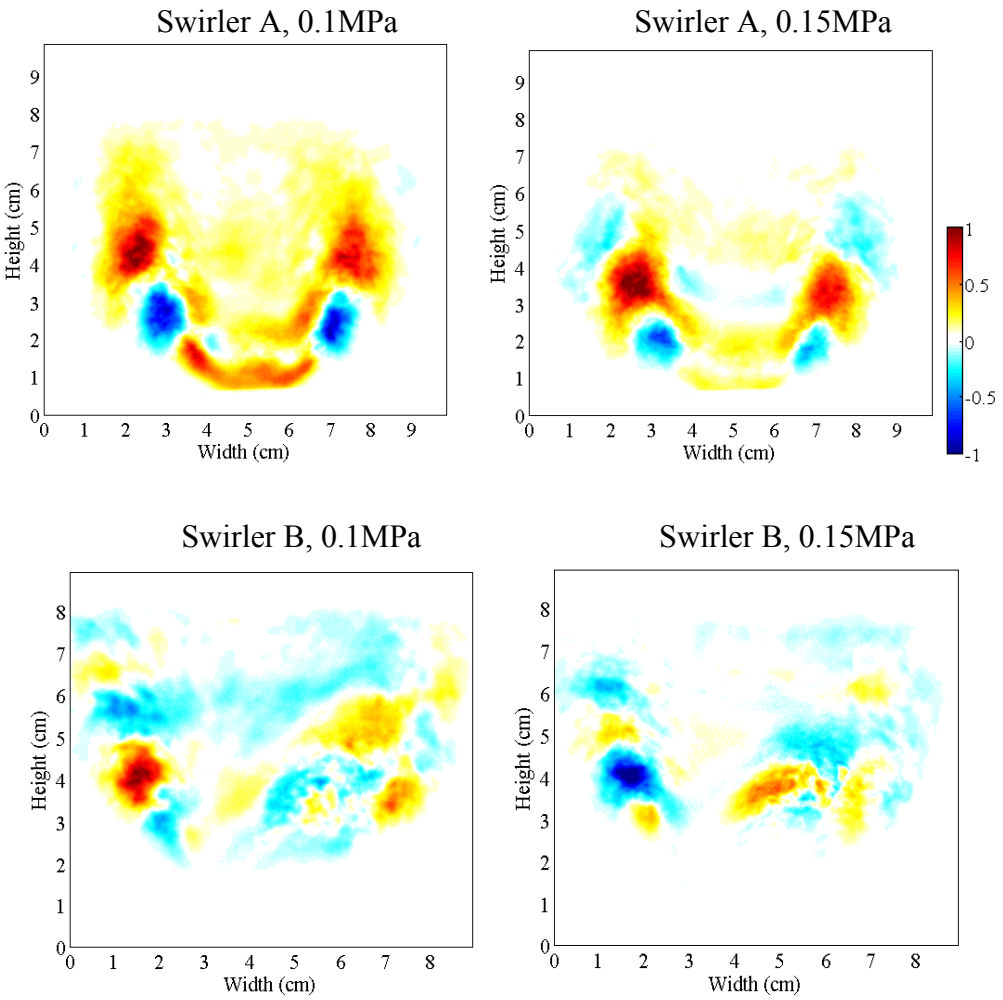

Figure 6.4 Local Rayleigh Index distributions

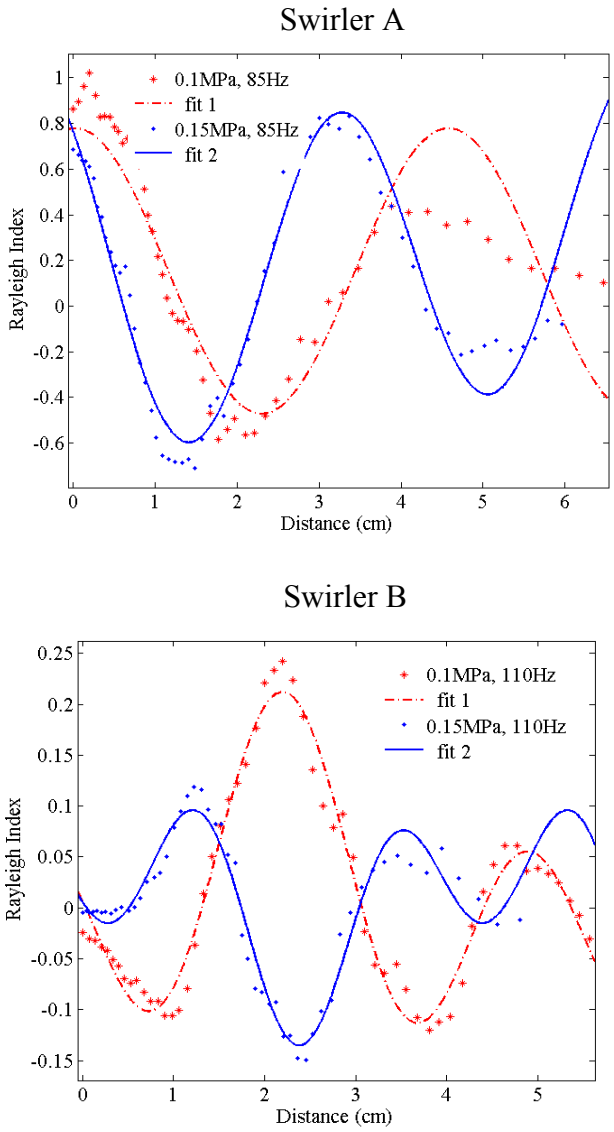

Figure 6.5 Rayleigh Index along the centerline of the vortices

6.1.3 Comparison at 0.15MPa

The flame response at a chamber pressure of 0.15MPa was also measured to examine the effect of pressure and density changes on the previously described flow and Rayleigh Index structures. Figure 6.4 illustrates the Rayleigh Index distributions at 0.1MPa and 0.15MPa. Reynolds numbers for flame A are fixed at 8547 so that the mass flow rate remains fixed. Reynolds number for flame B is 7362 and the acoustic excitation is 110Hz. For the two kinds of flames, the toroidal structure persists to 0.15MPa. Raising the mean pressure makes the flame shorter and the mean velocity of the reactants decreases with pressure as their mass flow rates are fixed. Therefore, the flame tends to propagate back to the burner and appears shorter.

Rayleigh index along the centerline of the structures are extracted in Figure 6.5 For flame A, the wave numbers are approximately 128/m at 0.1 MPa and 185/m at 0.15 MPa. Flame B, the wave numbers are approximately 209 at 0.1 MPa and 251 at 0.15 MPa. The wave numbers at 0.15 MPa are higher than that of 0.1 MPa, which is consistent with their decrease in velocity since $k=2\pi f/v$. This shows that the vortices are still convected by the mean flow at 0.15 MPa. The slight increase in pressure doesn't inherently change the coupling mechanism.

In summary, the combustion dynamics of two lean premixed swirl burners, A and B with swirl numbers of 0.5 and 0.2 respectively, were examined for insight into how swirl number affects flow structure and flame stability. It indicates that the configuration of flame A under swirl number of 0.5 was more stable and symmetrical. Without enough swirl to spread the flow field at the burner exit, the flame B behaves more like a jet flame, particularly in the associated sensitivity to anchoring. Rayleigh index maps were measured for both flames. Both flames A and B respond to the acoustic excitation within a certain frequency range, but only one side of flame B shows clear Rayleigh Index structure. The asymmetry of flame B suggests that the clear vortex structure in the

Rayleigh map is a property of the kind of flame that is relatively 'stable', has narrow flame brush and is only convectively unstable. Finally, the swirl burners were tested at 0.15 MPa, and similar coupling of the flame shear layer and acoustic responses were observed, which shows that the slight increase in mean pressure doesn't significantly affect the stability or the dominant flame physics.

6.2 Flame Sensitivity To Perturbation

It is clear that to induce coupling between the flame and the acoustics, the amplitude of the forcing frequency has to be sufficiently large. The next sets of experiments are carried out to capture the difference between the conditions when the acoustic excitation is strong and when it is weak. The mean pressure for these tests is fixed at one atmosphere.

Figure 6.6 shows the pressure oscillation of two excitations at 110Hz, where the plot on the left shows weak forcing ($p'/P=0.017\%$) and the plot on the right is a stronger forcing ($p'/P=0.035\%$). The 60Hz peak is from electric line noise. Figure 6.7 shows the corresponding Rayleigh index maps. Figure 6.8 and 6.9 show a similar comparison at 65Hz. The difference between the Rayleigh index maps for different levels of perturbation is significant. When the acoustic perturbation is not strong, the Rayleigh index map is basically at constant intensity and there are no fine structures. When the perturbation is more than 0.03% of the mean pressure, multi scale turbulence structures are triggered. This result would appear to have important implication for the application of the low swirl burner.

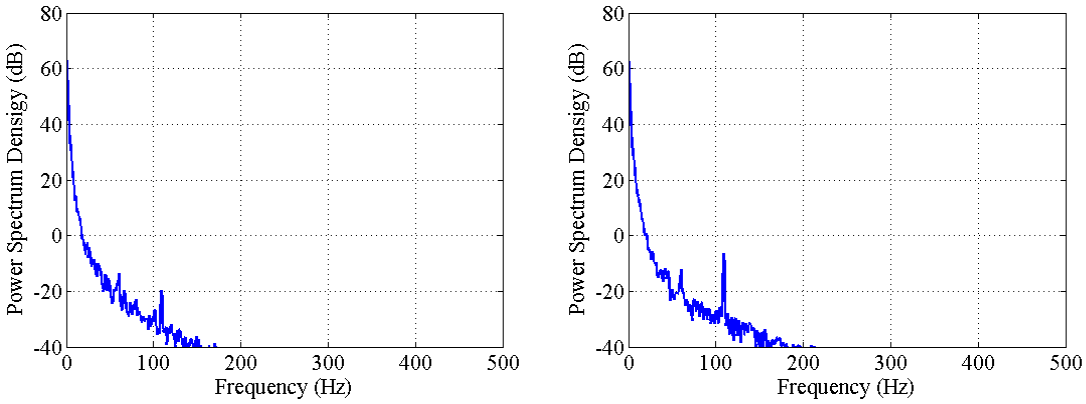

Figure 6.6 FFT of 110Hz excitations

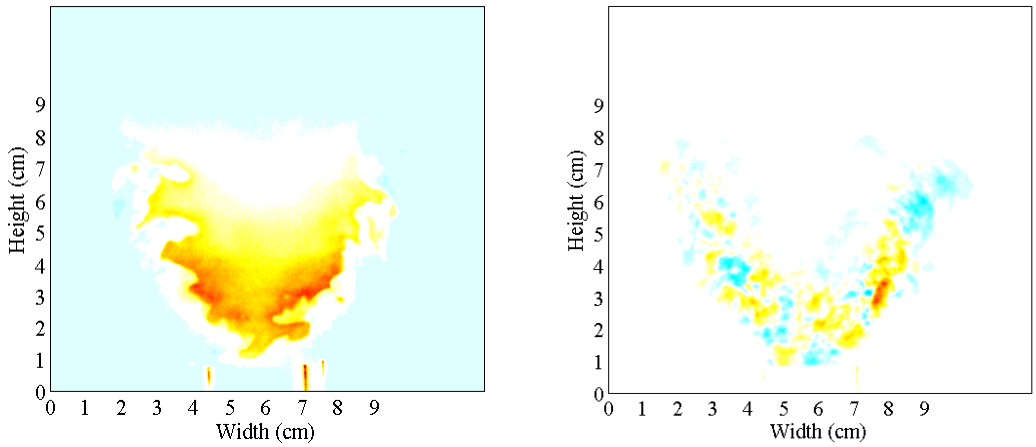

Figure 6.7 Rayleigh index maps at 110Hz (Re=6519, Φ=0.6)

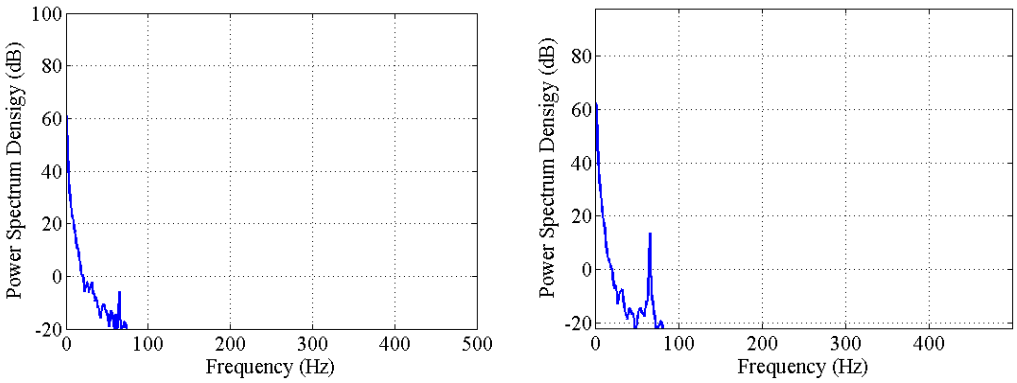

Figure 6.8 FFT of 65Hz excitations (Re=6519, Φ=0.6, f=65Hz)

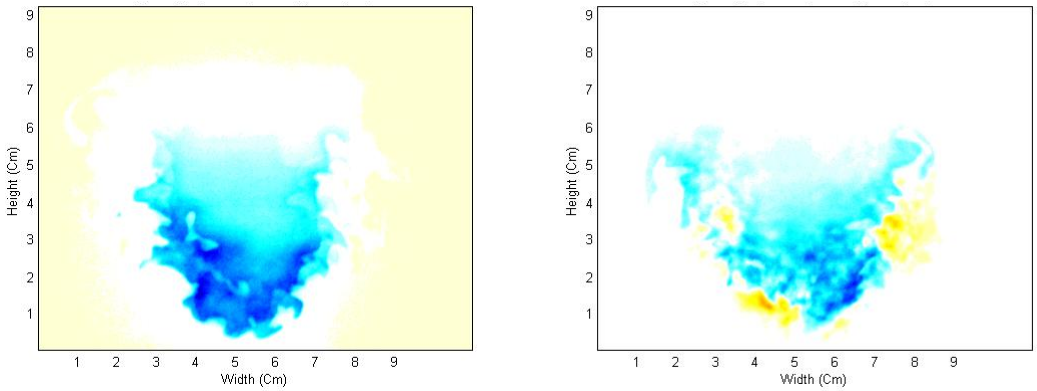

Figure 6.9 Rayleigh index maps at 65Hz (Re=6519, Φ=0.6)

Intermediate perturbations were also examined with experimental conditions in Table 6.1. Case 1 and 2 have the same mass supply of air and methane but at different mean pressure 0.1MPa and 0.2MPa respectively. Figure 6.10 is the OH chemiluminescence images of flame at 95Hz and 101Hz perturbations. The experiment was conducted at 0.1MPa. For weak forcing, the flame shapes are identical (at 95Hz and 120Hz). In other work (Kang et al., 2007; Huang and Ratner, 2009), the flame also had an identical shape across all weak forcing. This means that at levels of perturbation less

than 0.18%, the combustion field is not altered. The flame at 101Hz is different in that the height is smaller and the edge is wider. This implies that the acoustic perturbation changed the flow field, the flame speed, or both. Figure 6.11 is the Rayleigh index map for the cases in Figure 6.10. The structures in the shear layer are much clearer than Figure 6.9, and this implies acoustic coupling is occurring.

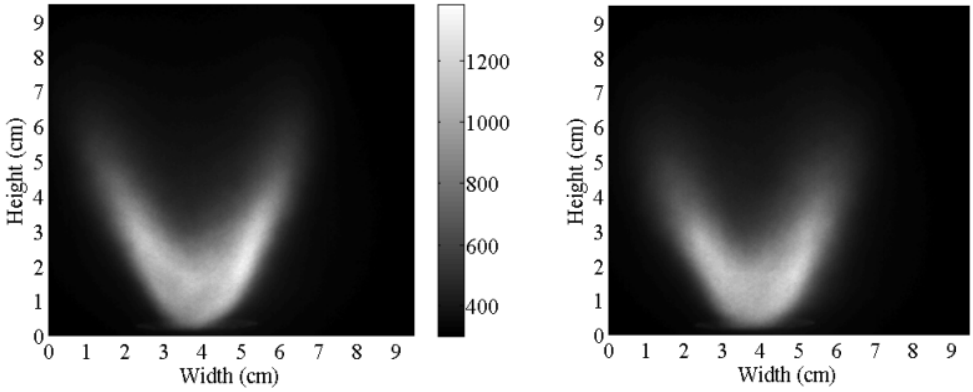

Figure 6.10 Mean flame at 0.1MPa
(left: 95Hz, *p'=0.18%P*; right: 101Hz, *p'=0.43%P*)

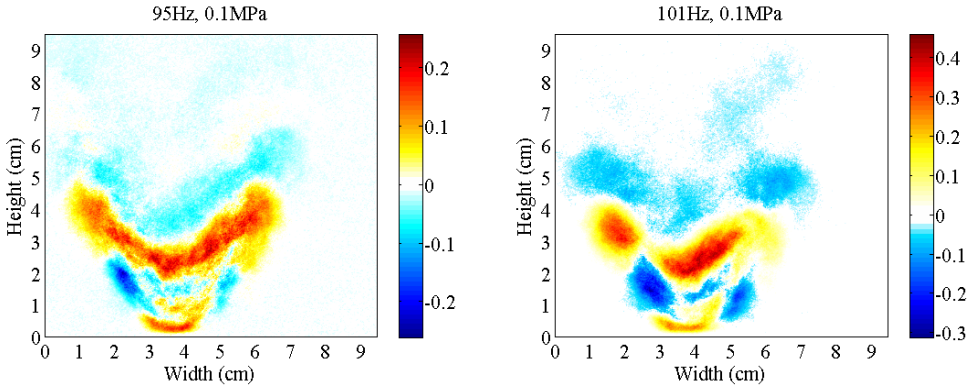

Figure 6.11 Rayleigh Index Maps

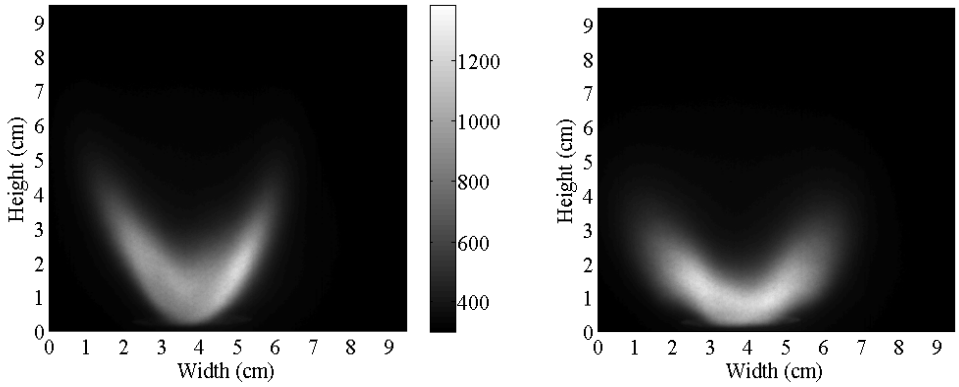

Figure 6.12 Flame at 0.2Mpa
(left:85Hz, *p'=0.08%P*; right:125Hz, *p'=0.19%P*)

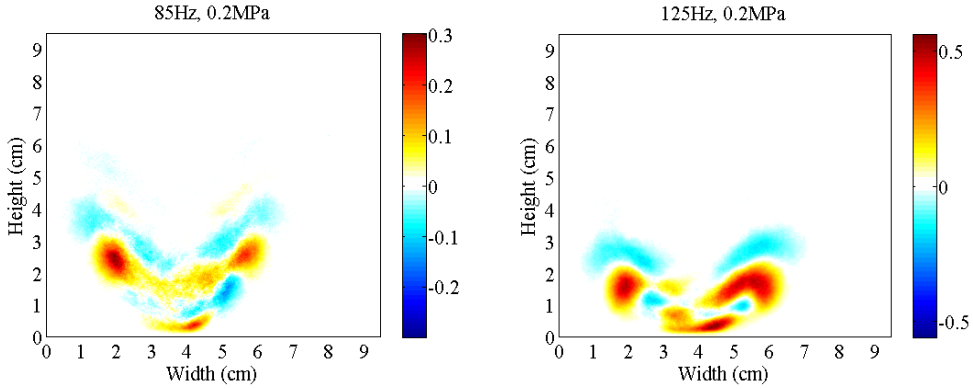

Figure 6.13 Rayleigh Index Maps

Table 6.1 Frequency and pressure conditions

	f (Hz)	95	101	120
Case 1	p’ (Pa)	185	435	144
	p’/P (%)	0.18	0.43	0.14
	f(Hz)	85	125	470
Case 2	p’(Pa)	156	378	145
	p’/P(%)	0.08	0.19	0.07

Figure 6.12 shows the OH images at a mean chamber pressure of 0.2MPa with same flow rates of methane and air. It is evident that the flame at 125Hz, when the amplitude is stronger than the others cases, is different. The Rayleigh index map shows clearer and more coherent structures. The effect of mean pressure on the thermoacoustic coupling was studied in chapter 5. It showed that the coupling persists through at elevated pressures. The observation here also showed similar flame behavior to strong perturbations at 2 atm and 1 atm.

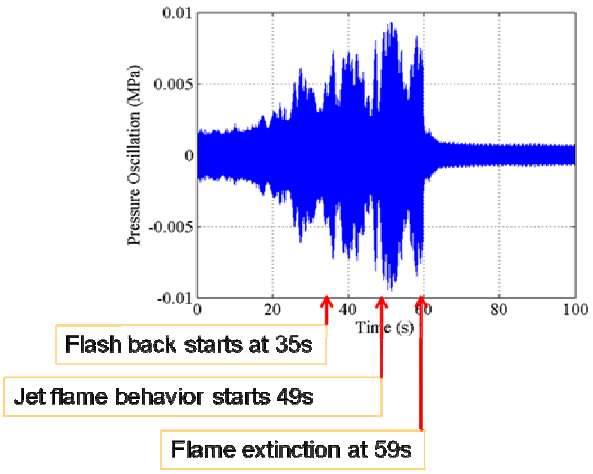

Figure 6.14 Pressure evolution (f=125Hz)

6.2.2 Natural Instability

One type of instability development was observed at 125Hz perturbation. As the perturbation was near the natural mode of the chamber mode, the initial pressure fluctuation was 0.2% of the mean pressure (one atm). The pressure oscillation in chamber starts to grow and after a few seconds, the flame starts to flash back and spatially oscillates. The large acoustic pressure oscillation (0.7% of mean pressure) soon

extinguishes the flame. Without combustion heat driving the flow in the chamber, the oscillation decreases quickly and dies out.

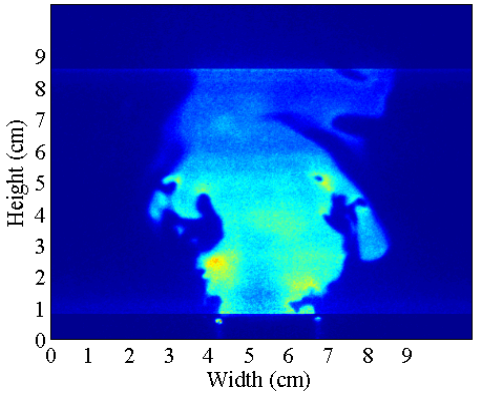

Figure 6.15 Unstable flame in the transition of instability (f=125Hz)

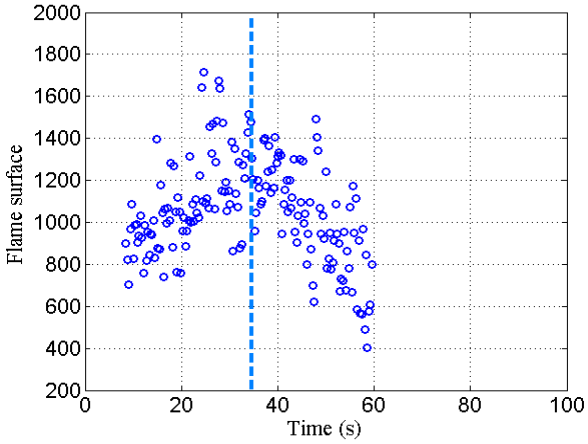

Figure 6.16 Flame surface length

The measured pressure growth is shown in Figure 6.14 and the transient flame is shown in figure 6.15. The length of flame surface in the imaged plane is calculated in

Figure 6.16. In chapter 4, the flame length stayed relatively constant across different frequencies. In this unstable case, the flame length grows with the increasing chamber pressure. The dashed line is the moment when part of the flame propagates back into the burner and an accurate measurement of the total flame surface is no longer possible.

The results described above show that the flame response changes from weak to strong acoustic forcing and the transition from unaffected to strongly affect is measured. The flame showed significantly different behavior to those acoustic perturbations. This leads to a more general question of how the acoustics actually affect the flow field. To stabilize a flame the flame speed should match the speed of the reactants. For turbulent flames, the flow speed needs to be high enough to prevent flame propagation into the burner. This also means that the natural turbulence velocity fluctuations will compete with the acoustic velocity fluctuations in influencing the flow structures. To better understand how these things work out, it is useful to decompose the fluctuations into three canonical types of disturbances (Eq. 6.1): vertical, entropy and acoustic (Lieuwen, 2003; Culick, 2006). The acoustic disturbances propagate with a characteristic velocity equal to the speed of sound, whereas vorticity and entropy disturbances have a characteristic velocity equal to the mean flow velocity with which they are convected. Velocity oscillation due to entropy wave can be neglected since they are generally small.

$$u' = u'_a + u'_v + u'_s \approx u'_a + u'_v \tag{6.1}$$

$$p' \sim \bar{\rho} c u' \tag{6.2}$$

According to the typical acoustic scaling (Eq. 6.2), then the velocity fluctuation induced by acoustic wave can be estimated assuming the mean temperature 330K. The turbulence velocity fluctuation is estimated as 10% of the mean flow. A comparison of the two fluctuation velocities, listed in Table 6.2, finds the acoustic induced fluctuations to be 0.5m/s and the turbulence fluctuations to be 0.25m/s. The common aspect of these

two types of analysis is that the condition when the flame changed its shape is when the acoustic velocity is larger than the turbulence velocity.

Table 6.2 Acoustic velocity fluctuation

Case 1 U=0.5m/s	p'(Pa)	185	435	144
	u'(m/s)	0.47	1.12	0.37
Case 2 U=0.25m/s	p'(Pa)	156	378	145
	u'(m/s)	0.20	0.48	0.19

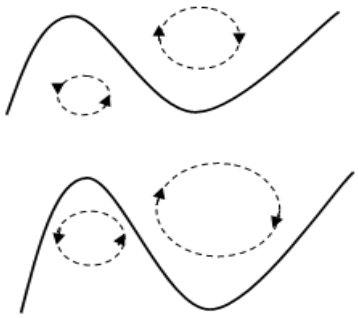

Figure 6.17 Flame-Vortex interactions

The low swirl stabilized lean premixed methane air flame has a very low Mach number (M), on the order of 0.006, assuming turbulent flame speed 2m/s. The ratio of the characteristic length of pressure disturbance to diffusion length (N) at 400Hz is 450 assuming flame thickness 2mm; therefore, $N \approx 1/M : \tau \approx 1$. For such a flame, the pressure/premixed flame interaction are not important, nor are pressure gradients in the combustion region, and neither is the pressure field interaction with the inner reaction zone. There is a fair amount of theoretical work on the interaction of acoustic wave and planer laminar flames (Macintosh, 1991; Clavin et al., 1990), and all of the predicted

coupling is likely through velocity perturbations. At large amplitudes, when the acoustic velocity fluctuation overwhelms the local velocity, the induced vortex in the shear layer is strong enough that it stretches the flame surface and increases the flame brush thickness (Fig. 6.17). This is consistent with the flame surface density measurements. For weak forcing, turbulent velocity fluctuation dominates.

6.3 Conclusion

A comparison was performed between two burners, A and B, with swirl numbers of 0.5 and 0.2 respectively, to examine how the swirl number affects flow structure and flame stability. The results indicate that the configuration of flame A, with a swirl number of 0.5, is more stable and symmetric. Without enough swirl to spread the flow field at the burner exit, flame B behaves more like a jet flame, particularly in the associated sensitivity to anchoring. The comparison between the two burners also suggests that the clear vortex structure in the Rayleigh map is a property of the kind of flame that is relatively 'stable', has narrow flame brush, and is only convectively unstable.

Second, the flame response was measured for different amplitudes of acoustic forcing. It was found that when the acoustic pressure perturbation is less than 0.03% of the mean pressure, the vortices do not lock-in to the forcing frequency and the large coherent structures in the shear layer do not form. It shows that the flame dynamics are significantly affected when the acoustic excitation is sufficiently strong to initiate shear layer vortex formation. The low swirl stabilized lean premixed methane-air flame is sensitive to acoustic perturbation when the velocity fluctuation induced by acoustic perturbation is comparable with that of the turbulence. An unstable oscillation was observed when the acoustic forcing is close to the natural mode of the chamber. The flame becomes unstable when the perturbation is higher than 0.7%.

CHAPTER 7 CONCLUDING REMARKS

This thesis has examined the combustion dynamics and the stability of a low swirl burner. The flame response under different acoustic perturbations has been measured and the impact of changing a range of system parameters has also been examined. The main diagnostic method employed in this thesis is OH-PLIF. The OH-PLIF images were used for calculating Rayleigh index maps of the flame and for the associated flow field structure study.

It was found that toroidal structures exist in the flow field when the acoustic excitation amplitude is above 0.034% of mean pressure and the frequency is between 60 and 150 Hz. Outside of this frequency range, the flow/flame showed no coherent response and acoustic forcing below 0.03-0.35% was insufficient to trigger structure formation even in the acoustically sensitive range. Raising the amplitude above 0.04% also had little effect on the flow structures, although large amplitude pressure forcing (0.7%) would induce flash-back or blowout.

The system response in the range of sensitivity induces changes in the shear layer between the unburned reactants and the products, which becomes unstable and creates periodic vortex structures. The vortices deform the flame surface and create regions of high and low flame surface which then advect with the shear layer. Calculation and comparison of local flame surface and integrated OH intensity validate this hypothesis. The frequency condition for when this coupling occurs can be categorized in terms of Reynolds and Strouhal numbers of the flow field.

These coupling and shear layer instability effects are found to persist across a range of chamber pressures, flow swirl values, and other parameter changes. In general, the coupling behavior continues to the highest pressure tested 0.34MPa. While the flame changes shape due to changes in mass flow and increases in flame speed, the coupling range of frequency is unaffected and the structure intensity weakens slightly. In terms of

sensitivity to swirl number, it was found that for both 0.5 and 0.2 swirl number cases, the flow was responsive to acoustic forcing and clear structures would form. Conversely, the swirl number of 0.2 case was found to be sensitive to any type of flow disturbance and would easily induce flame anchoring on one side or the other. This indicates that while the swirl number 0.5 case is more stable and symmetric. But the shear layer instability mechanism is independent of anchoring or lifting flame behavior.

This thesis work has contributed to the understanding of combustion instability by clarifying the mechanism that causes the toroidal structures first observed in Kang's thesis (2006). It has also examined the low swirl burner flame characteristics in a wide range of conditions, including finding that the flame front response to acoustic perturbation is the key driver for heat release variations. This work also measures the transfer functions for the flame which can serve as an input for numerical simulations.

Future work

High pressure experiments should be continued and expanded. High pressure studies require a robust chamber to withstand high stress and high temperature, and due to the limitation of most other test rigs, most published research on combustion dynamics is limited to one atmosphere. However, real gas turbines operate at pressures that are much higher. Chapter 5 presented a preliminary work at elevated pressures. More work can be carried on to study the flame structure with different forcing level. The frequency range of the shear layer coupling may change with pressure and needs to be verified with more measurement. Conducting further experiments will help to elucidate combustion dynamics in real systems.

Due to climate change and limitation in supply of petroleum, alternative fuel will inevitably be used in many combustors. The most recent development has been in the utilization of syngas for Integrated Gasification Combined Cycle (IGCC). This then drives the need for understanding the combustion dynamics of the low swirl burner when

used with syngas. From a scientific perspective, the Lewis number of Methane-air flame is approximately unity, but this ideal condition will be changed by adding other fuels. Due to the change in Lewis number, other instability modes (such as thermal diffusive instability and cellular instability) will add to the complexity of the combustion dynamics of these systems.

In terms of flame diagnostics, OH-PLIF has been the primary method used in the current thesis. To have a more complete view of the flame behavior, temperature and velocity should also be measured. With these advanced measurements, better data could be produced to contribute to the fundamental study of combustion physics and provide data source of validation for numerical simulations.

APPENDIX COMPONENT SCHEMATICS

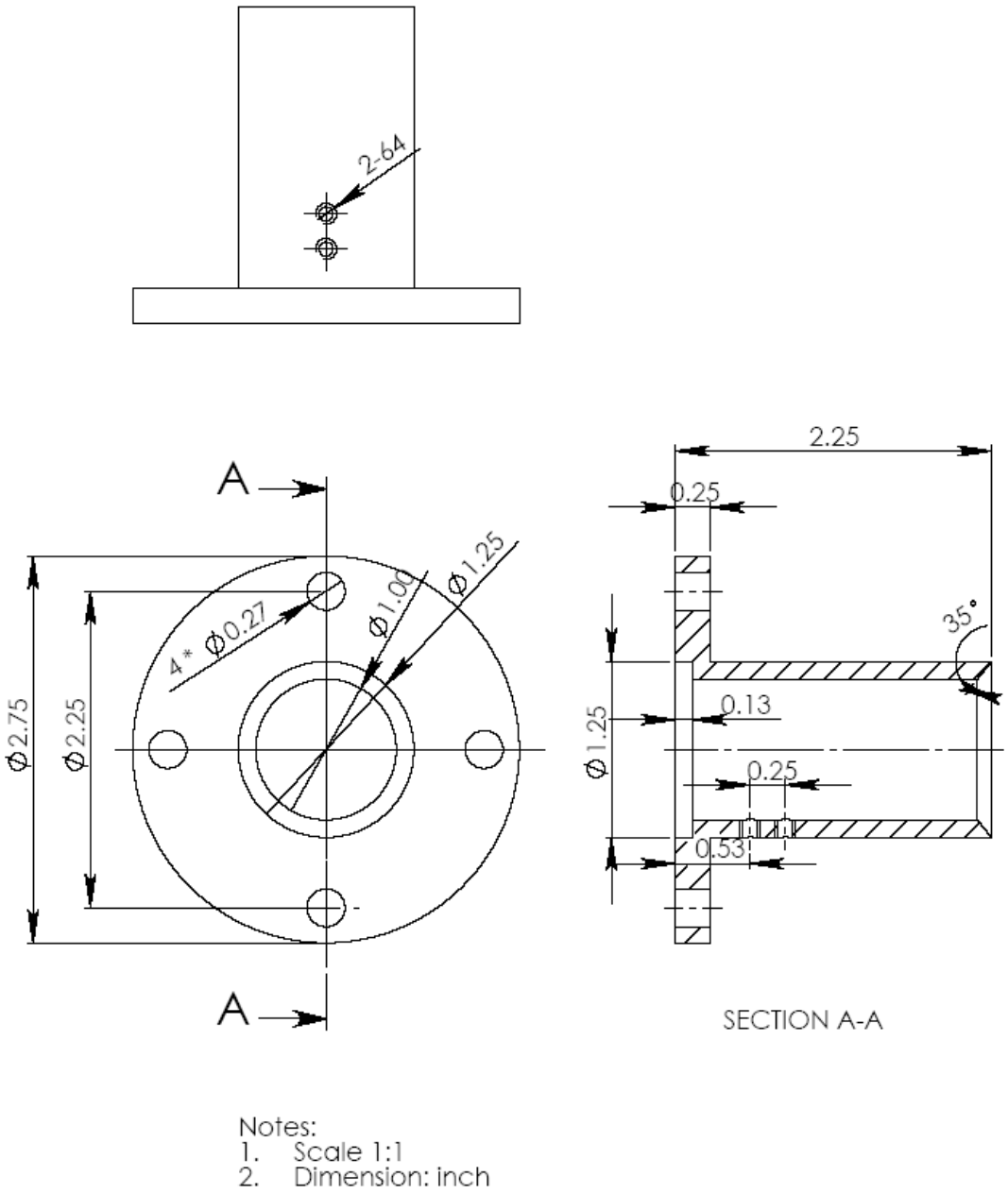

Figure A1 The 1-inch burner

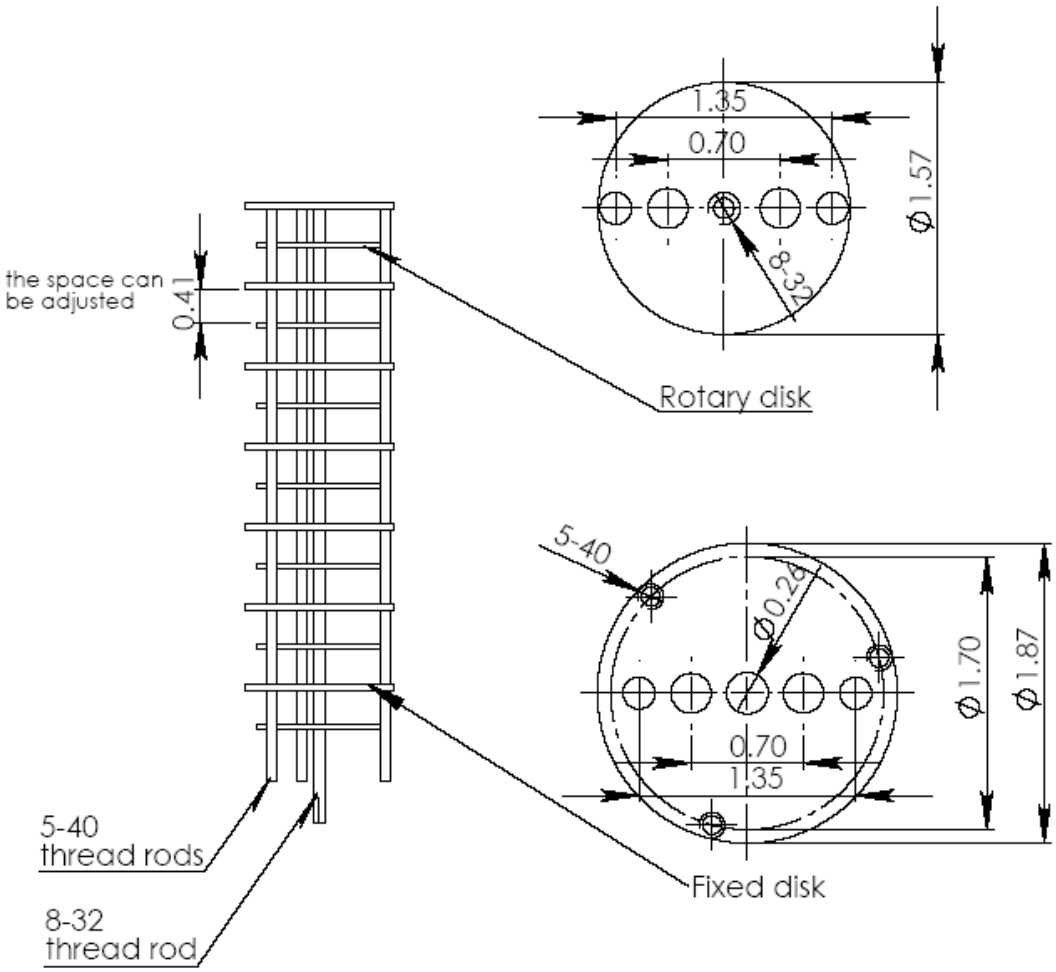

Notes:
1. Scale 1:1
2. Dimension: inch
3. Thickness of the disks: 0.08 inch
4. The fixed disks are fixed by thread rods and nuts
5. By rotaing the center thread rod, different degree of mixing can be obtained

Figure A2 Drawing of the mixer

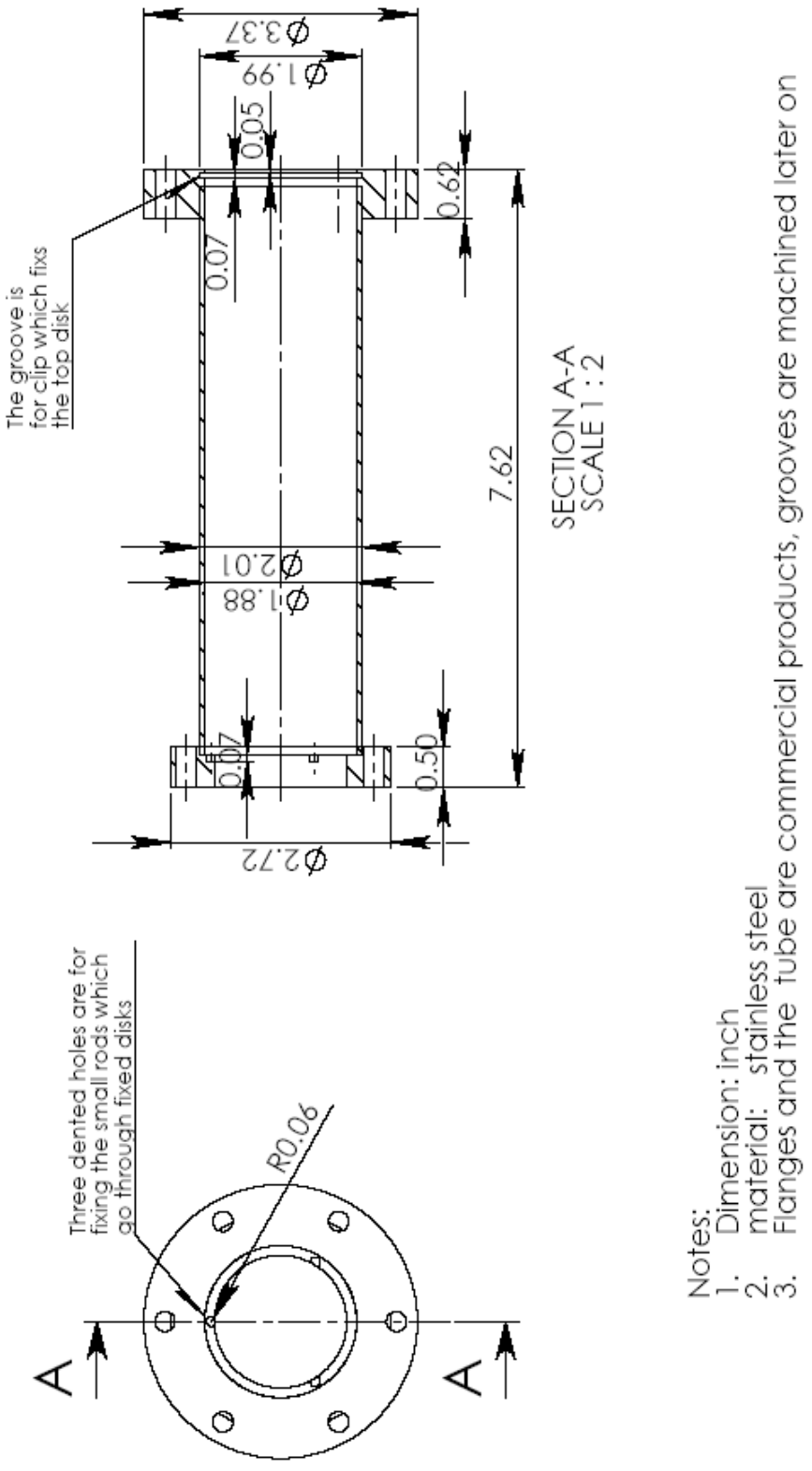

Figure A3 Drawing of the burner

REFERENCES

Aldredge, R.C., and Killingsworth, N.J., "Experimental evaluation of Markstein-number influence on thermoacoustic instability," *Combustion and Flame*, Vol. 137, No. 1-2, 2004, pp. 178-197

Allen., M.G., Mcmanus, K.R., Sonnenfroh, D.M., and Paul, P.H., "Planar Laser-Induced-Fluorescence imaging measurements of OH and Hydrocarbon fuel fragments in High-Pressure Spray-Flame combustion," *Applied Optics*, Vol. 34, No. 27, 1995, pp. 6287-6300

Anderson, J.D., Computational Fluid Dynamics, McGrawllHill, 1995

Ayoola, B.O., Balachandran, R., Frank, J.H., Mastorakos, E. and Kaminski, C.F., "Spatially resolved heat release rate measurements in turbulent premixed flames," *Combustion and Flame*, Vol.144, 2006, pp.1-16

Balachandran, R., Ayoola, B.O., Kaminski, C.F., Dowling,A.P., "Experimental investigation of the nonlinear response of turbulent premixed flames to imposed inlet velocity oscillations," *Combustion and Flame*, Vol. 143, 2005, pp. 37-55

Baillot, F., Durox, D., Ducruix, S., "Parametric response of a conical flame to acoustic waves," *Combustion Science and Technology*, Vol. 142, No. 1, 1999, pp. 91-109

Battles, B.E., and Hanson, R.K., "Laser-induced fluorescence measurements of NO and OH mole fraction in fuel-lean, high-pressure (1-10 atm) methane flames: fluorescence modeling and experimental validation," *Journal of Quantitative Spectroscopy and Radiative Transfer*, Vol. 54, No. 3, 1995, pp. 521-37

Bellows, B.D.1., Neumeier, Y.1., and Lieuweir, T.1., "Forced response of a swirling, premixed flame to flow disturbances," *Journal of Propulsion and Power*, Vol. 22, No. 5, 2006, pp. 1075-84

Birbaud, A.L., Durox, D., and Candel, S., "Upstream flow dynamics of a laminar premixed conical flame submitted to acoustic modulations," *Combustion and Flame*, Vol. 146, No. 3, 2006, pp. 541-552

Boschek, E., Griebel, P., Erne, D., Jansohn, P., "Lean blow out limits and NOx emissions of turbulent, lean premixed, high pressure CH4/H2/AIR flames," Eighth International Conference on Energy for a Clean Environment: cleanair 2005 27-30 June, 2005 Lisbon – Portugal

Bourehla, A., and Baillot, F., "Appearance and stability of a laminar conical premixed flame subjected to an acoustic perturbation," *Combustion and Flame*, Vol. 114, No. 3, 1998, pp. 303-318

Candel, S., "Combustion dynamics and control: progress and challenges," *Proceedings of the Combustion Institute*, Vol. 29, 1991, pp.561-606

Cattolica, R.J., "OH Radical Nonequilibrium in Methane-Air Flat Flames," *Combustion and Flame*, Vol. 44, 1982, pp.43-59

Chakravarthy, S.R., Sivakumar, R., and Shreenivasan, O.J., "Vortex-acoustic lock-on in bluff-body and backward-facing step combustors," *Sadhana - Academy Proceedings in Engineering Sciences*, Vol. 32, No. 1-2, 2007, pp. 145-154

Chang, A.Y., Battles, B.E., and Hanson, R.K., "Simultaneous measurements of velocity, temperature, and pressure using rapid CW wavelength-modulation laser-induced fluorescence of OH," *Optics Letters*, Vol. 15, No. 12, 1990, pp. 706

Cheng, R.K., Littlejohn, D., Nazeer, N., Smith, K.O., "Laboratory studies of the flow field characteristics of low-swirl injectors for adaption to fuel-flexible turbines," *2006 ASME Turbo Expo, GT2006-90878*

Cheng, R.K., Yegian, D.T., Miyasato, M.M., Samuelsen, G.S., Benson, C.E., Pellizzari, R. and Loftus, P., "Scaling and development of Low-Swirl burners for low emission furnaces and boilers," *Proceedings of the Twenty-Eighth Symposium on Combustion*, The Combustion Institute, Pittsburgh, 2000, pp. 1305-1313

Chigier, N.A., Beer, J.M., "Velocity and static pressure distributions in swirling air jets issuing from annular and divergent nozzles," *Trans ASME J Basic Eng 86D*, 1964, 788-796

Cho, J.H., and Lieuwen, T.C., "Modeling the response of premixed flames to mixture ratio perturbations," *2003 ASME Turbo Expo*, Vol. 2, American Society of Mechanical Engineers, New York, NY 10016-5990, United States, Atlanta, GA, United States, 2003, pp. 67-76

Chu, B.T., "Mechanism of generation of pressure waves at flame fronts," *National Advisory Committee for Aeronautics -- Technical Notes*, 1956, pp. 20

Clanet, C., Searby, G., "First experimental study of the Darrieus-Landau instability," *Physical Review Letters*, 80, 1998, pp.3867-3870

Clavin, P., Pelce, P., He, L.T., "One-dimensional vibratory instability of planer flames in propagating in tubes," *J. Fluid Mech.*, Vol. 216, 1990, pp. 299-322

Coats, C.M., "Coherent structures in combustion," *Progress in Energy and Combustion Science*, Vol.22, 1996, pp.427-509

Coker, A., Neumeier, Y., Zinn, B.T., "Active instability control effectiveness in a liquid fueled combustor," *Combustion Science and Technology*, Vol. 178, No. 7, 2006, pp. 1251-1261

Conrad, T., Bibik, A., Shcherbik, D., "Control of the stability margin in a liquid fueled combustor using a "smart" fuel injector," *AIAA/ASME/SAE/ASEE 42nd Joint Propulsion Conference*, Vol. 6, American Institute of Aeronautics and Astronautics Inc., Reston, VA 20191-4344, United States, Sacramento, CA, United States, 2006, pp. 4775-4788

Culick, F.E.C., "Nonlinear behavior of acoustic waves in combustion chambers, Part I," Acta Astonautica, Vol. 47, No. 13, 1976, pp.715-734

Culick, F.E.C, "Combustion instabilities in propulsion systems," *American Society of Mechanical Engineers, Noise Control and Acoustics Division (Publication)* NCA, v 4, 1989, p 33-52

Culick, F.E.C, "Dynamics of combustion systems: fundamentals, acoustics, and control", A short course of lectures, 2001

Culick, F.E.C., and Yang, V., "Overview of combustion instabilities in liquid-propellant rocket engines," *Liquid Rocket Engine Combustion Instability*, Vol. 169, Progress in Astronautics and Aeronautics, AIAA, Washington, DC, USA, 1995.

Culick, F.E.C., Unsteady Motions in Combustion Chambers for Propulsion Systems, NATO, AG-AVT-039, 2006

Docquier, N., Belhalfaoui, S., Lacas, F., Darabiha, N., Rolon, C., "Experimental and numerical study of chemiluminescence in methane/air high pressure flames for active control applications," *Proceedings of the combustion institute*, Vol. 28, 2000, pp.1765-1774

Dowling, A.P., and Morgans, A.S., "Feedback control of combustion oscillations," *Annual Review of Fluid Mechanics*, Vol. 37, 2005, pp. 151-182

Dowling, A.P., and Stow, S. R, "Acoustic analysis of gas turbine combustors," *Journal of Propulsion and Power*, Vol. 19, 2003, pp. 751-764

Durbin, M.D., and Ballal, D.R., "Optimizing the performance of a step swirl combustor," *Proceedings of 29th Intersociety Energy Conversion Engineering Conference - IECEC'94*, Vol. 2, AIAA, Monterey, CA, USA, 1994, pp. 631-635

Durbin, M.D., and Ballal, D.R., "Studies of lean blowout in a step swirl combustor", *Journal of Engineering for Gas Turbines and Power*, Vol. 118, No.1, 1996, pp.72-77

Durox, D., Ducruix, S., and Baillot, F., "Strong acoustic forcing on conical premixed flames," *Symposium (International) on Combustion*, Vol. 1, 1998, pp. 883-889

Durox, D., Schuller, T., and Candel, S., "Combustion dynamics of inverted conical flames," *Proceedings of the Combustion Institute*, Vol. 30, 2005, pp. 1717-24

Durox, D., Schuller, T., Noiray, N., Candel, S., "Experimental analysis of nonlinear flame transfer functions for different flame geometries," *Proceedings of the Combustion Institute*, Vol. 32, 2009

Duwig, C., Fuchs, L., Griebel, P., "Study of a confined turbulent jet: Influence of combustion and pressure," *AIAA Journal*, Vol. 45, No. 3, 2007, pp. 624-639

Eckbreth, A.C., Laser diagnostics for combustion temperature and species, Gordon and Breach Publishers, 1996

Fleifil, M., Annaswamy, A.M., Ghoneim, Z.A., "Response of a laminar premixed flame to flow oscillations: a kinematic model and thermoacoustic instability results," *Combustion and Flame*, Vol. 106, No. 4, 1996, pp. 487-510

Fritsche, D., Furi, M., and Boulouchos, K., "An experimental investigation of thermoacoustic instabilities in a premixed swirl-stabilized flame," *Combustion and Flame*, Vol. 151, No. 1-2, 2007, pp. 29-36

Ghoniem, A.F., Annaswamy, A., Wee, D, Yi, T. and Park, Sungbae, "Shear flow driven combustion instability evidence simulation and modeling," *Proceedings of the Twenty-Ninth Symposium on Combustion*, The Combustion Institute, Sapporo, Japan, 2002, pp. 53-60

Ghoniem, A.F., Park, S., Wachsman, A., "Mechanism of combustion dynamics in a backward-facing step stabilized premixed flame," *30th International Symposium on Combustion*, Vol. 30 II, United Kingdom, Chicago, IL, United States, 2005, pp. 1783-1790

Giezendanner, R., Keck, O., Weigand, P., Meier, W., Meier, U., Stricker, W. and Aigner, M., "Periodic combustion instabilities in a swirl burner studied by Phase-locked planar laser induced fluorescence," *Combustion Science and Technology*, Vol.175, 2003, pp.721-741

Griebel,P., Siewert, P., Jansohn, P., "Flame characteristics of turbulent lean premixed methane/air flames at high pressure: Turbulent flame speed and flame brush thickness", *Proceedings of the Combustion Institute*, 31, 2007, 3083-3090

Gupta, A.K., Lewis, M.J., and Daurer, M., "Swirl effects on combustion characteristics of premixed flames," *Journal of Engineering for Gas Turbines and Power*, Vol. 123, No. 3, 2001, pp. 619-626

Gupta, A.K., Lilley, D.G., Syred, N., Swirl Flows, Abacus Press, 1984

Gutmark, E., Parr, T.P., Parr, D.M. and Schadow, K.C., "Planar imaging of vortex dynamics in flames," *Journal of Heat Transfer*, Vol. 111, 1989, pp. 148-155

Hardalupas Y., and Orain, M., "Local measurements of the Time-Dependent heat Release rate and equivalence ratio using chemiluminescent emission from a flame," *Combustion and Flame*, Vol. 139, 2004, pp188-207

Hassel, E.P., and Linow, S., "Laser diagnostics for studies of turbulent combustion," *Meas. Sci. Technol*., Vol.11, 2000, pp37-57

Heinz Pitsch, "Large-Eddy simulation of turbulent combustion," *Annu. Rev. Fluid. Mech.* 2006.38:453-482

Huang, Y., Ratner, A., "Experimental investigation of thermoacoustic coupling for low-swirl stabilized lean premixed flames," *Journal of Propulsion and Power*, in press, 2009

Huang, Y., "Modeling and simulation of combustion dynamics in Lean-Premixed Swirl-Stabilized gas-turbine engines," Thesis, Pennsylvania State University, 2003

Huang, Y., and Yang, V., "Effect of swirl on combustion dynamics in a lean-premixed swirl-stabilized combustor," *Proceedings of the Combustion Institute*, Vol. 30, 2004, pp. 1775-82

Huang, Y., Wang, S.W., and Yang, V., "A systematic analysis of combustion dynamics in a Lean-Premixed Swirl-Stabilized combustor," *AIAA Journal*, Vol. 44, 2006, pp. 724-740

Huerre, P., Monkewitz,P.A., "Local and global instabilities in spatially developing flows," *Annual Review of Fluid Mechanics*, Vol.22, 1990, pp.473-537

Hult, J., Burns, I.S., and Kaminski, C.F., "Two-line atomic fluorescence flame thermometry using diode lasers," *Proceedings of the Combustion Institute*, Vol 30, 2005, pp 1535-1543

Joulin, G., and Clavin, P., "Linear stability analysis of nonadiabatic flames: diffusional-thermal model," *Combustion and Flame*, Vol. 35, No. 2, 1979, pp. 139-153

Kang, D.M., Measurements of combustion dynamics with laser-based diagnostic techniques, Thesis, California Institute of Technology, 2006

Kang, D.M., Culick, F.E.C., Ratner, A., "Combustion dynamics of a Low-Swirl combustor", *Combustion and Flame*, Vol. 151, 2007, pp 412-425

Kaskan, W.E., and Noreen, A.E., "High-frequency oscillations of flame held by bluff body," *American Society of Mechanical Engineers -- Meeting A-66*, American Society of Mechanical Engineers (ASME), 1954, pp. 14

Katharina, K., Meier, U., Brigitte, A., "Laser-induced fluorescence study of OH in flat flames of 1-10 bar compared with resonance CARS experiments," *Applied Optics*, Vol. 29, No. 10, 1990, pp 1560-1569

Keller, J.J., "On the Interpretation of Vortex Breakdown," *AIAA Journal*, Vol.33, No.12, 1995, pp. 2280-2287

Kiefer, J., Li, Z.S., Zetterberg, J., Bai, X.S., Alden, M., "Investigation of local flame structures and statistics in partially premixed turbulent jet flames using simultaneous single-shot CH and OH Planar Laser-Induced Fluorescence imaging," *Combustion and Flame*, Vol., 154, 2008, pp.802-818

Kohse-Hoinghaus. K., Barlow, R.S., Alden, M., and Wolfrum, J., "Combustion at the focus: laser diagnostics and control," *Proceedings of the Combustion Institute*, Vol. 30, 2005, pp 89-123

Kojima, J., Ikeda, Y., and Nakajima, T., "Basic aspects of OH(A), CH(A), and C2(d) chemiluminescence in the reaction zone of laminar methane-air premixed flames," *Combustion and Flame*, Vol. 140, No. 1-2, 2005, pp. 34-45.

Kornilov, V.N., Schreel, K.R.A.M., and De Goey, L.P.H., "Experimental assessment of the acoustic response of laminar premixed Bunsen flames," *31st International Symposium on Combustion*, Vol. 31 I, United Kingdom, Heidelberg, Germany, 2007, pp. 1239-1246

Kulsheimer, C., Buchner, H., "Combustion Dynamics of Turbulent Swirling Flames," *Combustion and Flame*, Vol. 131, 2002, pp. 70-84

Landau, D., "Factors influencing wear in machines," *Machine Design*, Vol. 16, No. 9, 1944, pp. 105-108

Law, C.K, "Combustion Dynamics" Cambridge, 2006

Law, C.K., and Sung, C.J., "Structure, aerodynamcs, and geometry of premixed flamelets," *Prog. Energy Combust. Sci*, Vol. 26, 2000, pp. 459-505

Law, C.K., "Structure, and Limit phenomena of laminar flames at elevated pressure," *Combustion. Sci. Tech*., 178, pp. 335-360

Lawn, C.J., Evesque, S., and Polifke, W., "A model for the thermoacoustic response of a premixed swirl burner, part one: acoustic aspects," *Combust. Sci. and Tech.*, Vol. 176, 2004, pp.1331-1358

Lee, C. L., Jou, C.J.G., Tsai, C.H., "Improvements in the performance of a medium-pressure-boiler through the adjustment of inlet fuels in a refinery plant," *Fuel*, Vol. 86, No. 5-6, 2007, pp. 625-631

Lee, D., and Lieuwen, T.C., "Premixed flame kinematics in a longitudinal acoustic field," *Journal of Propulsion and Power*, Vol. 19, No. 5, 2003, pp. 837-846

Lee, J.G., and Santavicca, D.A., "Experimental diagnostics for the study of combustion instabilities in lean premixed combustors," *Journal of Propulsion and Power*, Vol. 19, No. 5, 2003, pp.735-750

Lee, S.Y., Seo, S., Broda, J.C., Pal, S., and Santoro, R.J., "An experimental estimation of mean reaction rate and flame structure during combustion instability in a lean premixed gas turbine combustor," *Proceedings of the Combustion Institute*, Vol. 28, 2000, pp. 775-782

Lee. J.G., Lee, T.W., Nye, D.A., and Santavicca, D.A., "Lewis number effects on premixed flames interacting with turbulent Karman vortex streets," *Combustion and Flame*, Vol. 100, 1995, pp.161-168

Li, H., Zhou, X., Jeffries, J.B., Hanson, R.K., "Sensing and control of combustion instabilities in swirl-stabilized combustors using Diode-Laser absorption," *AIAA Journal*, Vol. 45, No. 2, 2007, pp. 390-398

Lieuwen, T., "Modeling premixed combustion-acoustic wave interactions: a review," *Journal of Propulsion and Power*, Vol.19, 2003, pp.765-781

Lieuwen, T., and Zinn, B.T., "On the experimental determination of combustion process driving in an unstable combustor," *Combustion Science and Technology*, Vol. 157, No. 1-6, 2000, pp. 111-127

Lieuwen, T., Neumeier, Y., and Zinn, B.T., "Role of unmixedness and chemical kinetics in driving combustion instabilities in lean premixed combustors," *Combustion Science and Technology*, Vol. 135, No. 1-6, 1998, pp. 193-211.

Lieuwen, T.C. and Yang, V.(eds), Combustion Instabilities in Gas Turbine Engines: Operational Experience, Fundamental Mechanisms, and Modeling, AIAA Progress in Astronautics and Aeronautics, Vol. 210,2005, 657 pages

Lieuwen, T.C., "Statistical characteristics of pressure oscillations in a premixed combustor," *Journal of Sound and Vibration*, Vol. 260, No. 1, 2003, pp. 3-17

Littlejohn, D., and Cheng, R.K., "Fuel effects on a low-swirl injector for lean premixed gas turbines," *31st International Symposium on Combustion*, Vol. 31 II, Elsevier Ltd, Oxford, OX5 1GB, United Kingdom, Heidelberg, Germany, 2007, pp. 3155-3162

Locke, R.J., Hicks, Y.R., Anderson, R.C., "Two-dimensional imaging of OH in a lean burning high pressure combustor," NASA, Washington, DC, USA, 1995

Markstein, G.H., Guenoche, H., and Putnam, A.A., "Nonsteady flame propagation," *AGARDograph 75*, 1964, pp. 328

Matalon, M., "Intrinsic flame instabilities in premixed and nonpremixed combustion," *Annu. Rev. Fluid Mech.*, Vol. 39, 2007, pp.163-191

Matalon, M., and Matkowsky, B.J., "On the stability of plane and curved flames," *SIAM Journal on Applied Mathematics*, Vol. 44, No. 2, 1984, pp. 327-43

Matveev, K.I., and Culick, F.E.C., "A model for combustion instability involving vortex shedding," *Combustion Science and Technology*, Vol. 175, No. 6, 2003, pp. 1059-1083

Mcintosh, A.C., "Pressure disturbances of different length scales interacting with conventional flames," *Combust. Sci. and Tech.*, 1991, Vol. 75, pp. 287-309

McKinney, R.G., Sepulveda, D., Sowa, W., Cheung, A.K., "The Pratt&Whitney TALON X low emissions combustor: revolutionary results with evolutionary technology," 45th AIAA Aerospace Sciences Meeting and Exhibit, January, 2007

Miles, R.B., Udd, E., and Zimmermann, M., "Quantitative flow visualization in sodium vapor seeded hypersonic helium," *Applied Physics Letters*, Vol. 32, No. 5, 1978, pp. 317-19

Najm, H.N., and Ghoniem, A.F., "Coupling between vorticity and pressure oscillations in combustion instability," *Journal of Propulsion and Power*, Vol. 10, No. 6, 1994, pp. 769-776

Paschereit, C.O., and Gutmark, E., "Active control of combustion instabilities in gas turbine burners," *2006 ASME 51st Turbo Expo*, Vol. 1, American Society of Mechanical Engineers, New York, NY 10016-5990, United States, Barcelona, Spain, 2006, pp. 161-171

Paschereit, C.O., Gutmark, E., and Weisenstein, W., "Coherent structures in swirling flows and their role in acoustic combustion control," *Physics of Fluids*, Vol. 11, No. 9, 1999, pp. 2667-2678

Petchenko, A., Bychkov, V., Eriksson, L.E., "Flame propagation along the vortex axis," *Combustion, Theory and Modelling*, Vol. 10, No. 4, 2006, pp. 581-601

Peters, N., Turbulent Combustion, Cambridge, 2000

Poinsot, T.J., Trouve, A.C., Veynante, D.P., "Vortex-Driven Acoustically Coupled Combustion Instabilities," *Journal of Fluid Mechanics*, Vol. 177, 1987, pp. 265-292

Pope, S.B., Turbulent flows, Cambridge, 2005

Pun, W., Measurements of Thermo-Acoustic Coupling, Thesis, California Institute of Technology, 2001

Pun, W., Palm, S.L., and Culick, F.E.C., "Combustion dynamics of an acoustically forced flame," *Combustion Science and Technology*, Vol. 175, No. 3, 2003, pp. 499-521

Putnam, A.A., General considerations of autonomous combustion oscillations, The MacMillan Co., New York

Rani, S.L., Smith, C.E., Hemchandra, S., "Reduced-order stability analysis model for predicting dynamic instabilities in bluffbody flameholder geometries," *43rd AIAA/ASME/SAE/ASEE Joint Propulsion Conference*, Vol. 7, American Institute of Aeronautics and Astronautics Inc., Reston, VA 20191-4344, United States, Cincinnati, OH, United States, 2007, pp. 6334-6349

Rayleigh, J.W.S., The theory of sound Vol. II, Dover publications, 1945

Renard, P.H., Thevenin, D., Rolon, J.C., Candel, S., "Dynamics of flame/vortex interactions," *Progress In Energy and Combustion Science*, Vol. 26, 2000, pp. 225-282

Roberts, W.L., Driscoll, J.F., Drake, M.C., and Goss, L.P., "Images of quenching of a flame by a vortex-to quantity regimes of turbulent combustion," *Combustion and Flame*, Vol. 95, 1993, pp.58-69

Rodriguez-Martinez, V.M., Dawson, J.R., O'Doherty, T., and Syred, N., "Low-frequency combustion oscillations in a swirl burner/furnace," *Journal of Propulsion and Power*, Vol. 22, No. 1, pp217-221

Rogers, D.E., and Marble, F.E., "Mechanism for high-frequency oscillation in ramjet combustor and afterburners," *Jet Propulsion*, Vol. 26, No. 6, 1956, pp. 456-462

Roux, S., Lartigue, G., Poinsot, T., Meier, U., Berat, C., "Studies of mean and unsteady flow in a swirled combustor using experiments, acoustic analysis, and large eddy simulations," *Combustion and Flame*, Vol., 141, 2005, pp. 40-54

Samaniego, J.M, Yip, B., Poinsot, T. and Candel, S., "Low-frequency combustion instability mechanisms in a side-dump combustor," *Combustion and Flame*, Vol. 94, No.4, 1993, pp. 363-380

Santhanam, V., Knopf, F.C., Acharya, S., and Gutmark, E., "Fluorescence and temperature measurements in an actively forced swirl-stabilized spray combustor," *Journal of Propulsion and Power*, Vol. 18, No. 4, 2002, pp855-865

Scarinci, T., Freeman, C., and Day, I., "Passive control of combustion instability in a low emissions aeroderivative gas turbine," *2004 ASME Turbo Expo*, Vol. 1, American Society of Mechanical Engineers, New York, NY 10016-5990, United States, Vienna, Austria, 2004, pp. 487-499

Schadow, K.C., and Gutmark, E., "Combustion instability related to vortex shedding in dump combustors and their passive control," *Progress in Energy and Combustion Science*, Vol. 18, No. 2, 1992, pp. 117-132

Schildmacher, K.-U. , Hoffmann, A., Selle, L., Koch, R., Schulz, C., Bauer, H.-J., Poinsot, T., Krebs, W., Prade, B., "Unsteady flame and flow field interaction of a premixed model gas turbine burner," *Proceedings of the Combustion Institute,* 31, 2007, 3197-3205

Seitzman, J.M., Kychakoff, G., and Hanson, R.K., "Instantaneous temperature field measurements using planar laser-induced fluorescence," *Optics Letters,* Vol. 10, No. 9, 1985, pp. 439-41

Shanbhogue, S.J., Plaks, D.V., and Lieuwen, T., "The K-H instability of reacting, acoustically excited bluff-body shear layers," *43rd AIAA/ASME/SAE/ASEE Joint Propulsion Conference,* Vol. 7, American Institute of Aeronautics and Astronautics Inc., Reston, VA 20191-4344, United States, Cincinnati, OH, United States, 2007, pp. 6631-6647

Shepherd, I.G., and Cheng, R.K., "The burning rate of premixed flames in moderate and intense turbulence," *Combustion and Flame,* Vol. 127, 2001, pp. 2066-2075

Sivashinsky, G.I., "Diffusional-Thermal Theory of Cellular Flames," *Combustion Science and Technology,* Vol. 15, No. 3-4, 1977, pp. 137-146

Smith, D.A., and Zukoski, E.E., "Combustion instability sustained by unsteady vortex combustion," *AIAA/SAE/ASME/ASEE 21st Joint Propulsion Conference,* AIAA, New York, NY, USA, Monterey, CA, USA, 1985, pp. 9

Sung, H.G., "Combustion dynamics in a model lean-premixed gas turbine with a swirl stabilized injector," *Journal of Mechanical Science and Technology,* Vol. 21, No. 3, 2007, pp. 495-504

Swift, G.W., Thermoacoustics: a unifying perspective for some engines and refrigerators, Acoustical Society of America, 2002

Syred, N., "A review of oscillation mechanisms and the role of the precessing vortex core (PVC) in swirl combustion systems," *Progress in Energy and Combustion Science,* Vol. 32, No. 2, 2006, pp. 93-161

Syred, N., and Beer, J.M., "The damping of precessing vortex cores by combustion in swirl generators," *Proceedings of the 3rd Colloquium on Gasdynamics of Explosions and Reactive Systems,* Vol. 17, Marseille, France, 1972, pp. 783-801

Taupin, B., Cabot, G., Martins, G., Vauchelles, D., and Boukhalfa, A., "Experimental study of stability, structure and CH* chemiluminescence in a pressurized lean premixed methane turbulent flame," *Combust. Sci. and Tech.,* Vol. 179, 2007, pp 117-136

Poinsot, T., Veynante, D., Theoretical and Numerical Combustion (Second Edition), Edwards, 2005

Thumuluru, S.K., Bobba, M.K., and Lieuwen, T., "Mechanisms of the nonlinear response of a swirl flame to harmonic excitation," *2007 ASME Turbo Expo,* Vol. 2, American Society of Mechanical Engineers, New York, NY 10016-5990, United States, Montreal, Que., Canada, 2007, pp. 721-731

Turns, S.R., An introduction to Combustion, Mcgraw Hill, 2000

Turrell, MD, Stopford, PJ, Syed, K, Buchanan, E., "CFD simulations of the flow within and downstream of high swirl lean premixed gas turbine combustors," *Proceedings ASME turbo-expo 2004*, vol.1, pp.31-38

Venkataraman, K.K., Preston, L.H., Simons, D.W., Lee, B.J., Lee, J.G. and Santavicca, D.A., "Mechanism of combustion instability in a lean premixed dump combustor," *Journal of Propulsion and Power*, Vol.15, 1999, pp. 909-917

Wang, H., "Oscillation and extinction in flames," PhD thesis, Princeton University, 2007, pp. 6-10

Wangher, A., Searby, G., Quinard, J., "Experimental investigation of the unsteady response of premixed flame fronts to acoustic pressure waves," *Combustion and Flame*, Vol. 154, 2008, pp. 310-318

Wolfrum, J., "Lasers in combustion: from basic theory to practical devices," *Proceedings of the Combustion Institute*, 27, 1998, 1-41

Williams, F., Combustion Theory, Addison-Wesley Pub., Reading, MA, 1985

Zhang, Y., Ishzuka, S., Zhu, H., Kee, R.J., "Effects of stretch and pressure on the characteristics of premixed swirling tubular methane-air flames," *Proceedings of the Combustion Institute*, 33, 2009

Zinn, B.T., "Combustion instabilities: problems, solutions, and research needs." *Chemical and Physical Processes in Combustion: 1986 Fall Technical Meeting.* Combustion Inst, Pittsburgh, PA, USA, San Juan Bautista, PR, 1987, pp. 1-12

Zinn, L.T., "A mechanism of combustion instability in lean premixed gas turbine combustors," *Journal of Engineering for Gas Turbines and Power*, Vol. 123, No. 1, 2001, pp. 182-189